Detection thresholds for large to great paleoseismic subduction earthquakes in south-central Alaska from coastal marsh records.

WOOD, KAITLIN,LOUISE

Detection thresholds for large to great paleoseismic subduction earthquakes in south-central Alaska from coastal marsh records.

Abstract

Coastal paleoseismic evidence currently provide records of the recurrence of great earthquakes in the Prince William Sound section, Alaska, with widespread evidence of vertical surface displacement ≥ 1 m during seven great earthquakes in the past 4000 years. The established criteria for detecting land level changes ≥ 1 m relies heavily on identifying and tracing abrupt changes in sediment stratigraphy, peat-silt couplets which indicate ≥ Mw 8 earthquake produced subsidence. While methods are well developed for identifying displacement of ≥ 1 m, very little is known about the lower detection limit of vertical land displacement. Briggs and Barnhart (2017) suggest that subduction earthquakes < Mw 8 displace the coast by < 0.3 m and likely leave no geologic evidence in coastal marshes. However, recent studies suggest that a detection limit of ~0.1 to 0.2 m is possible within vegetated marsh environments.

Consequently, this thesis aims to identify the lower detection limits of co-seismic vertical deformation in coastal marshes of Prince William Sound to reveal large (Mw 7-7.9) to great (≥ Mw 8) earthquakes, which may have occurred between the 1964 CE and the preceding earthquake (~771 cal yr BP). The sampling design of previous studies looking at ≥ 1 m subsidence focuses on marsh-front locations, which may not detect smaller earthquakes. Thus, fieldwork was undertaken in Alaska to test a new methodology which focuses on high marsh environments; peat forming communities where the most precise quantitative estimates of deformation can be reconstructed.

The stratigraphic contact of the 771 ± 10 cal yr BP earthquake was traced inland where it is expressed as a peat-to-peat contact. AMS dating, shifts in diatom assemblages, and a pronounced fall in PMSE at the contact provide evidence of the ~771 cal yr BP earthquake. However, I argue that the magnitude of this subsidence is dependent on training set selection. Furthermore, I suggest that using a regional peat only training set provides the lowest detection limit (< 0.1 m) for the ~771 cal yr BP earthquake whilst still providing a suitable number of analogues. No additional earthquakes were identified in the peat at Girdwood, raising questions about the suitability of diatom transfer functions for detecting smaller seismic events in high marsh environments.

Detection thresholds for large to great paleoseismic subduction earthquakes in south-central Alaska from coastal marsh records.

Kaitlin Wood

Thesis submitted for the degree of MSc by Research

Department of Geography, Durham University

September 2024

Table of Contents

List of Figures

List of Tables

List of Acronyms

AMS	Accelerator Mass Spectrometry
CPS	Counts Per Second
CT	Computed Tomography
EQ	Earthquake
HAT	Highest Astronomical Tide
LW-WA	Locally Weighted-Weighted Averaging
MAT	Modern Analogue Technique
MINDC	Minimum Dissimilarity Coefficient
MHHW	Mean Higher High Water
MLLW	Mean Lower Low Water
ML	Maximum Likelihood
MSCL-XCT	Multi Sensor Core Logging - X-ray Computed Tomography
Mw	Moment Magnitude
NOSAMS	National Ocean Sciences Accelerator Mass Spectrometry Facility
PMSE	Palaeo Marsh Surface Elevation
RMSEP	Root Mean Square Error of Prediction
RSL	Relative Sea Level
R^2	Coefficient of Determination
SWLI	Standardised Water Level Index
WA	Weighted Averaging
WA-PLS	Weighted Averaging- Partial Least Squares
XRF	X-ray Fluorescence

Statement of copyright

Acknowledgements

Firstly, I would like to thank my supervisors Professor Sarah Woodroffe and Dr Simon Engelhart. I am extremely grateful for the opportunity to do this project - and for all the wisdom, guidance and patience you have given me. The knowledge I have gained has been invaluable.

Sarah – Thank you being a calm presence when I needed it most, and for all the time you have given to me and my project over the past year. I couldn't have asked for a better lead supervisor. You have shaped my interest in palaeosiesmology and academic research more broadly. I hope we get to work together again one day.

Simon – Thank you for your insights on this project, and for your guidance over the past year. Your knowledge on Alaskan palaeosiemology have been truly invaluable.

Secondly, I would like to thank Emeritus Professor Ian Shennan. Ian's knowledge regarding Alaskan diatoms has been extremely helpful.

I would also like to thank Robert Witter, our contact at the USGS, for his insights during fieldwork in Alaska. Also, Grace Summers, for keeping me sane during fieldwork, and for all the diatom knowledge you have given me as a total novice.

I would also like to acknowledge the USGS. This project would not have been possible without their financial funding.

Finally, I would like to thank my friends and family for their love and support throughout my masters. Special thanks go to Erin, who has been the most supportive office buddy I could've ask for, and to Will, who has always supported me throughout my undergraduate and postgraduate studies.

Chapter 1: Introduction

South-central Alaska is located on the Aleutian Megathrust boundary, where the Pacific and North American plates converge at 6.3 cm per year. This results in the area being profoundly seismically active, with seven ≥ Moment Magnitude (Mw) 9 earthquakes being recorded in the last 4000 years in this region (Shennan et al. 2008). Large (Mw 7-7.9) to great (≥ Mw 8) earthquakes within south-central Alaska pose significant threats to society, as evidenced by a magnitude 9.2 earthquake which ruptured the Prince William Sound, Kenai and Kodiak segments of the Aleutian Megathrust in 1964 CE (Figure 1.1).

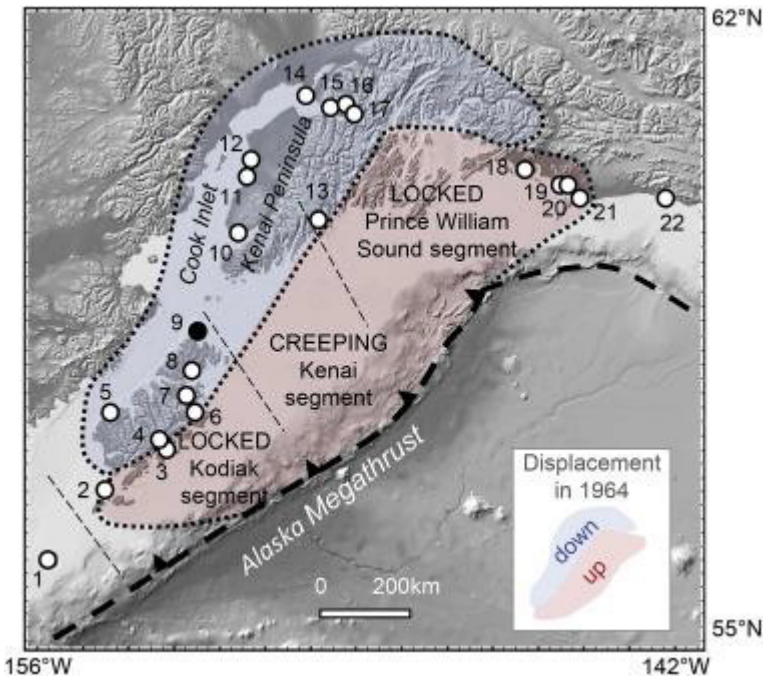

Figure 1.1. The various rupture segments and spatial extent of the subsidence and uplift associated with the 1964 CE earthquake. Schematic is taken from Shennan et al. (2018).

Coastal marshes adjacent to subduction zones in south-central Alaska act as proxies for historical earthquakes. This is owed to the rapid changes in relative sea level experienced during earthquakes, which is reflected in the litho- and bio- stratigraphy of their sedimentary sequences (Shennan and Hamilton, 2006). Coastal paleoseismic evidence currently provides records of the recurrence of great earthquakes in the Prince William Sound segment, with widespread evidence of surface deformation ≥ 1 m during these great earthquakes. However, very little is known about the lower detection limit of vertical displacement, and smaller earthquakes (< Mw

8) causing < 1 m displacement have yet to be identified (Briggs and Barnhart, 2017; Shennan et al. 2014a; Shennan et al. 2016; Brader et al. 2021).

Based on records from numerous subduction zones, Briggs and Barnhart (2017) suggest that subduction earthquakes < Mw 8 displace the coast by < 0.3 m and likely leave equivocal or no geologic evidence in coastal marshes. However, in certain circumstances, such as in the high marsh environment, it has been suggested a detection limit of ~ 0.1 to 0.2 m is considered possible (Shennan et al. 2016, 2018; Brader et al. 2021). This thesis will take a different sampling design to previous studies, which focus on marsh front locations, by looking at high marsh environments to investigate whether the sedimentary signature of a known earthquake (referred to as EQ1 occuring ~770 cal yr BP, Barclay et al. 2024) is visible and possible to quantify. This signature which can be seen as a peat-silt couplet at the marsh front may also be recorded as a peat-peat couplet in the high marsh environment at Ocean View, Anchorage. I will then investigate part of the interseismic period between the EQ1 and the 1964 CE events at Girdwood, to see if there is any evidence for as-yet unknown subsidence events in high marsh (peat) sediment lithology and bio- stratigraphy.

Recent research regarding subduction zones in Alaska question whether the segment boundaries identified for large and great earthquakes in the 20th and 21st centuries remain consistent across multiple earthquake cycles, or if smaller segments with different boundaries are capable of rupturing and generating significant hazards (Shennan et al. 2016). Thus, a better understanding of the ability of high marsh environments to provide estimates of subsidence is important for assessing seismic hazards of large (Mw 7.0-7.9) and great (≥ Mw 8.0) earthquakes. Furthermore, this knowledge is crucial for reducing uncertainties related to future earthquake hazards in south-central Alaska, and for effectively integrating paleoseismic records into seismic hazard assessments (Wesson et al. 2007; Mueller et al. 2015).

This thesis will begin with a review of the existing literature regarding historical earthquakes in south-central Alaska and the application of microfossils in paleoseismology. Chapter 3 details the methods employed in this thesis, while Chapter 4 presents the results of this research. Finally, Chapter 5 and 6 discusses the implications of the findings, conclusions and suggests areas for future work.

2.0. Literature Review

2.1. Seismic controls on relative sea level

Changes in Holocene relative sea level are influenced by multiple factors, including variations in land ice mass and ocean thermal expansion, glacio- and hydro-isostatic adjustment, ocean dynamics, tectonic activity, and local factors such as sediment compaction (Plafker et al. 1992). Variations in relative sea level, sediment availability, erosion and tidal range influence the deposition and preservation of sediment sequences within coastal salt marshes, and can thus provide a stratigraphic record of Holocene sea-level changes. Within Alaska, coastal marsh stratigraphy has been shown to preserve records of relative sea-level changes caused by co-seismic vertical land deformation associated with large to great earthquakes (e.g. Shennan and Hamilton, 2006, Shennan et al. 2018).

2.1.1. Earthquake deformation cycle and the formation of peat-silt couplets

The 1964 CE Alaska earthquake occurred at the boundary between the North American and Pacific tectonic plates, where the Pacific plate subducts beneath the North American plate, resulting in the area being profoundly seismically active. During an interseismic period, strain slowly accumulates along the locked portion of the plate boundary – causing the upper continental plate to shorten. This results in subsidence close to the trench and uplift further landward. However, during co-seismic subsidence, the accumulated strain is released along the locked segments of the plate boundary. This release of strain results in a sudden slip that allows the upper continental crust to extend. Consequently, areas close to the plate boundary experience abrupt uplift, whilst sites further landward from the plate boundary experience subsidence (Nelson et al. 1996) (Figure 1.1). At sites close to the plate boundary, deformation dissipates more quickly whereas sites further away experience a slower rate of deformation, with subsidence persisting for a long period. Plafker (1969) notes that Girdwood, one of the field sites used in the project, lies close to the zone of maximum subsidence, experiencing up to 1.5 m of subsidence during the 1964 CE earthquake. This period of co-seismic subsidence is followed by the interseismic period until another earthquake occurs. During this interseismic period, deformation can occur by the process of ‘relocking’, whereby after an earthquake, the previously slipped segments of the fault become locked again, and strain accumulates. Alternatively, deformation can occur during the interseismic period due to ‘afterslips’, which is the continued slip along a fault after the main release of stress during co-seismic activity. This is caused by only a portion of the stress on the megathrust being released during the earthquake – resulting in additional slipping along the fault. The various mechanisms causing land

deformation in seismically active regions such as south-central Alaska highlight the complexities of the earthquake deformation cycle.

In coastal marshes affected by co-seismic subsidence, organic sediment falls to a lower elevation resulting in this layer becoming overlain by lower-intertidal sediment such as silt. The drop in elevation during co-seismic subsidence results in the creation of a peat-silt couplet, with a sharp stratigraphic boundary between the two units (Brader et al. 2021). Following co-seismic subsidence, rapid post-seismic uplift results in relative sea level fall and a gradual return to the peat-forming environment (Barlow, 2010). This uplift continues at a slower rate during the inter-seismic period, which persists until the occurrence of the next large or great earthquake. Consequently, stratigraphic sequences featuring multiple peat–silt couplets indicate the occurrence of multiple earthquake cycles (e.g. Shennan and Hamilton, 2006) (Figure 2.1).

2.1.2. Identifying seismic activity within peat-silt couplets

While peat-silt couplets are predominantly associated with large and great earthquakes, they may also form due to non-seismic factors, including storm surges, localized flooding and variations in tidal range, all with various degrees of abruptness (Scholl, 1964, Allen, 2000). This led Nelson et al. (1996) to propose five criteria that a peat-silt couplet should satisfy before attributing its formation to seismic activity. However, this critera was critiqued and subsequently expanded on by Shennan et al. (2016) who added a further sixth critera, in order to better inform paleaeoseismological studies. Shennan et al. (2016) argues that the importance of different criteria changes as our knowledge of a tectonic region increases, as thus Nelson et al's (1996) criteria may not always be sutiable. Shennan et al. (2016) suggests as model testing for subduction zone ruptures in segments of variable length in different earthquakes increases, sites close together within a segment should show the same co-seismic inference. Thus, they argue that if one site has a buried peat with tight age constraints but with weak criteria (e.g. amount of vertical change across the contact), the lack of a correlation in age to nearby buried peats with strong co-seismic criteria is a good indication that the dated peat with weak criteria may be of non co-seismic origin. In order to reflect developments in research of salt marsh paleoseismological studies since Nelson et al. (1996), Shennan et al. (2016) proposes assessing sediments based on the following criterion:

1. Lateral extent of peat-mud or mud-peat couplets with sharp contacts (usually 10-50 m apart for hundred of metres is common across most studies).
2. Suddenness of submergence or emergence, replicated within each site (sequence of interbedded mud-peat couplets rather than thick peat).

3. Amount of vertical motion, quantified with 95% error terms (mud with plants typical of low marsh overlain by peaty soil with remains of high-marsh plants, attributed to change in relative sea level of decimetres to a metre).
4. Syncroneity of submergence and emergence (age of sediments formed within a few hundred years of one another)
5. Spatial pattern of submergence and emergence
6. Possible additional evidence, such as evidence of a tsunami or liquefaction concurrent with submergence or emergence (laterally extensive sand beds immediately overlie intertidal mud and lie below buried wetland soils, attributed to surge of sandy water concurrent with submergence or emergence).

In addition to the previously mentioned criteria, seismic events can be inferred from microfossils within sedimentary archives. Microfossils such as diatoms and foraminifera are useful for distinguishing between seismic and non-seismic origins of peat–silt couplets since microfossils record variations in environmental conditions, including relative sea level (Horton and Sawai, 2010). Changes in relative sea level influence microfossil distributions, which can be used alongside evidence of peat-silt couplets to quantify the subsidence associated with large to great earthquakes (e.g. Pilarczyk et al. 2014).

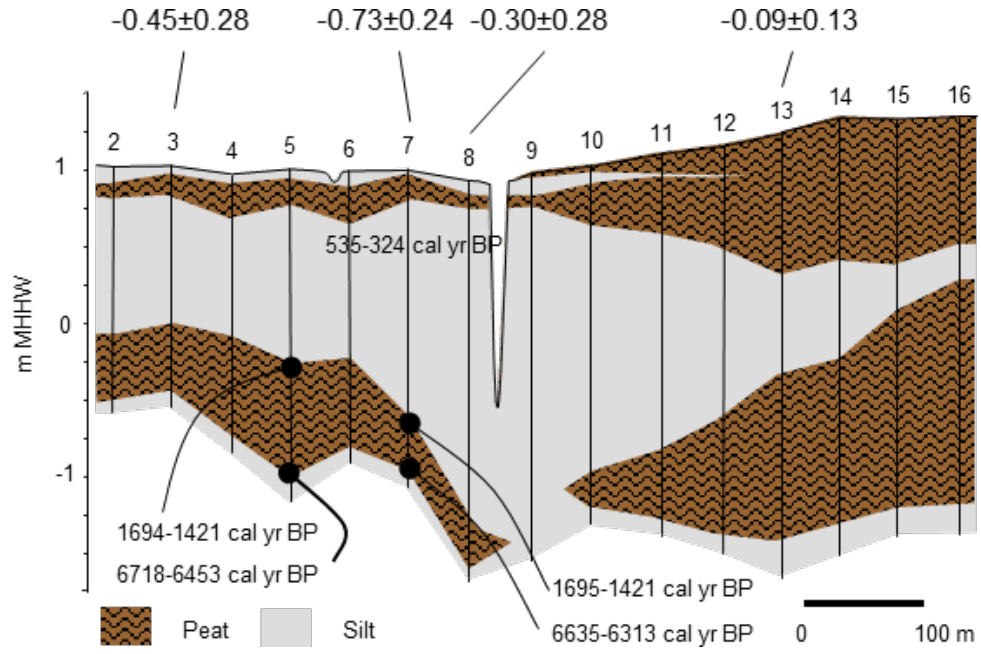

Figure 2.1. Marsh stratigraphy at Kenai, Alaska (from Hamilton & Shennan, 2005). There are two peat-silt couplets within the marsh stratigraphy. Lithostratigraphy of southern transect (vertical lines represent each core) and radiocarbon ages (black dots), shown as 95% probability range, cal. yr BP.

2.2. South-central Alaskan earthquakes

2.2.1. The 1964 CE earthquake

The 1964 CE earthquake was the second-largest earthquake on record and the largest in US history. The earthquake's focus occurred at a depth of approximately 25 km, with the epicentre located 125 km east of Anchorage. The earthquake caused significant vertical tectonic deformation over an area of 170,000 to 200,000 km^2, including the Kenai and Prince William Sound segments, as well as a second smaller rupture in the Kodiak segment of the megathrust (Plafker, 1965) (Figure 1.1). The earthquake also caused a cascade of hazards, including thousands of smaller aftershocks and hundreds of landslides, submarine slumps, and tsunamis (Brocher et al. 2014). Extensive evidence of peat-silt couplets has been documented across numerous marshes in south-central Alaska, with the most recent couplet formed during the 1964 CE earthquake. Litho- and bio- stratigraphic analysis of this peat-silt couplet has been the subject of considerable research since the earthquake, with the aim of enhancing understanding of subduction-zone earthquakes and the hazards they present (e.g. Shennan et al. 1999, Zong et al. 2003).

2.2.2. Seismic displacement associated with the 1964 CE earthquake

Co-seismic subsidence occurred over most of the Cook Inlet and Prince William Sound area, with a maximum subsidence of 2.3 m along the southwest coast of the Kenai Peninsula (Plafker, 1969). At Girdwood, Plafker (1969) documented 1.5 m of regional subsidence, with an additional 0.9 m of localized subsidence attributed to sediment compaction. Shennan and Hamilton (2006) used quantitative analysis of diatom assemblages across 3 sites to confirm whether a peat–silt couplet found in the top ~1 m of marsh sediment records relative land subsidence as well as to determine the amount and suddenness of the subsidence. Their findings indicated subsidence of up to 1.5 m at Girdwood, 0.7 m at Kenai, and 0.6 m at Ocean View. Additionally, Plafker (1969) reported 1.7 m of co-seismic subsidence during the 1964 CE earthquake on Kodiak Island.

Several researchers have also investigated the post-seismic uplift following the 1964 CE earthquake to gain insights into earthquake deformation cycles within Alaska (Suito and Freymueller (2009), Hamilton and Shennan (2005), Zweck et al. (2002)). Brown et al. (1977) combined levelling data carried out by the National Geodetic Survey between Anchorage and Whittier with an analysis of relative sea level measurements at Anchorage to indicate up to 0.55 m of land uplift in the decade following the 1964 CE earthquake, and 0.4 m of land uplift at Girdwood by 1975 CE. Building on this work, Cohen and Freymueller (1997) estimated an average uplift rate of 3 cm per year from 1964 to 1995 CE, although they also note a potential slowing of uplift rates over time. This is supported by Savage and Plafker (1991), who used

annual mean sea levels to suggest that 15 cm of uplift occurred around the Turnagain Arm in the first year after the 1964 CE event, followed by post-seismic relaxation.

In addition to the observed post-seismic uplift, Zong et al. (2003) investigated the occurrence of a preceding phase of gradual land subsidence prior to the 1964 CE earthquake. They proposed that Caesium (^{137}Cs) records indicate that subsidence began approximately 15 years before the 1964 CE earthquake. They used coastal marsh sediment sequences to identify changes in diatom and pollen assemblages, suggesting the change in microfossil assemblages provides evidence of 0.15 m pre-seismic land subsidence at Girdwood, followed by co-seismic subsidence of 1.8 m. However, evidence of pre-seismic land subsidence is limited, highlighting the need for further investigation into vertical land movements associated with earthquakes.

2.2.3. EQ1

Due to the limited duration of the instrumental record in recording earthquakes, changes in litho- and bio- stratigraphy have been employed to reconstruct the longer- term geological record of earthquakes (Pilarczyk et al. 2014; Shennan and Hamilton, 2006; Hamilton et al. 2005). Peat-silt couplets within coastal marsh sediments at various sites in south-central Alaska provide evidence of rapid subsidence and uplift, recording up to seven great earthquakes over the past 4,000 years. These inferred seismic events are comparable to the 1964 CE earthquake, with recurrence intervals ranging from 420 to 610 years (Shennan et al. 2014).

The peat-silt couplet associated with EQ1 is found within a bed of tree stumps now situated in the intertidal zone at Girdwood, which is indicative of co-seismic submergence. Karlstrom (1964) argued that several lines of evidence indicate that the coastal forest was submerged and buried because of sudden subsidence as opposed to a non-seismic relative sea level rise. Rubin and Suess (1955) first dated EQ1 between 1176 – 267 cal yr. BP, whilst Combellick and Reger (1994) suggest EQ1 occurred between 918-741 cal yr. BP. Hamilton and Shennan's (2005) analysis of the 1964 CE earthquake and EQ1 estimated the latter event at approximately 850 cal. yr BP. More recently, radiocarbon dating of tree stumps associated EQ1 by Barclay et al. (2024) suggest a date of 781–761 cal. yr BP, with a 95% confidence interval. They propose that the interseismic interval between the 1964 CE and EQ1 events was approximately 785 ± 10 years.

The EQ1 event caused 1.45 ± 0.34 m subsidence at Girdwood, comparable to that of the 1964 CE earthquake (Hamilton and Shennan, 2005). At Ocean View, 40 km to the west and close to the city of Anchorage, co-seismic subsidence is estimated at ~ 0.2 m (Shennan and Hamilton, 2006), although a later reconstruction using updated transfer function models gives an estimate of between 0.9 ± 0.4 and 1.5 ± 0.9 m of subsidence depending on which transfer function model is chosen (Watcham et al. 2013).

2.2.4. Previous earthquakes

At Girdwood, Shennan et al. (2014) analysed diatom assemblages across six peat–silt couplets to represent six phases of rapid co-seismic land subsidence prior to the 1964 CE earthquake. Each earthquake shows different spatial patterns of co-seismic subsidence when compared between sites. For example, Shennan et al. (2009) suggest that some earthquakes were limited to single segments, whilst others ruptured multiple segments of the megathrust. Shennan et al. (2014) also note a recurrence interval of 420-610 years for the earthquake deformation cycle in south-central Alaska. However, Barclay et al. (2024) identified an interseismic interval of 785 ± 10 years between the 1964 CE earthquake and the EQ1 event, indicating an unusually long interval compared to previous cycles. The spatial patterns of co-seismic activity between sites, as well as the irregularity in occurrence intervals underscores the need to better understand the behaviour of multiple great earthquakes but also smaller magnitude earthquakes during the late Holocene in south-central Alaska (Hamilton, 2003).

2.2.5. Rationale

2.2.5.1. Earthquake recurrence intervals

At Girdwood, peat-silt couplets within salt marsh sediments record seven great earthquakes in the last 4000 years (Shennan et al. 2008). Shennan et al. (2008) argue that no earthquake exhibits the same pattern of deformation as the 1964 CE earthquake, and some earthquakes documented within the Prince William Sound area may not have extended across the Kenai segment to the Kodiak segment (Figure 1.1). Current seismic hazard maps for Alaska model great earthquakes for the 1964 CE rupture zone, featuring a ≥ Mw 9 recurring every 650 years (Figure 2.2).

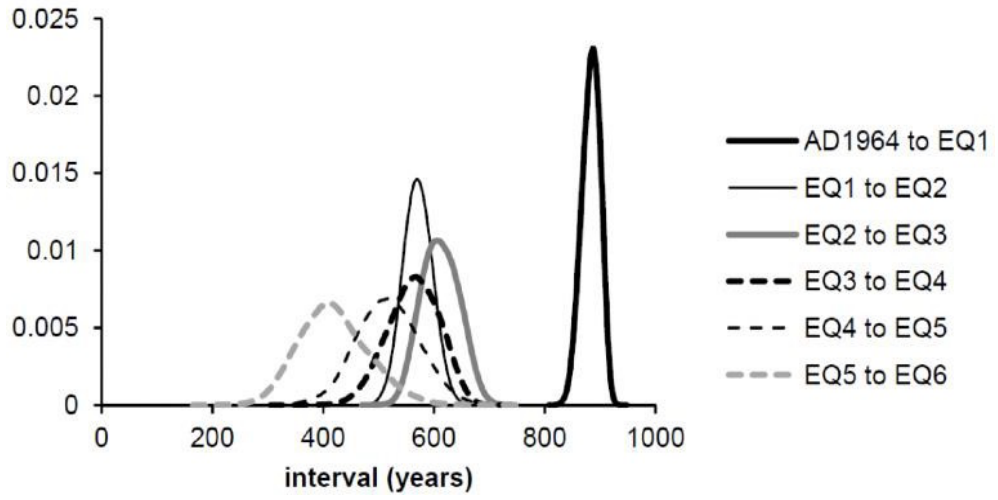

Figure 2.2. The interval period between great earthquakes in the Prince William Sound Segment. The interval between the 1964 CE and EQ1 is uncharacteristically long. Graph taken from Shennan et al. (2014).

However, as previously stated, Barclay et al. (2024) suggest an interseismic interval between the 1964 CE and EQ1 events as approximately 785 ± 10 years, revealing a temporal inconsistency in the paleoseismic record for the past 4,000 years. This irregular time interval may reflect the natural variability in the time-dependent behaviour of the megathrust. Conversely, it may instead relate to smaller earthquakes occurring in the Prince William Sound segment during the interseismic period, releasing stress on the megathrust. Whilst great earthquakes (≥ Mw 8) have been identified within palaeomarsh stratigraphic records, smaller earthquakes (Mw 7-7.9) have not yet been identified. Identifying smaller earthquakes is crucial for understanding their frequency, hazard risk, and significance in strain release (Brader et al. 2021). For instance, the November 2018 earthquake in Anchorage, Alaska, with a magnitude of 7.1, had widespread impacts across various sectors, causing an estimated $30 million in damages, including $10 million for pipe repairs and $10 million to repair public facilities. This highlights that Mw 7-7.9 earthquakes can have significant societal impacts, underscoring the urgent need to better understand the recurrence patterns of earthquakes within this magnitude range. Very few studies regarding the lower detection limit for subduction earthquakes have been carried out. Brader et al. (2021) was the first to investigsate high marsh wetlands as recorders of large megathrust earthquakes. They present evidence of land-level change resulting from the 2016 Mw 7.6 Chiloé earthquake to test criteria for the detection of low-level, < 0.1 m, co-seismic land-level change. However, no studies in south-central Alaska have investigated using high marsh sediments to better understand subsidence limits associated with Mw 7-7.9 earthquakes, highlighting the novelty of this study. Additionally, understanding the subsidence associated with Mw 7-7.9 earthquakes and their recurrence intervals is essential for integrating paleoseismic records into seismic hazard assessments.

2.3. Investigation of co-seismic sea-level change using microfossils

2.3.1. Environmental reconstructions using diatoms

Microfossils such as diatoms, foraminifera and ostracods have been widely used in paleaoenvironmental studies, and more specifically sea level studies (i.e. Guilbault et al. 1996; Hawkes et al. 2010; Shennan et al. 1999). Diatoms, the microfossil used within this project, are unicellular microscopic algae with a shell wall structure formed of opaline silica. They are valuable in reconstructing seismic activity within stratigraphic sequences found in coastal marsh sediments. Among the most precise quantitative reconstructions of earthquake-related land-level changes are those derived from diatom analysis (Pilarczyk et al. 2014). Diatoms serve as reliable proxies due to their sensitivity to subtle environmental changes. Their zonation across marsh surfaces, which is tied to tidal inundation and therefore marsh altitude, makes

them strong indicators of relative sea-level changes (Patterson et al. 2000). Marine diatoms, which prefer highly saline conditions, are more prominent in the tidal flats and lower marsh, whereas low salinity diatoms are found within the mid and high marsh elevations. Thus, diatom species inhabit a wide range of ecological niches across the environmental gradient with specific optimums and tolerances, from marine tidal flats to freshwater environments, which enable high-resolution reconstructions (Figure 2.3). They occur in substantial numbers in coastal sediments, making it possible to obtain statistically significant populations of the diatom species within core samples relative to the elevation (Birks, 1995). All paleoenvironmental studies follow the principles of uniformitarianism, which assumes that past environments resemble those of the present. Therefore, diatoms found in specific environments within the environmental gradient of a fossil core are assumed to have lived in similar tidal conditions to those species found at the marsh surface today.

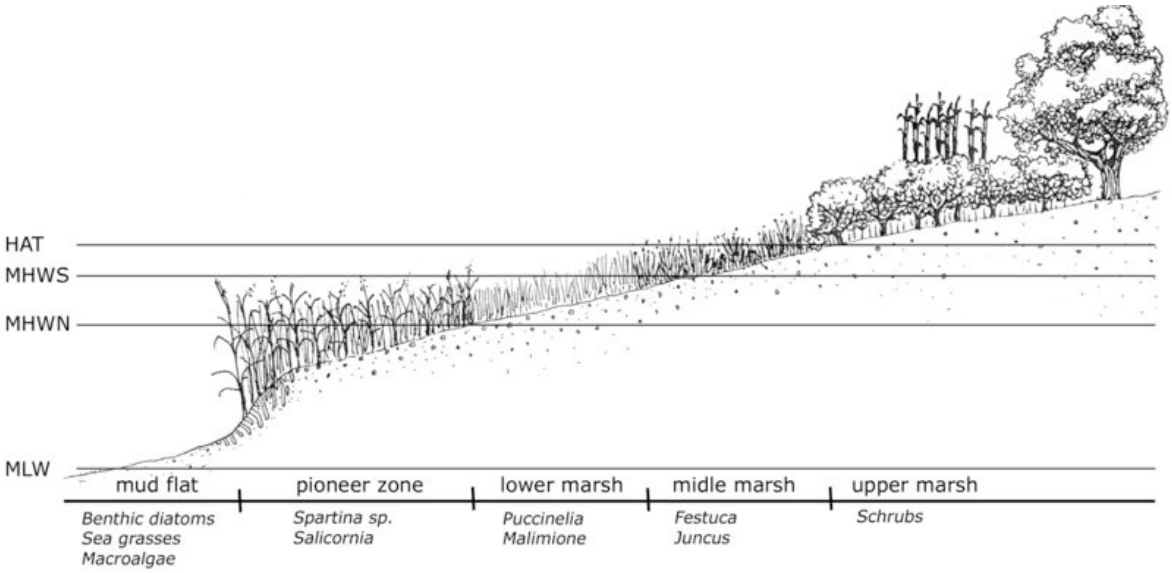

Figure 2.3. Schematic of the various zones in relation to elevation. Different abundances of diatom species are found in varying zones depending on their elevation optima and tolerance. Modified from Bertness et al. (2002).

2.3.2. Use of diatom-based transfer functions in paleoseismic studies

Early diatom research aimed at reconstructing co-seismic subsidence and uplift during large to great earthquakes often relied on semi-quantitative methods or broad distinctions between intertidal elevation zones (Hustedt and Aleem, 1951, Sancetta, 1979). These approaches, when combined with litho- stratigraphic data, provided land-level reconstructions with a precision of approximately ±0.5 m (Nelson et al. 1996). One method to overcome the ambiguity associated with semi-quantitative land-level reconstructions was the development of transfer functions (Juggins et al. 2015). Transfer functions were first established by Imbrie and Kipp (1971) to estimate sea surface temperatures from fossil foraminifera. Trasnfer functions utilise factor

analysis and multiple regression to develop equations to quantify the vertical relationship between a proxy (e.g., microfossils such as diatoms) and an environmental variable (i.e. tidal elevation) (Wright, 2011). Since Imbrie and Kipp (1971), transfer functions have since been widely adopted for quantitatively reconstructing relative sea-level changes linked to vertical land movements and relative sea level changes caused by earthquakes (e.g. Hamilton and Shennan 2005, Shennan and Hamilton 2006, Wang et al. 2013, Engelhart et al. 2013, Zong et al. 2003). Unlike qualitative methods, diatom transfer functions offer increased accuracy and precision in reconstructing relative sea-level changes since they they leverage abundance information of a range of diatom species, as opposed to single-species indicators, making them valuable in earthquake research (Kemp and Telford, 2015) . Regression analysis is used to develop a model from contemporary surface samples (the modern training set), which is then applied to fossil core assemblages to infer past marsh surface elevations (Kemp and Telford, 2015). Notable work in Alaskan palaeosiesmology includes Shennan et al. (2018), who utilises a modern training set of 356 samples from nine sites within south-central Alaska (Figure 2.4). This training set was first established by Hamilton and Shennan (2005) who included modern diatom data from three locations (Girdwood, Ocean View, Kenai). This was then further developed by Watcham et al. (2013) who added an additional four study sites (Alaganic Slough, Hartney Bay, Hope, Middlebay) as well as Shennan et al. (2016) who added one further study site (Beluga Slough). Shennan et al. (2018) published the most recent version of the modern training set, with the addition of Bear Trail Marsh, Shuyak Island. Shennan et al. (2018) argues that the creation of a large training set with samples collected from a wide range of marshes across ~1000 km of south-central Alaska allows the best fit between fossil and modern diatom assemblages.

2.3.3. Lithologically constrained transfer function models

Hamilton and Shennan (2005) show that sample specific reconstruction errors when using a transfer function can be reduced by using sediment lithology to constrain which samples to include in the modern training set – since model estimates become increasingly precise when smaller training sets from higher elevations are used (e.g. Table 2.1). They created a peat-only training set consisting of modern samples above a standardised water level index (SWLI) of 225, as peat only forms in Alaskan coastal marshes roughly above this elevation (equivalent to ~0.7-1 m above Mean Higher High Water (MHHW)) (SWLI is defined as a standardised elevation relative to MHHW and is the difference in elevation between MHHW and mean sea level (MSL) in order to accommodate for varying tidal ranges). They used this training set to reconstruct palaeomarsh surface elevations during interseismic periods in fossil peats. They

also created a training set using modern samples above 180 SWLI to reconstruct changes in fossil silts with rootlets, since vegetation does not grow on tidal flats below this elevation.

Importantly, Hamilton and Shennan (2005) did not attempt to reconstruct earthquake subsidence within peat units. Instead, the lithologically constrained transfer functions were used to infer relative sea level changes during interseismic periods and immediately prior to co-seismic subsidence. There is however potential to use lithologically-constrained transfer function models to identify and reconstruct earthquake subsidence at peat-peat contacts with greater precision than the longer gradient (the full range of SWLI values) transfer function models required at peat-silt contacts. This would allow reconstruction of smaller (Mw 7-7.9) events that may have occurred between great earthquakes over the past few thousand years.

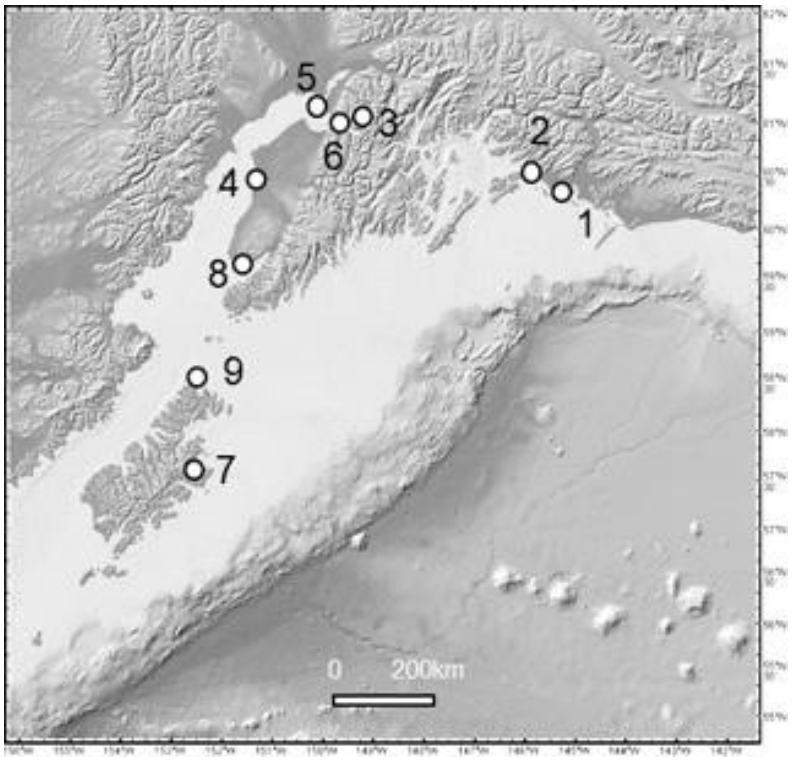

1. Alaganic Slough, Copper River Delta.
2. Hartney Bay, Cordova
3. Girdwood
4. Kenai
5. Ocean View, Anchorage
6. Hope
7. Middle Bay, Kodiak Island
8. Beluga Slough, Homer
9. Bear Trail Marsh, Shuyak Island

Figure 2.4. Location of nine sites within south-central Alaska where modern samples were collected in Shennan et al. (2018).

Scale, model and samples included	Number of samples	Bootstrapped R^2	Bootstrapped RMSEP
Subregional scale, Cook inlet model			
> 100 SWLI	166	0.77	13.73
> 180 SWLI	145	0.76	8.23
> 225 SWLI	74	0.73	3.11
Subregional scale, outer coast model			
> 100 SWLI	90	0.86	16.93
> 180 SWLI	61	0.81	13.03
> 225 SWLI	26	0.74	9.6
Regional scale, south central Alaska			
> 100 SWLI	225	0.67	17.26
> 180 SWLI	206	0.69	11.84
> 225 SWLI	100	0.75	6.24

Table 2.1. Modified table from Watcham et al. (2013) showing how the bootstrapped RMSEP values are reduced when the training sets are constrained to > 180 or > 225 SWLI units.

2.4. Research objectives

This research investigates the potential of peat-peat contacts to provide precise estimates of co-seismic land level changes at Ocean View, Anchorage and also aims to analyse the fossil peat record at Girdwood for any evidence of previously undetected earthquakes between the EQ1 and 1964 CE events at this location.

2.4.1. Identifying a known earthquake in a high marsh setting

Whilst up to seven great earthquakes have been recorded within marsh stratigraphy in the Prince William Sound, these earthquake signatures have not been investigated in high marsh environments, where they may instead be manifested as a peat-peat couplet. Hamilton and Shennan (2005) traced peat-silt couplets in their Coral Lane transect at Ocean View landward until the signature of the EQ1 event turned into a peat-peat couplet. However they did not sample this peat-peat couplet to investigate its bio- stratigraphy. Within vegetated marsh environments, from the pioneer marsh to the upper limit of tides, sediment lithology and diatom assemblages can provide increasingly more precise model estimates of elevation. Reconstruction model estimates are tidal range dependent. For example, scaled for Girdwood, the

root mean squared error of prediction increases from 0.16 m in peat-forming environments, to 0.36 m in vegetated intertidal marsh, to 0.52 m in unvegetated tidal flat (Shennan et al. 2016). This change in precision reflects the increasing strength of the environmental gradient as higher elevations are less frequently inundated by the tides, but also the shortening of the environmental gradient which limits the range of the tolerances of many diatom species. By identifying a known earthquake in a high marsh setting where it would be manifested as a peat-peat couplet, the lowest sample specific errors may be produced. This study will investigate whether litho- and bio- stratigraphic evidence of EQ1 is detectable in peat cores from Ocean View.

2.4.2. Detecting smaller earthquakes in coastal marshes

While understanding smaller (Mw 7-7.9) earthquakes is crucial, limited research has focused on determining the detection thresholds of such events. For instance, the pattern and magnitude of deformation associated with the November 2018 Anchorage earthquake, with a magnitude of 7.1, falls below current estimates for detection limits in coastal marshes. Although methods for identifying ≥ Mw 8 earthquakes, which produce vertical displacements of < 1 m across hundreds of kilometres, are well-established, the detection threshold for smaller earthquakes remains poorly understood (Briggs and Barnhart, 2017, Shennan et al. 2014, Shennan et al. 2016, Brader et al. 2021). Based on records from numerous subduction zones, Briggs and Barnhart (2017) suggest that subduction earthquakes < Mw 8 displace the coast by < 0.3 m and likely leave equivocal or no geologic evidence in coastal marshes. However, Shennan et al. (2016), through investigations at several sites across south-central Alaska, suggest that a detection limit as low as 0.1–0.2 m of co-seismic vertical change may be possible in certain settings. Characterising Mw 7-7.9 earthquakes with decimetre-scale (0.1 - 1 m) surface deformation would enable better assessment of their frequency, hazard risk, and role in strain accumulation and release cycles. At Girdwood, a peat layer is recorded by Shennan et al. (2016) to have formed 515-318 cal yr BP to 1964 CE, during interseimic uplift following EQ1. This peat layer will be analysed for evidence of smaller magnitude co- seismic events during this period.

2.5. Aims and research questions

The overarching research aims will be answered by addressing the following research questions:

1. *How do new high marsh modern diatom samples collected at Girdwood in 2023 compare to data in the existing modern training set described by Shennan et al. (2018) and high marsh diatoms regionally and globally?*

The modern diatom training set developed over ~20 years and summarised in Shennan et al. (2018) was created to provide quantitative palaeomarsh surface estimates across peat-silt contacts. Therefore, modern sampling is concentrated on low/mid marsh and tidal flat settings. For this project which focuses on reconstructing palaeomarsh surface elevation changes in high marsh environments, I needed to collect additional modern diatom data from higher elevations (above MHHW) up to the Highest Astronomical Tide (HAT) level) to add to the existing training set. This data is collected from Girdwood which has a large area of high marsh to the rear of the coastal lowland plain.

2. *Is EQ1 detectable within the high marsh stratigraphy at Ocean View, Anchorage?*

There is an existing record of EQ1 at Ocean View, Anchorage which suggests ~0.2 m of subsidence at the marsh front where there is a buried peat-silt contact (Shennan and Hamilton, 2006). This peat-silt contact transitions horizontally into a peat-peat contact towards the rear of the marsh. This project investigates the litho- and bio- stratigraphic signature of this known (already dated and magnitude estimated) great earthquake in the palaeo-high marsh at Ocean View.

3. *How does training set selection influence the magnitude of the reconstructed surface deformation?*

Shennan et al. (2018) used a diatom-based transfer function to quantitatively reconstruct elevation change across peat-silt contacts using the training set described above. When working in a peat-forming environment, does it make sense to include the whole elevation range of the training set which includes samples from low-intertidal mudflats?

This issue is tackled by this research question that looks at transfer function models with different environmental gradient lengths and the impact of this on reconstructed surface deformation.

4. *Using the EQ1 event in the high marsh at Ocean View as an analogue, is there any evidence of decimetre-scale surface deformation caused by additional earthquakes between the EQ1 and 1964 CE events in the high marsh stratigraphy at Girdwood, Upper Turnagain Arm?*

EQ1 caused 1.7 +/- 0.8 m of subsidence at Girdwood allowing the high marsh to flood and silt to be deposited (Hamilton and Shennan 2005, Watcham et al, 2013). Rapid initial and later slower post-seismic uplift returned the marsh to a peat-forming environment by at least 455 cal. yr BP (Hamilton and Shennan 2005). From then until the great earthquake in 1964 CE, the marsh stratigraphy is peat, with no visual evidence of sudden subsidence events (peat-silt

couplets). However, there may have been smaller earthquakes here which could be recorded in the peat lithology and diatom stratigraphy. This research question will investigate this using the peat-peat contact at Ocean View as a template for the litho- and bio- stratigraphic signature of earthquakes in high-marsh settings.

2.6. Site descriptions

2.6.1. Ocean View

The primary site for this project is Ocean View, a marsh located in the Ocean View neighbourhood of Anchorage, Alaska, along the southeastern edge of the city, and has a tidal range of 8 m (tidal data recorded at Anchorage (NOAA, 2024)) (Figure 2.5). Shennan and Hamilton (2006) identified evidence of three earthquakes at Ocean View, represented by peat-silt couplets, dated to 1964 CE, 900 cal. yr BP (EQ1), and 1500 cal yr BP. Based on mapping conducted during the summers of 1964 and 1965 CE, Plafker (1969) estimated 0.7–1.5 m of co-seismic subsidence at Ocean View during the 1964 CE earthquake, while more recent work by Shennan and Hamilton (2005) recorded 0.6 m of subsidence associated with the same event. Shennan and Hamilton (2005) also noted that, while EQ1 was not recorded at Kenai or Kasilof, the marsh at Ocean View showed evidence of 0.2 m of subsidence. Additionally, Hamilton et al. (2005) recorded multiple peat-silt couplets linked to multiple great earthquakes. In their Coral Lane transect, the peat-silt couplet associated with EQ1 was traced landward until it transitioned into a peat-peat couplet. For this project, a transect was taken at Ocean View at the location of Hamilton et al's. (2005) transect, to trace the transition from peat-silt into peat-peat couplet and to further investigate the nature of the peat-peat EQ1 contact in the high marsh.

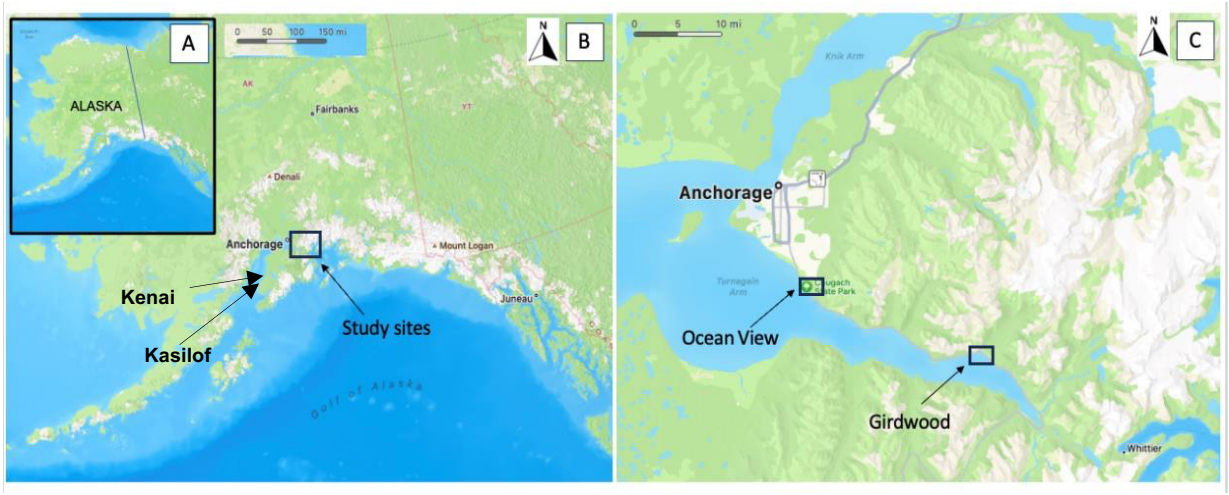

Figure 2.5. Location of Ocean View and Girdwood within the upper Turnagain arm, south-central Alaska.

2.6.2. Girdwood

A second site visited for this project is a small town which lies 65 km southeast of Anchorage along the upper Turnagain Arm; a narrow and elongated waterway that branches off from the Cook Inlet and stretches approximately 72 km long (Figure 2.5). There are several rivers within the Turnagain Arm, including Glacier Creek and Tidewater Slough which feed Girdwood marsh. The rivers discharging into the Turnagain Arm have an annual sediment discharge rate of 7 million m^3, but the main sediment source to the estary originates in areas seaward of the estuary (Bartsch-Winkler & Ovenshine, 1984). Nearly a metre of sediment (starting as marine-sourced silt but later replaced by organic sedimentation at the rear of the marsh) has been deposited on Girdwood marsh since the 1964 earthquake, indicating extremely rapid modern rates of sediment deposition in the intertidal zone. As the marsh is progressively uplifted due to post-seismic rebound, the rate of sediment deposition will slow as the marsh surface comes closer to the highest tide levels (Hamilton and Shennan 2005).

Girdwood has a tidal range of 9.2 m (data from Sunrise, 12 km west of Girdwood, (NOAA, 2024)). The marsh lies close to the zone of maximum subsidence during the 1964 CE earthquake and has extensive evidence of peat-silt couplets going back ~4000 years (Shennan and Hamilton, 2006). At low tide (approximately 1 m Mean Lower Low Water (MWWL)), extensive tidal flats are exposed, as well as a small cliff (~1 m) that separates the tidal flats from the marsh front. The marsh is intersected by the Seward Highway and the Alaska Railroad, beyond which it transitions into a more freshwater environment. Shennan et al. (1999) agure that their estimate of 1.7 m co-seismic subsidence during the 1964 CE earthquake led to a tidal flat environment slightly below MHHW, which allowed for the rapid colonisation of the accumulating silt by low marsh vegetation, which can be seen in the changes in sediment and vegetation since 1964 CE. Additionally, previous studies have identified several buried peat-silt couplets here, indicative of multiple earthquake cycles. Combellick (1997) attributed the first two peat-silt couplets to the 1964 CE earthquake and the EQ1 event, dating the latter to ~ 730 cal yr BP. I collected modern surface samples here to add to the existing diatom training set (Shennan et al. 2018) and to focus on coring the rear part of the marsh to reconstruct palaeomarsh surface elevation changes during the time period between the EQ1 and 1964 CE events when the marsh was a peat-forming environment.

Chapter 3: Methodology and Research Design

This chapter describes in detail the methods used to answer the proposed research questions. Research design includes collection of modern and fossil samples, lithological and microfossil analysis, transfer function development, Accelerator Mass Spectrometry (AMS) dating and additional supplementary methods including X-ray Fluorescence (XRF) and computed tomography (CT) core scanning.

3.1. Collection of modern surface samples at Girdwood

In September 2023, I collected 26 contemporary diatom samples across two transects from the tidal marsh at Girdwood to increase the sampling density of the upper part of the intertidal zone in the Alaska diatom training set described in Shennan et al. (2018) (Figure 3.1). The new samples were intended to enhance the likelihood of acquiring a reliable analogue within the modern training set when employed in reconstructions in the upper part of the intertidal zone. A transect of 15 samples was taken across a levee of Tidewater Slough in the middle part of the marsh, between the Seaward Highway and the Alaska railroad, and a transect of 11 samples was taken towards the back of the marsh, where the highest elevations are found. Whilst Hamilton (2003) suggest that the railroad causes ponding of freshwater, making Girdwood inappropriate for modern sample collection, my fossil cores are taken from ponded high marsh landward of the Alaskan railroad, and therefore I took modern samples from this location to capture this environment. For each sample, a 10x10x1 cm thick section of surface sediment was taken, the standard size used in diatom studies (Medoli and Scott, 1989).

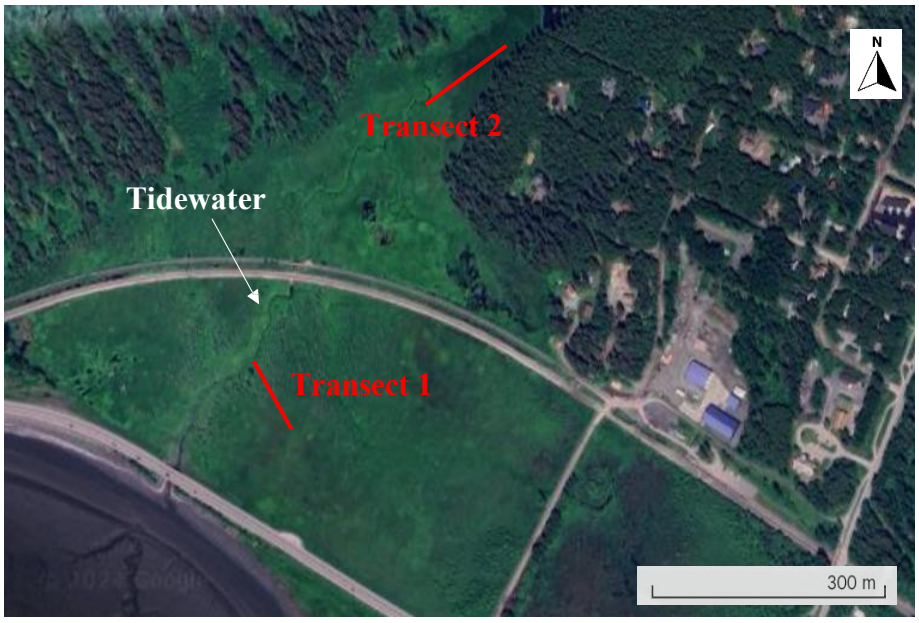

Figure 3.1. Location of the new modern samples taken across Girdwood marsh.

3.2. Marsh stratigraphy and collection of fossil cores at Girdwood and Ocean View

I collected four transects of cores (n= 29), with 24 cores at Girdwood and five cores at Ocean View. The aim was to describe the sub-surface stratigraphy and to trace peat-silt couplets from the 1964 CE earthquake and the EQ1 event into the upper part of the intertidal zone where co-seismic subsidence may be recorded as peat-peat couplets. Samples were then sealed in bags for transporting back to the UK where they were refrigerated until analysis.

At Ocean View, I was guided by previous coring at the same location (Coral Lane transect) by Hamilton et al. (2005), who had identified the presence of a peat-peat contact from EQ1 but had not sampled this horizon in the high marsh for laboratory analysis. Cores were extracted using a Russian corer since it encloses sediment within a chamber, which results in less contamination and mixing of layers (Janigian, 2018). The stratigraphy of the cores was recorded following the Troels-Smith (1955) classification to distinguish between silt, herbaceous 'turfa' peat, and sphagnum peat deposits (Nelson et al.1996). Five cores were taken, and a core thought to be the most representative of the marsh stratigraphy was identified as the sample core (Ocean View core 5 in figure 3.2). The core was transported back to Durham for laboratory analysis.

At Girdwood, I described the stratigraphy along three transects (24 cores). A main transect was taken from the marsh front landward to the highest elevations (Figure 3.2). Two additional transects were taken to the centre of the marsh from the steep hillslope at the edge of the marsh with the aim of showing lateral continuity in peat-peat couplets both across and landwards up marsh (Nelson et al. 1996). All cores were extracted using a Russian corer and described using the Troels-Smith (1955) classification. This allowed me to identify a sediment core thought to contain the most complete record (Girdwood core 1, blue transect in figure 3.2), which was then transported back to Durham and used as the focus for laboratory and statistical analysis.

Figure 3.2. Location of the coring transects taken at Ocean View and Girdwood marshes. Orange dot shows the location of the temporary benchmarks.

3.3. Surveying

The elevation of each modern sample and fossil cores from Girdwood was recorded by levelling from the core top or modern sample location to a temporary benchmark used in previous studies at Girdwood (defined as 100.00 m) using a standard level and staff. The height of this temporary benchmark had previously been tied to North American Vertical Datum (NAVD) using tidal loggers deployed in the Upper Turnagain Arm estuary close to Girdwood (Bender et al. 2015).

At Ocean View, a benchmark with a known height in NAVD from previous work (Hamilton et al. 2005) close to the Coral Lane transect was used to relate new cores on the Coral Lane transect to vertical datum.

To allow the new modern samples to be included in the existing Alaskan diatom training set (Shennan et al. 2018), I converted sample heights in m MHHW to Standardised Water Level Index (SWLI) using MSL and MHHW within the equation outlined by Hamilton and Shennan (2005):

$$\mathrm{SWLI_n} = \frac{100\ (h_n - h_{MSL})}{(h_{MHHW} - h_{MSL})} + 100$$

where $\mathrm{SWLI_n}$ is the standardised water level index for sample n, h_n the elevation of sample n (m) relative to MHHW, h_{MSL} the mean sea level elevation (m), and h_{MHHW} the elevation of MHHW (m). The equation produces a SWLI value for each modern sample with 100 representing MSL and 200 representing MHHW. The standardized water level index was employed as the environmental variable in the transfer functions for each modern sample, ultimately producing a reconstructed SWLI value for each fossil sample (Kemp and Telford, 2015).

3.4. Diatom preparation

Both the modern samples and fossil cores were analysed for diatoms to allow palaeomarsh surface elevation and relative sea level reconstructions. Within the fossil cores, sampling intervals varied from 1 cm to 4 cm, in order to obtain a higher resolution of sampling at stratigraphic contacts. Laboratory preparation of diatom samples followed standard procedure outlined by Palmer and Abbott (1986). For preparation, 1 cm^3 of sediment was treated with 20% hydrogen peroxide and heated to digest the organic material. This process was carried out several times until all the organic material was digested. After the organic matter was

removed, samples were centrifuged, and the hydrogen peroxide was decanted. Distilled water was then added, and the desired concentration was dried onto a cover slip at 55 degrees Celsius. These were subsequently mounted onto microscope slides using Naphrax. Slides were examined using a Leica DM LB2 microscope with an oil-immersion lens at x1000 magnification. To ensure statistical robustness and ecological accuracy, a minimum of 250 diatoms were counted for most samples (Fatela and Taborda, 2002). Diatom identification followed taxonomy by Van der Werff and Huls (1958-1974) and Hartley et al. (1996).

3.5. Cluster analysis

The paleoenvironmental software C2 version 1.8 (Juggins, 2018) was used to create diatom assemblage diagrams for both modern and fossil data. Developed by Hemphill- Haley (1993), diatoms species were plotted using the halobian classification system, which classifies species into five groups based on their salinity tolerances. Constrained clustering of the fossil diatom data within the R package 'Rioja V1.0-7' (Juggins, 2024) was used to produce dendrograms using CONISS (Grimm, 1987), which delineates zones based on the similarity of assemblages between adjacent samples. The number of zones was determined automatically in Rioja using a broken-stick model (Bennett, 1996).

3.6. Diatom Training Sets

3.6.1. Regional and local training sets

When generating diatom training sets, there has been debate regarding whether local or regional training sets are most appropriate. In south-central Alaskan marshes, diatoms often require large regional training sets due to their considerable species diversity across sites, in order to obtain a suitable analogue (Watcham et al. 2013). Watcham et al. (2013) also suggest that regional transfer functions are important for reconstructing relative sea level changes from older sediments (> 100 years old) because environmental conditions (and therefore diatom assemblages) become increasingly dissimilar to the local contemporary environment. In contrast, local training sets tend to produce reconstructions with reduced uncertainty because some less important environmental variables (e.g., grain size) are more consistent across samples at a single site, thereby minimizing the influence of factors other than elevation. Consequently, both local and regional training sets were developed to compare the influence on transfer function performance. The regional training set consists of modern samples across nine sites in south-central Alaska, whereas the local training set consists of samples from three sites within the Upper Turnagain Arm (Girdwood, Ocean View, Hope). The Upper Turnagain Arm

is a lower salinity estuary environment which may have different relationships between diatom species and elevations than sites at the fully marine open Pacific coast. As the fossil data being analysed is from this location, I wanted to explore whether training sets only from the Upper Turnagain Arm provide better modern analogues than when using the Full Alaskan training set. The 26 new modern samples from Girdwood were integrated with the Alaskan training set compiled by Shennan et al. (2018), which includes modern samples from an additional eight sites within south-central Alaska. The Full Alaskan training set used in transfer function development consists of 382 samples. The Upper Turnagain Arm training set consists of 126 samples.

3.6.2. Lithologically constrained training sets

Using the Full Alaskan and Upper Turnagain Arm framework described above, additional training sets were also developed that are constrained to specific elevations based on the lithology of the fossil core. Observations of the contemporary marsh indicate that peat does not form below an elevation of 225 SWLI, and vegetation does not live in environments below 180 SWLI (Hamilton and Shennan, 2005). As a result, Hamilton and Shennan (2005) suggests that if a fossil sample is formed of peat, it is appropriate to apply a transfer function using only those samples in the modern training set from elevations above 225 SWLI. Conversely, if a fossil sample contains silt with rootlets, a transfer function incorporating samples above 180 SWLI should be used. If the sample is composed entirely of silt, then the entire training set containing SWLI values below 180 SWLI must be used, as silt accumulates lower in the environmental gradient on the unvegetated tidal flat. However, instead of using the entire training set, Hamilton and Shennan (2005) suggests constraining the silt only transfer function to 100-250 SWLI, in order to reduce the low predictive capacities associated with the extreme low and high ends of the environmental gradient.

The Full Alaskan training set was subdivided by different SWLI-value ranges into smaller training sets; 100-250 SWLI units (352 samples) for reconstruction across peat-silt couplets, > 180 SWLI units (306 samples) for reconstruction in silts with rootlets, > 225 SWLI units (142 samples) for reconstruction within peat (Figure 3.3).

I further constrained the > 225 SWLI training set to 225-250 SWLI units (129 samples) because of the potential for the relationship between elevation and diatom assemblages to break down at the highest elevations; the possibility that Highest astronomical tide (HAT) is higher at Ocean View and Girdwood (our fossil sites) than at the Anchorage tide gauge (recorded as 217 SWLI), and also because samples in the training set become very widely spaced above 250 SWLI units.

Similar to the Full Alaskan training set, the Upper Turnagain Arm training set was also subdivided to 100-250 SWLI units (126 samples), > 180 SWLI units (116 samples) and > 225 SWLI units (47 samples). No samples within the Upper Turnagain Arm training set are found above 250 SWLI units, and thus only 1 training set was created for samples above > 225 SWLI (UTA > 225). In total, 9 training sets were produced using the Full Alaskan and Upper Turnagain Arm modern diatom data (Figure 3.3).

3.7. Transfer Function Development

The second stage in transfer function development involved empirically modelling the ecological response of diatom assemblages to elevation using the modern training sets (Kemp and Telford, 2015). This was done by modelling the predicted SWLI elevation for each sample within the training set based on their diatom assemblages. Five types of regression models were applied to the nine training sets described in section 2.6, resulting in 45 transfer function models. The five types of transfer function model used are Weighted averaging (WA) (Ter Braak and Prentice (1988)), Weighted Averaging- Partial Least Squares (WA-PLS), (Ter Braak and Juggins, 1993), Modern Analogue Technique (MAT) (Hutson 1979), Maximum Likelihood (ML) (Ter Braak and van Dame, 1989) and Locally Weighted - Weighted Averaging (LW-WA) (Juggins, 2001). As well as the five main models presented in the main body of this thesis, the performance of nine additional varitaions of these models are included in Appendix 1 and 2. They model species responses in different ways, therefore if down-core changes are driven by changes in elevation, I would expect trajectories from different models to be similar. I therefore developed multiple diatom-based transfer functions to test whether they consistently reconstruct palaeomarsh surface elevation changes.

3.8. Transfer Function Performance

The Root Mean Square Error of Prediction (RMSEP) and the coefficient of determination (R^2) was used to assess transfer function performance. The RMSEP is the square root of mean squared differences between measured tidal elevation (observed) and those predicted for the same sample by the transfer function under cross validation. The cross-validation method used to produce the RMSEP values is bootstrapping, since it also produces specific standard errors for individual fossil samples (Birks, 1995). A lower RMSEP value indicates better transfer function performance (Birks, 1995). The R^2 value reflects the proportion of variation in predicted tidal elevation based on the observed elevation of the same sample; a higher R^2 value suggests a strong predictive relationship between the observed and predicted SWLI values (Birks, 1995).

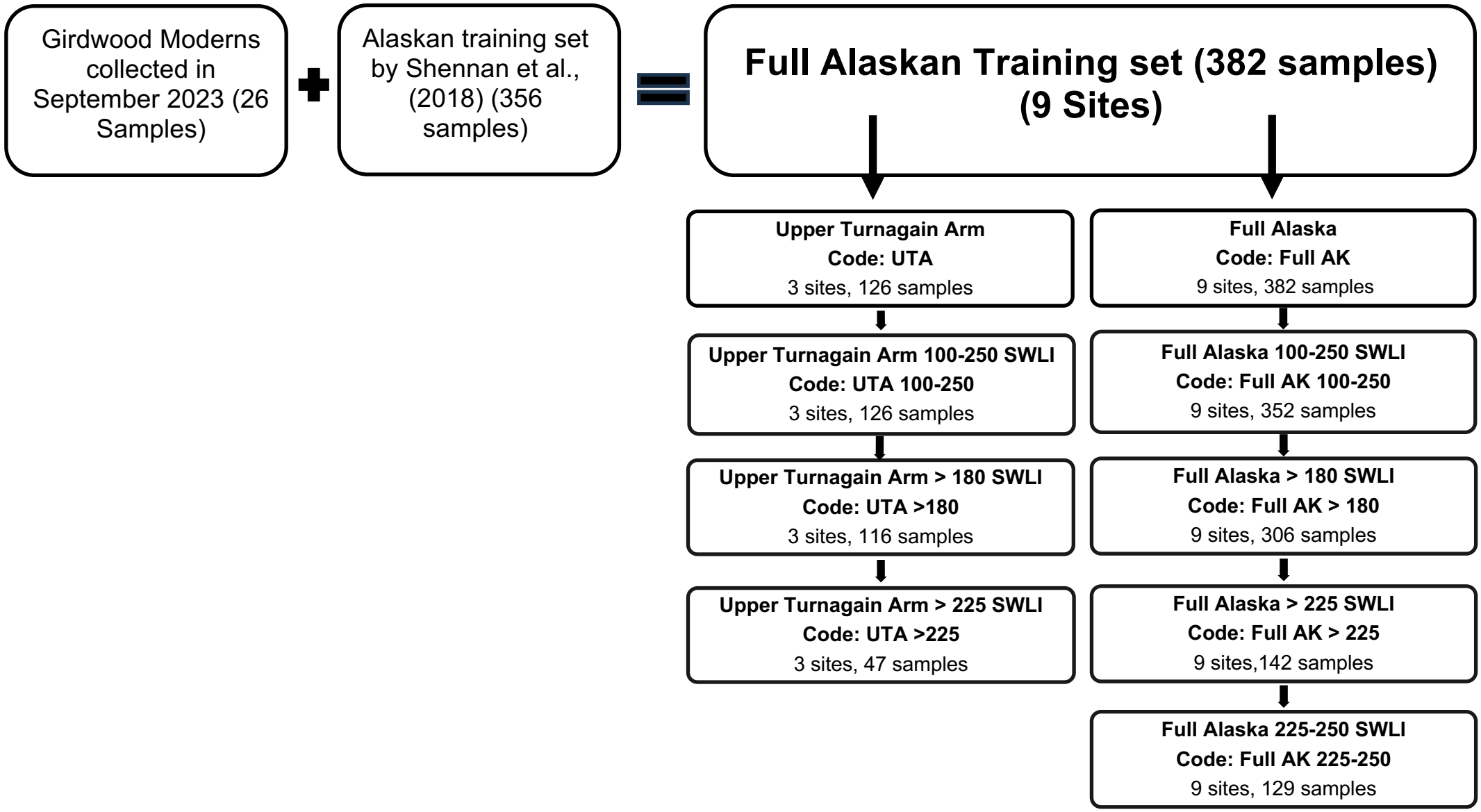

Figure 3.3. Flow chart of the various training sets derived from the Full Alaskan training set.

The transfer function performance (RMSEP and R^2) and the standard errors were compared between different transfer functions to assess the validity of each in turn.

3.9. Modern Analogue Technique

As well as a reconstruction technique, MAT was also employed to evaluate the ecological plausibility of reconstructions by assessing the similarity between modern and fossil samples. The 5th and 20th dissimilarity percentiles were used to classify 'good' and 'close' modern analogues (Hamilton et al. 2005, Watcham et al. 2013). Samples with dissimilarity below 5% were considered to have a good modern analogue, while those below 20% were deemed to have a close analogue. For each fossil sample, the closest modern analogue (minDC) was used to determine whether it fell within or outside these thresholds (As proposed by Kemp and Telford, (2015) and Watcham et al. (2013)). The number of modern analogues was used to determine and compare the validity of reconstructions produced by the various models.

3.10. Paleoenvironmental reconstruction

Each transfer function developed using the different modern training sets was applied to the fossil assemblages from Girdwood and Ocean View, producing outputs of reconstructed SWLI and a sample-specific estimate of SWLI uncertainty (indicative range). The reconstructed SWLI values were then converted back to palaeomarsh surface elevation in metres MHHW and relative sea level by reversing the equation in Section 3.3. This ultimately allowed for the quantification of changes in paleaomarsh surface elevation or relative sea level associated with seismic events (Shennan et al. 2005).

3.11. X-ray fluorescence (XRF)

X-ray fluorescence (XRF) spectrometry is a well-established and widely utilized technique for determining the major elemental compositions of sedimentary archives. XRF enables the non-destructive analysis of solid samples through X-ray radiation, allowing for the identification of various elements within sediment cores (Rothwell and Croudace, 2015). Various elements can be used to confirm the nature of the sediments within fossil cores. 20 elements were traced within the fossil core at Ocean View. However, only those elements which show noteworthy changes in composition were used to act as supplementary data to support the transfer function reconstructions. A GeoteK MSCL-S core scanner (Vatandoost et al. 2008) was used to obtain

the data at a 1mm resolution. The output is raw data containing the number of counts per second (CPS) of element- specific fluorescent X-ray energies received in the XRF instrument detector. The CPS for each element was plotted against core depth to see if there are any changes in sediment composition not visible in the litho- stratigraphy, as specific elements such as aluminium, calcium and silicon can serve as proxies for marine or terrestrial environments (Rothwell and Croudace, 2015). Additionally, XRF analysis may support the nature of changes in diatom assemblages that are not apparent from lithological observations, thus, it may provide supplementary evidence for previously unknown seismic events.

3.12. X-ray Radiographs and Computed Tomography (CT)

The fossil cores from Girdwood and Ocean View were analysed using a Geotek X-ray CT Core Imaging System (MSCL-XCT) to acquire linear digital X-ray images. Furthermore, computed tomographic (CT) reconstructions were also produced, allowing for the visualization of three-dimensional structures within the cores as well as high-resolution radiographs. Given the nature of the cores and the peat-peat contacts present, this technique was carried out to identify geological features that may not be identifiable through visual core logging (Brader et al. 2021). The raw images were then analysed using the Geotek image processing software, 'CT Quick View' and modified in the editing software 'Image J' (Rasband, 1997-2007).

3.13. Chronology

At Ocean View, AMS dating on 11 plant macrofossils was carried out at evenly spaced intervals through the sample core, or where a change in the litho- and bio- stratigraphy were observed, to produce a high-resolution age-depth model for the core. At Girdwood, Hamilton et al. (2005) had previously dated lithological changes during the interseismic period between the EQ1 event and the 1964 CE event from marsh- front cores. This meant I was able to interpolate ages to our sample core at Girdwood rather than needing to date new samples from this sediment sequence. Plant macrofossils including wood fragments were favoured for AMS dating over bulk organic matter, since macrofossils are more reliable as their carbon source is known, and not comprised of heterogeneous material that may have been formed at different times (Hatté and Jull, 2007). Macrofossils were dried in a 30-degrees Celsius oven, and those with a dry weight exceeding 0.02 grams were selected for analysis at the National Ocean Sciences Accelerator Mass Spectrometry Facility (NOSAMS). Pretreatment was carried out at NOSAMS using a series of acid-base-acid leaches to eliminate inorganic carbon. AMS measurements then determined the ratio of ^{14}C to ^{12}C in the sample relative to concurrently measured standard samples. Ages were

given by NOSAMS as conventional radiocarbon years BP (relative to AD 1950) and as a percentage of modern ^{14}C (Roberts et al. 2019).

I used the P_sequence model in the software Oxcal (P_sequence, v4.4, Bronk Ramsey, 2009a) to develop an age-depth model for the Ocean View core. This model uses the IntCal20 calibration curve (Reimer et al. 2020). A 'K' value of 0.1 was applied in the P_sequence model because a low K value assumes less variability in the calibration curve. Since the rate of deposition is unknown, the low K value allows the model to assume a relatively constant sedimentation rate over time (Ramsey, 2008).

Chapter 4: Results

4.1. Modern diatom data

4.1.1. Girdwood modern diatom assemblages

In September 2023, I collected 26 contemporary diatom samples across two transects to increase the sampling density of the upper part of the intertidal zone in the Alaskan diatom training set described in Shennan et al. (2018). The new samples were intended to improve analogues within the modern training set when employed in reconstructions in the upper part of the intertidal zone. Transect one spans SWLI values from 230.5 to 238, a 28.5 cm vertical range (Figure 4.1) and comes from the levee next to Tidewater Slough. The samples in this transect are dominated by mesohalobian, oligohalobian-halophile, and oligohalobian-indifferent diatom species, with high abundance taxa including *Nitzschia sigma*, *Navicula cari var cincta*, *Navicula brockmannii*, and *Navicula lagerstedtii* (Figure 4.2). The prevalence of these taxa indicates that the samples were collected from a marine-influenced environment, which is consistent with transect one being taken from within the tidal marsh at Girdwood. There is little variability in assemblages across the elevation gradient sampled. Transect two spans SWLI values from 228

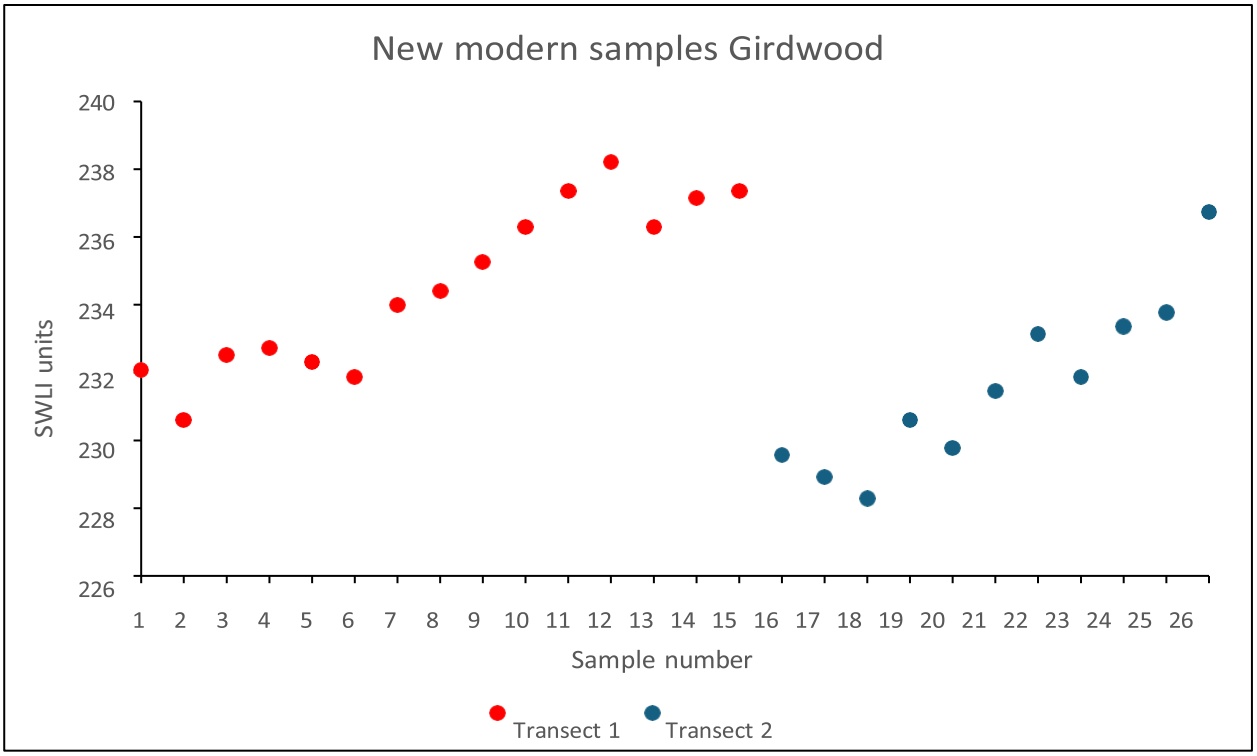

Figure 4.1. SWLI values of the new modern samples taken across Girdwood marsh.

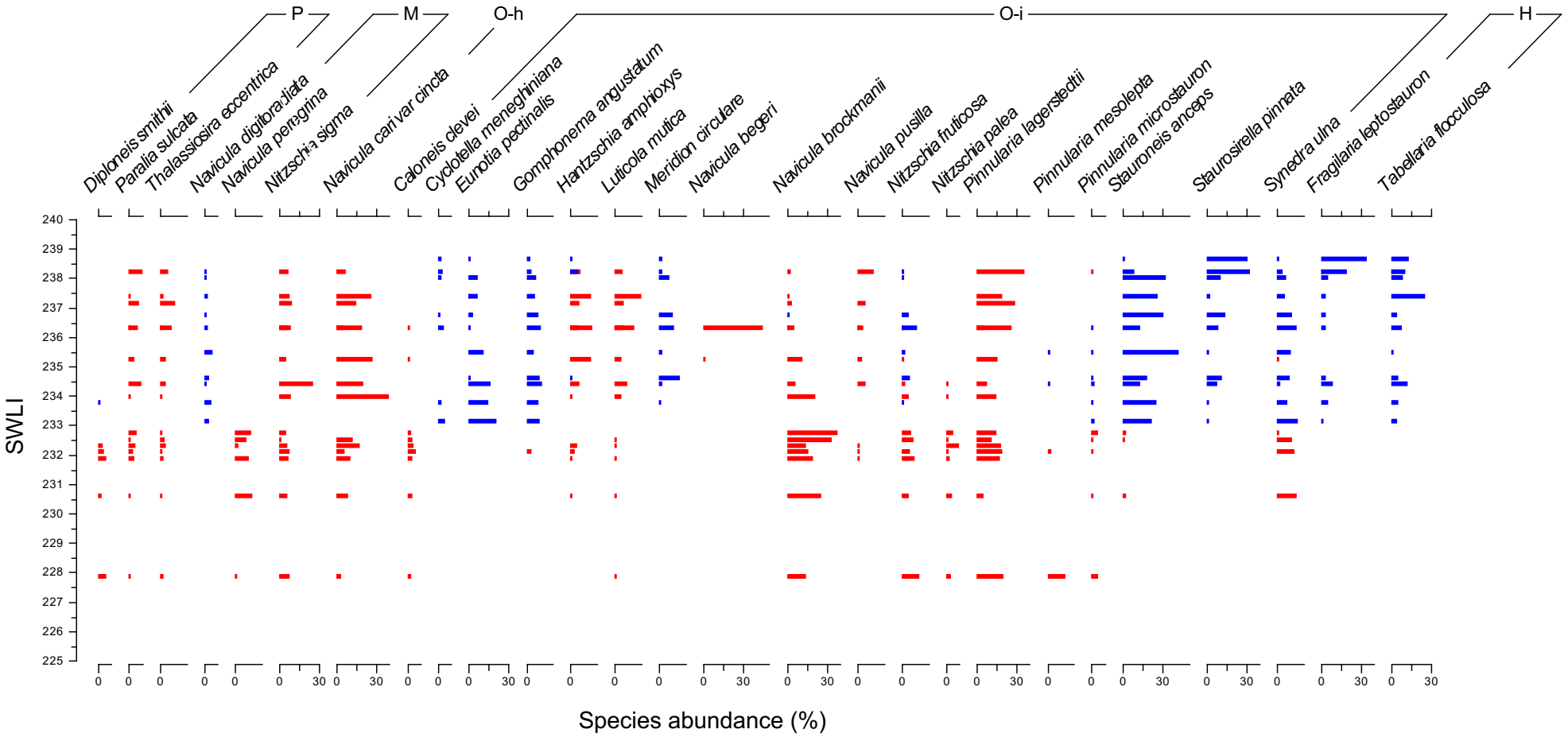

Figure 4.2. New contemporary diatom data from Girdwood marsh (> 5%). Transect one = Red. Transect two = Blue. Summary salinity classes: Polyhalobian (P), Mesohalobian (M), Oligohalobian-halophile (O-h), Oligohalobian-indifferent (O-i), Halophobe (H).

to 236, a 30.4 cm vertical range (Figure 4.1) and was taken from the rear of the marsh immediately downstream of a beaver dam across Tidewater Slough. Transect two is characterized by oligohalobian-halophile and halophobe species such as *Stauroneis anceps*, *Fragilaria leptostauron*, and *Tabellaria flocculosa* (Figure 4.2). The diatom data suggests a fresher environment compared to the samples from Transect one despite similar elevations. Transect two was taken from a more waterlogged high marsh environment which may be more influenced by freshwater flooding from nearby Tidewater Slough than Transect one. Given that these transects display differing assemblages at comparable SWLI values, the variation in species taxa is likely attributable to localised environmental conditions including freshwater input and waterlogging as well as differences in elevation.

4.1.2. Full Alaskan training set modern diatom assemblages

I added the 26 contemporary samples collected from Girdwood in September 2023 to an Alaskan training set containing 356 samples developed over 20 years from nine sites in south-central Alaska and summarised in Shennan et al. (2018) (map of study sites in Shennan et al. (2018) is shown in figure 2.4). Samples collected from Girdwood in September 2023 (26 samples) occupy a small part of the overall training set SWLI range and sit towards the upper end of the existing sampled elevation range (Figure 4.3). 92% of samples in the full training set are situated within SWLI values from 100 to 250 (352 samples). The relationship between increasing SWLI elevation and halobian classification is nuanced, with most species having broad elevation tolerances. For example, species such as *Navicula cari var. cincta* span the majority of SWLI values sampled in the training set. Nonetheless, as SWLI values increase, there is a slight increase in the number of oligohalobian-indifferent and halophobe species, illustrating the impact of changing elevation on species abundance.

4.1.3. Upper Turnagain Arm modern diatom assemblages

The 26 modern samples collected in September 2023 from Girdwood were also added to an existing subset of the Full Alaskan training set, which consists of 100 contemporary samples acquired by Shennan et al. (2018) from three sites within the Upper Turnagain arm of the Cook Inlet, Alaska; Ocean View, Girdwood, and Hope (Figure 4.4). The Upper Turnagain Arm is a lower salinity estuarine environment which may have different relationships between diatom species and elevations than sites at the fully marine (higher salinity) open Pacific coast. As the fossil data being analysed is from this location, I wanted to explore whether training sets only from this region provide comparable modern analogues compared to the Full Alaskan training set. The combined Upper Turnagain Arm training set consists of 126 samples with corresponding SWLI values ranging from 135 to 240 SWLI (Figure 4.4). New samples

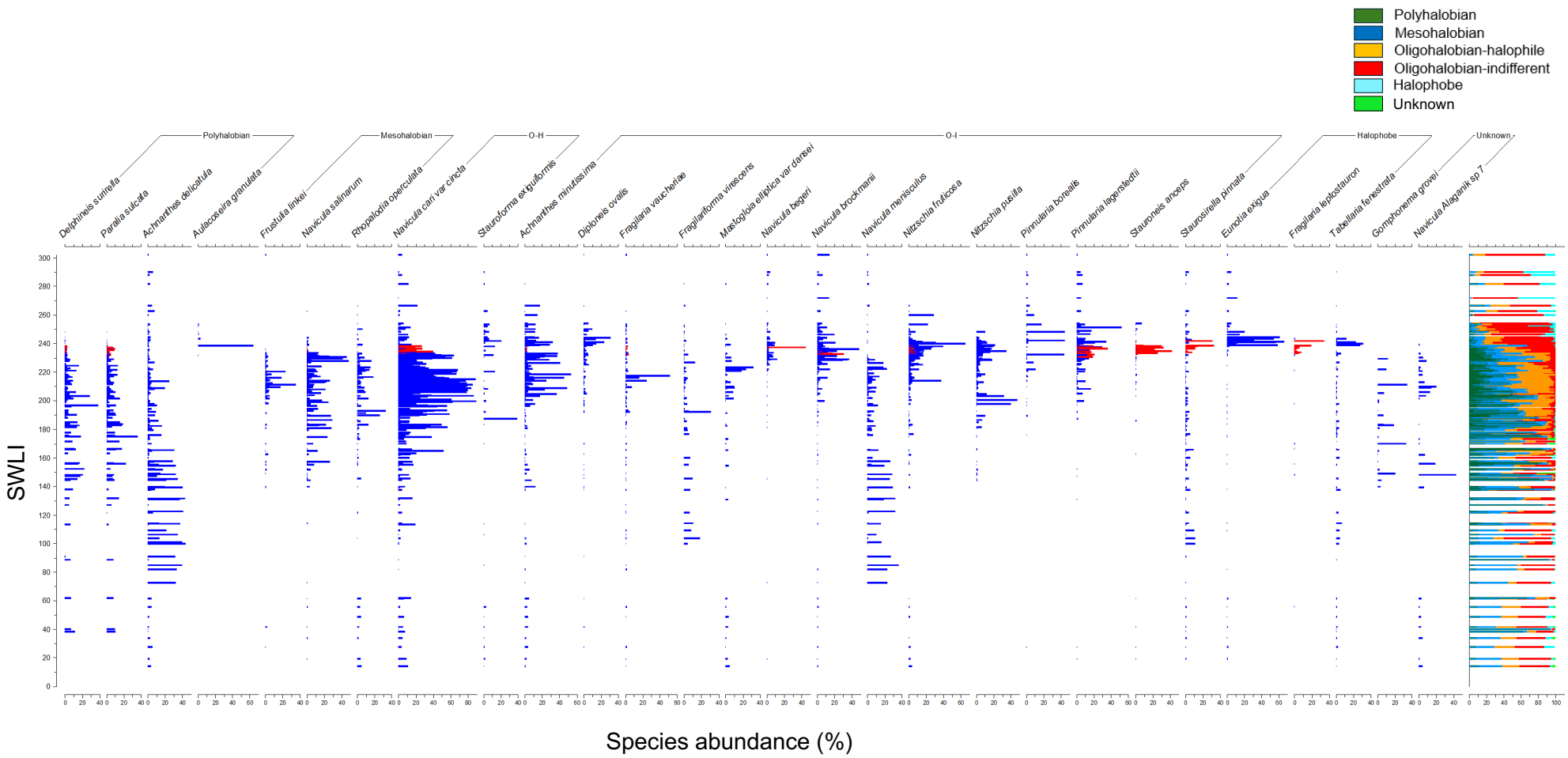

Figure 4.3. Contemporary diatom assemblages taken from nine sites within the Cook inlet (> 30%). New samples taken from Girdwood in 2023 are highlighted in red. Summary salinity classes: Polyhalobian (P), Mesohalobian (M), Oligohalobian-halophile (O-h), Oligohalobian-indifferent (O-i), Halophobe (H).

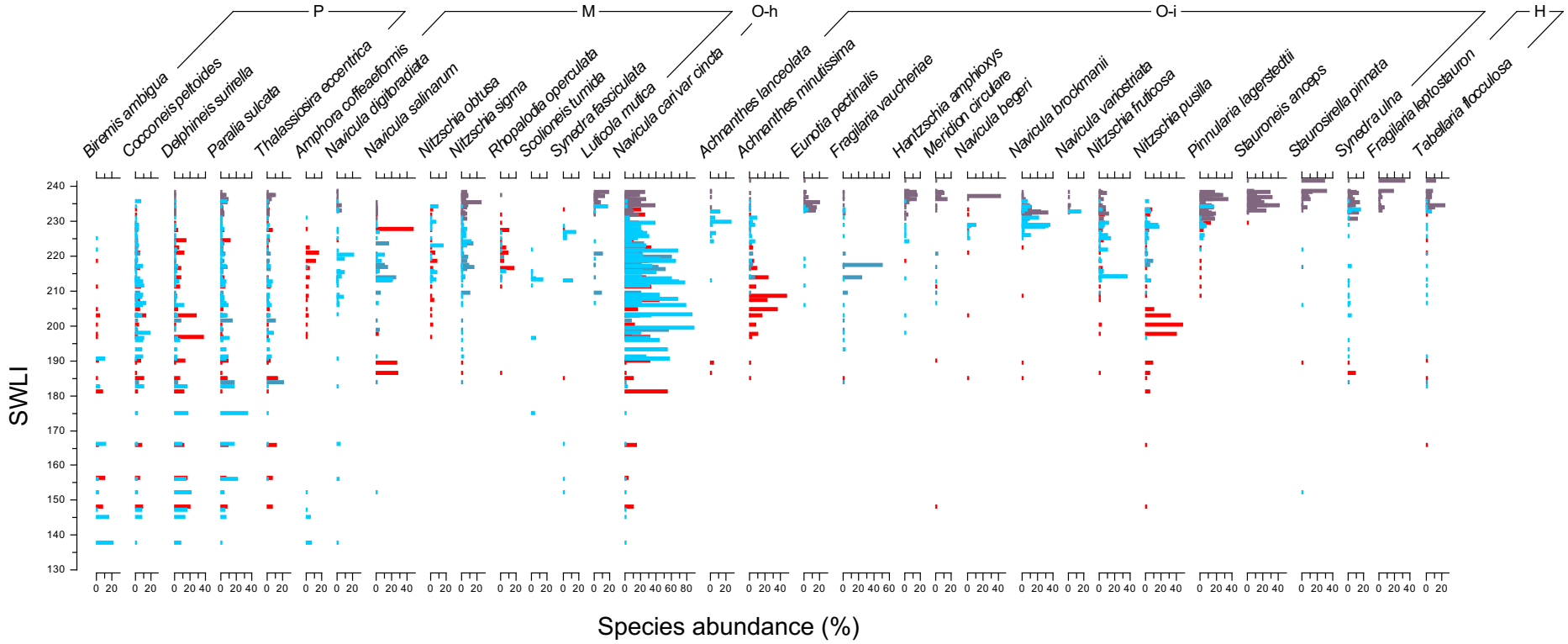

Figure 4.4. Contemporary diatom assemblages from the Upper Turnagain Arm of the Cook Inlet. New Girdwood samples are purple, older Girdwood samples are red, Hope samples are dark blue and Ocean View samples are light blue (> 15%).

collected from Girdwood predominantly correspond to the highest SWLI values, with nearly all halophobe species being exclusively from the new Girdwood samples, whereas the older Girdwood samples cover the full range of SWLI values (new samples marked in purple on Figure 4.4). Samples from Hope are primarily located in the mid-range of SWLI values (180–210), where polyhalobian and mesohalobian diatoms are prevalent. Notable species at Hope include *Navicula salinarum*, *Thalassiosira eccentrica*, and *Navicula cari var. cincta*, which have the highest abundances. Samples from Ocean View are dominated by *Navicula cari var. cincta* and polyhalobian species such as *Delphineis surirella*, *Cocconeis peltiodes*, and *Paralia sulcata*. The lowest elevations are predominantly occupied by polyhalobian species, with *Biremis ambigua*, *Cocconeis peltoides*, and *Delphineis surirella* exhibiting the highest abundances. Halophobe and oligohalobian-indifferent species are exclusively found at the highest SWLI values whilst polyhalobian species are exclusively found at the lower SWLI values, suggesting that elevation is likely the primary factor influencing species distributions in this training set.

4.2. Transfer function testing

4.2.1. Full Alaskan training sets testing

Five transfer functions were run using the Full Alaskan training set and the Full Alaskan subdivided training sets (100-250, > 180, > 225 and 225-250 SWLI) (see Appendix 1). The transfer functions are WA, WA-LPS, MAT, ML and LW-WA.

For the > 225 SWLI training set (Full AK > 225) (Figure 4.5d), low R^2 values in model development are partly attributable to samples being located very high in the intertidal zone, where freshwater input or standing water bodies may disrupt the relationship between diatom taxa and elevation. Highest astronomical tide is recorded at Anchorage at 217 SWLI (NOAA, 2024). Thus, I decided to further constrain the Full AK > 225 SWLI training set to 225-250 SWLI (Full AK 225-250) because of the potential for the relationship between elevation and diatom assemblages to break down at the highest elevations; the possibility that HAT is higher at Ocean View and Girdwood (our fossil sites) than at the Anchorage tide gauge, and also because samples in the training set become very widely spaced above 250 SWLI units (Figure 4.5d). I therefore decided to use the Full AK 225-250 training set (Figure 4.5e) instead of the Full AK > 225 SWLI training set in all subsequent model comparisons. This gave a total of 25 model runs. For simplicity, only the regression model performances for WAPLS component 2 are shown in the main body of the thesis as this model generally provides the highest overall model performance of the five models tested using each training set in turn. However, all model results can be found within Appendix 1.

4.2.2. Full Alaskan training set results

When the Full Alaskan training set is used in the transfer function, models produce the highest RMSEP values ranging between 22.8 and 38.1 SWLI. Using subdivisions of the Full Alaskan training set reduces the RMSEP values. When the training set is constrained to SWLI values between 100-250 (Full AK 100-250) (Figure 4.5b) the RMSEP values range between 13.9 - 26.16 SWLI (Table 4.1). The training set constrained to SWLI values above 180 (Full AK > 180) (Figure 4.5c) produce smaller RMSEP values than the Full AK 100-250 SWLI training set, with RMSEP for the five models ranging between 10.2 and 15.2 SWLI units. The Full AK 225-250 SWLI (Figure 4.5e) training set produces the smallest RMSEP, ranging between 3.9 - 5 SWLI. The WAPLS model with the Full AK 100-250 SWLI training set demonstrates the highest performance in terms of R^2, with the WAPLS component 2 model achieving a value of 0.82, indicating a strong relationship between observed and predicted SWLI values. The Full AK > 180 SWLI training set produces an R^2 value of 0.77 for WAPLS component 2 whilst the training set with SWLI constraints of 225-250 SWLI produces the lowest R^2 value of 0.5 for WAPLS component 2. The residuals for each training set show a slightly negative trend. However, this reduces as the training set size also reduces, most likely due to extreme ends of the environment gradient being included within the larger training sets (i.e. < 100 SWLI). These training sets include more of the environmental gradient, including elevations representing marsh tidal flats, which are associated with high amoutns of sediment mixing.

4.2.3. Upper Turnagain Arm training set

Similar to the Full Alaska training set, the Upper Turnagain Arm training set was also subdivided by different SWLI-value ranges into smaller training sets. Whilst two additional training sets were created within the Full Alaskan training set for samples > 225 and 225-250 SWLI units, no samples within the Upper Turnagain Arm training set are found above 250 SWLI units. Therefore, only 1 training set was created for the Upper Turnagain Arm for samples above > 225 SWLI (UTA > 225). The smaller training sets were also used to develop five different transfer function models, giving a total of 20 model runs for the Upper Turnagain Arm.

For simplicity again, only the regression model performances for WAPLS component 2 are shown as this model provides the highest model performance of the five models tested using each training set in turn (Figure 4.6 and Table 4.1).

4.2.4. Upper Turnagain arm training set results

Figure 4.6 shows the WAPLS component 2 performance for the Upper Turnagain Arm models using four different-sized training sets. The performance statistics for the other transfer function

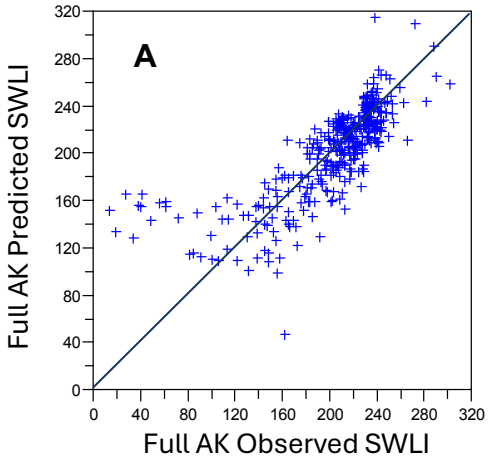
A
Full AK Predicted SWLI
Full AK Observed SWLI
0
40
80
120
160
200
240
280
320

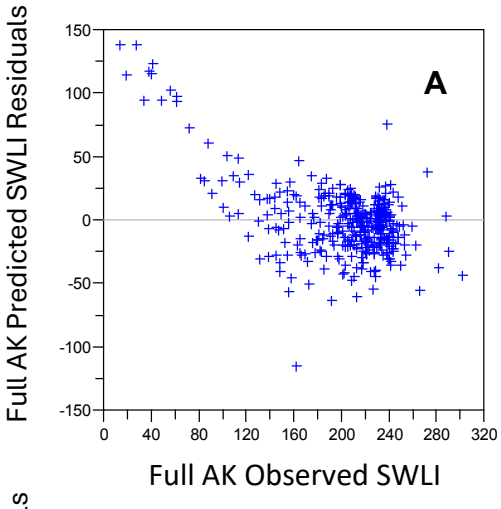
A
Full AK Predicted SWLI Residuals
Full AK Observed SWLI
150
100
50
0
-50
-100
-150
0
40
80
120
160
200
240
280
320

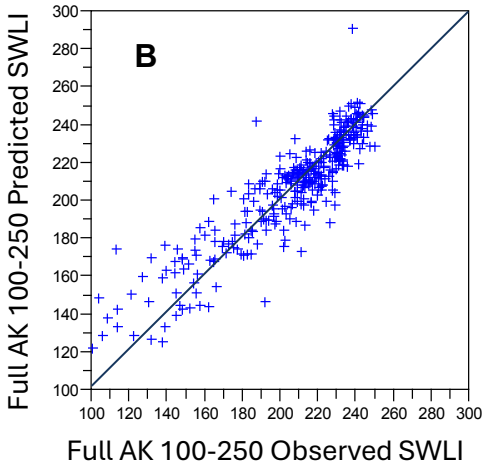
B
Full AK 100-250 Predicted SWLI
Full AK 100-250 Observed SWLI
300
280
260
240
220
200
180
160
140
120
100
100
120
140
160
180
200
220
240
260
280
300

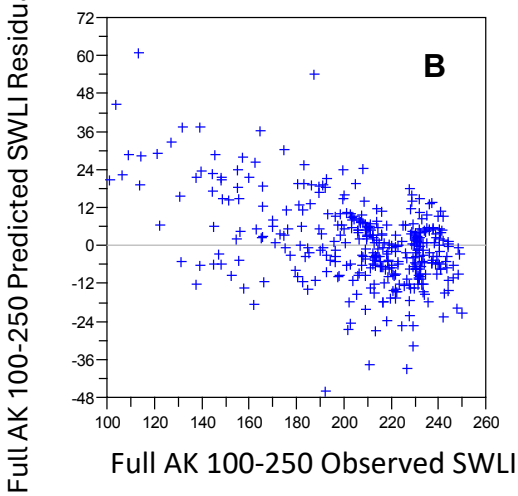
B
Full AK 100-250 Predicted SWLI Residuals
Full AK 100-250 Observed SWLI
72
60
48
36
24
12
0
-12
-24
-36
-48
100
120
140
160
180
200
220
240
260

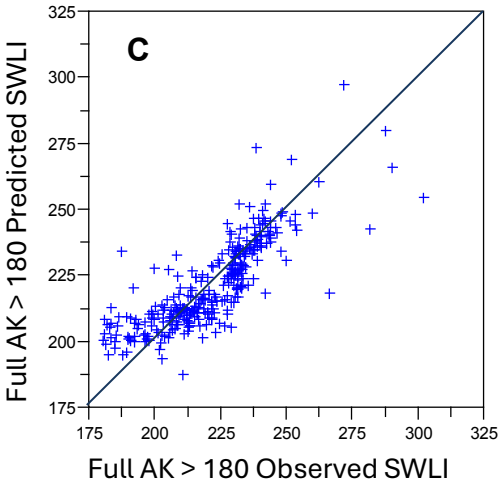
C
Full AK > 180 Predicted SWLI
Full AK > 180 Observed SWLI
325
300
275
250
225
200
175
175
200
225
250
275
300
325

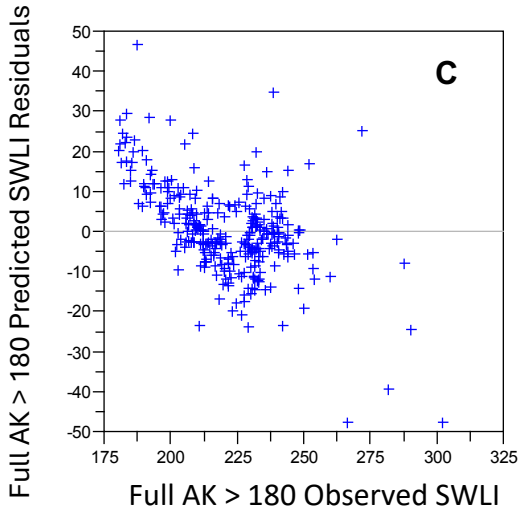
C
Full AK > 180 Predicted SWLI Residuals
Full AK > 180 Observed SWLI
50
40
30
20
10
0
-10
-20
-30
-40
-50
175
200
225
250
275
300
325

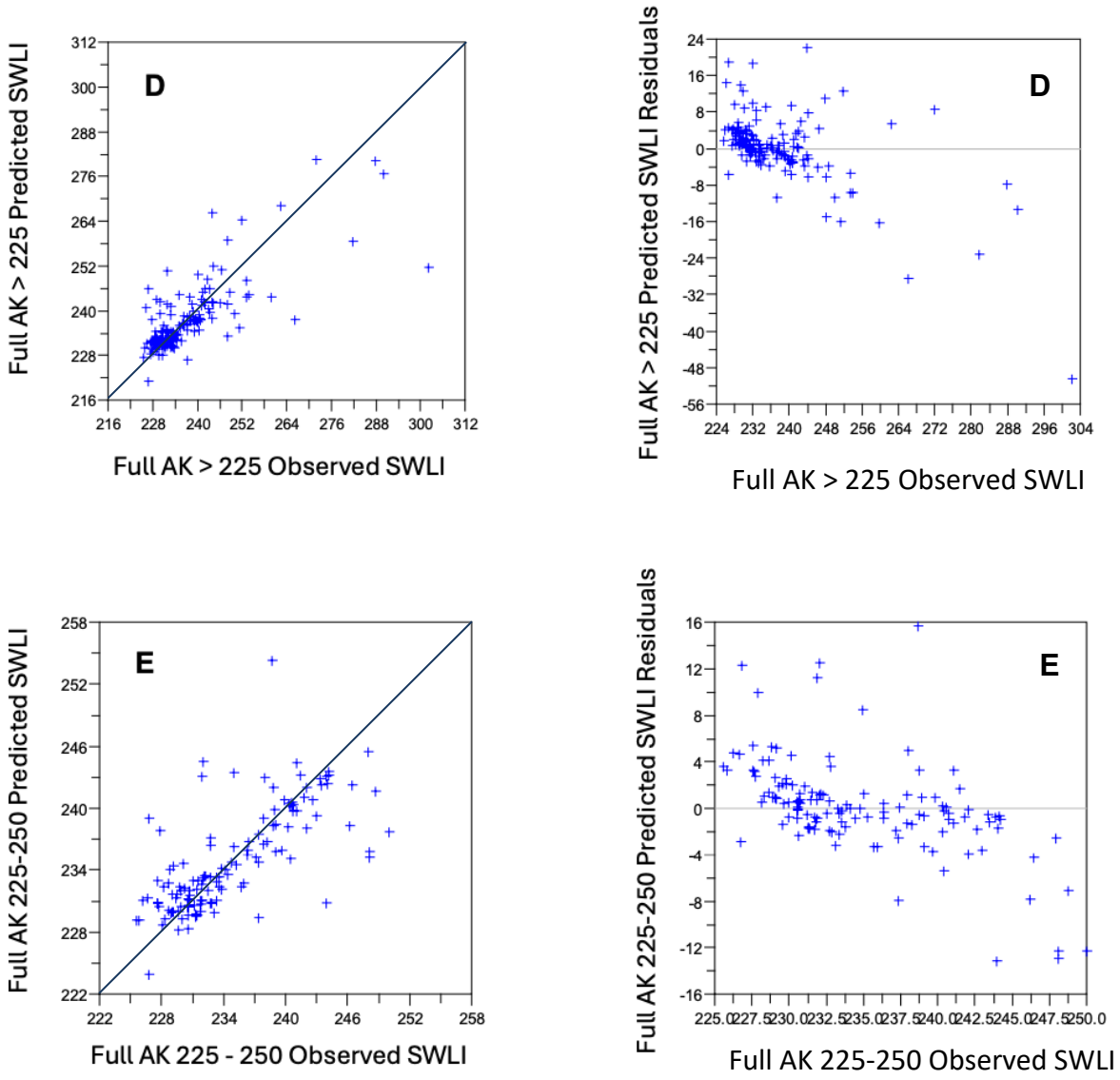

Figure 4.5. Observed vs predicted SWLI values and residuals for the Full Alaskan training sets using the WAPLS component 2 transfer function model. As the training sets size decreases so does the RMSEP. Letters are used to refer to indervidual graphs in text.

Training set	R2	RMSEP
Full AK	0.61	29.82
Full AK 100-250 SWLI	0.82	14.12
Full AK > 180 SWLI	0.67	11.84
Full AK > 225 SWLI	0.57	8.79
Full AK 225-250 SWLI	0.51	4.52
UTA	0.84	9.47
UTA 100-250 SWLI	0.84	9.47
UTA > 180 SWLI	0.72	8.16
UTA > 225 SWLI	0.48	2.54

Table 4.1. Transfer function model performance for the WAPLS component 2 model using 7 lithologically constrained training sets.

models can be found in Appendix 2. The models derived from the Upper Turnagain Arm training sets generally yield lower RMSEP values compared to those using the Full Alaskan training sets. The WAPLS model Full Upper Turnagain Arm training set (Full UTA) produces RMSEP values between 8.4 and 12.7 SWLI (Figure 4.6a) (RMSEP values for the Upper Turnagain Arm training set can be found in Appendix 1). Since all the samples within the Full Upper Turnagain Arm training set lie between 135-240 SWLI, the UTA 100-250 SWLI training set contains the same number of samples as the Full UTA training set (Figure 4.6b). The training set constrained to SWLI values above 180 (UTA > 180) (Figure 4.6c) produces results with lower RMSEP ranging from 7.2 to 10.5 SWLI. The WAPLS UTA > 225 SWLI training set has the smallest RMSEP values, ranging between 2.5 and 3.1 SWLI (Figure 4.6d). The R^2 values across all models are comparable to those found when using the Full Alaskan training set, indicating similar relationships between observed and predicted SWLI values. For each training set, the WA-PLS and the LW-WA models perform best. Using the subdivided training sets, although RMSEP values decrease as the number of samples in the training set decreases, R^2 values also decrease. Consquently, whilst the WA-PLS model provides the overall highest model performance (and is thus presented in the main body of the thesis), no single transfer function consistently outperforms others, and model selection should also consider ecological plausibility when comparing modern and fossil data. Ecological plausibility refers to how

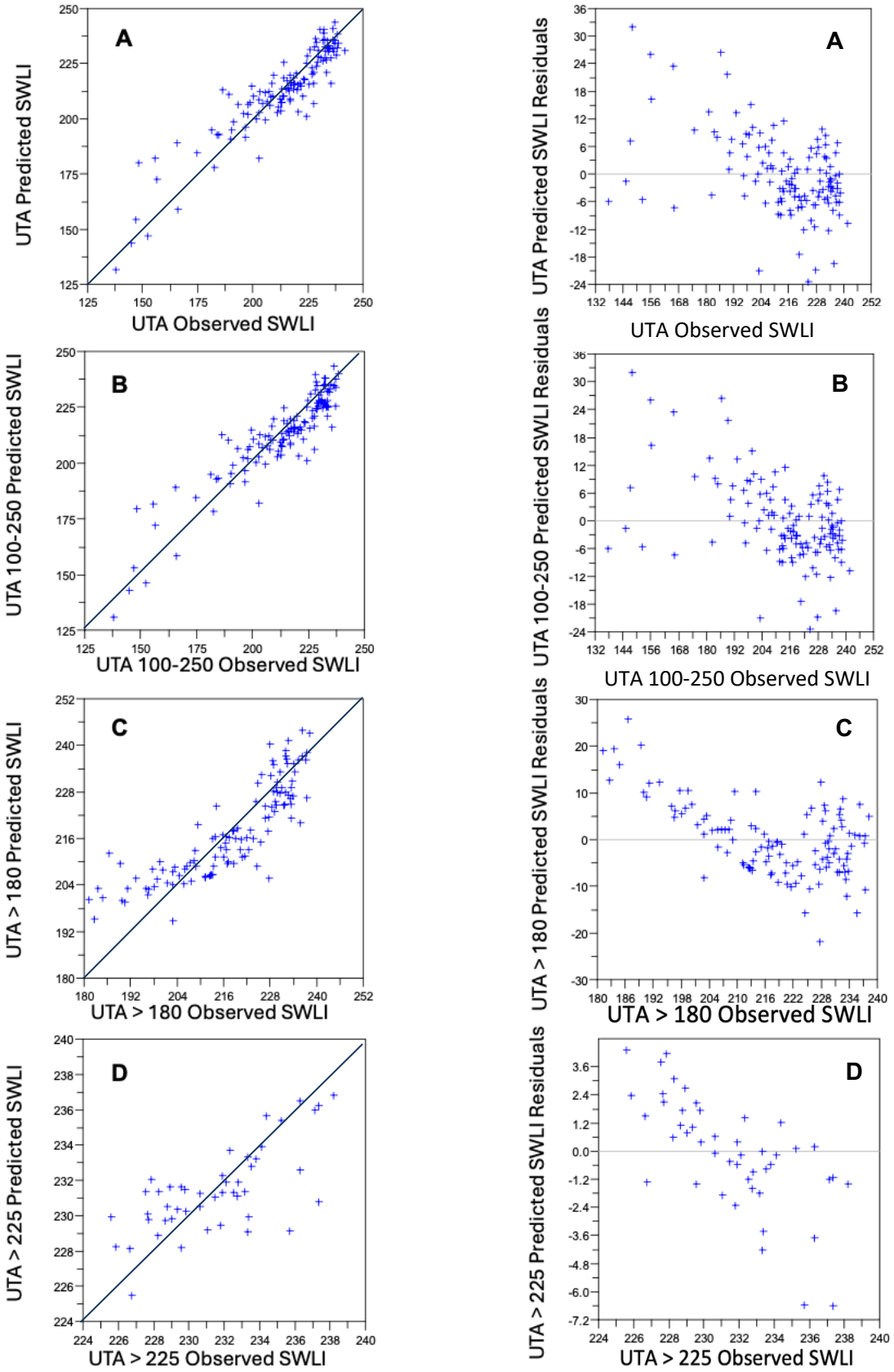

Figure 4.6. Observed vs predicted SWLI values and residuals for the Upper Turnagain Arm training sets using the WAPLS component 2 transfer function model. Letters are used to refer to indervidual graphs in text.

plausible it is that diatoms would be found within a certain environment. i.e. if we know *Delphineis surirella* is found within marine environments, but it reconstructs at very high elevations, it is not ecologically plausible. We can only know this (and must take this into account) after the reconstructions have been produced.

4.3. Fossil Results from Ocean View

4.3.1. Ocean View core litho- stratigraphy

Ocean View provides laterally extensive evidence of a peat-silt couplet from the ~1500 cal yr BP earthquake, a peat-silt and peat-peat couplet associated with EQ1, and a peat-silt couplet associated with the 1964 CE earthquake. The location of the cores taken within the Coral Lane transect by Hamilton et al. (2005) at Ocean View guided the location of new cores, as they had traced peat-silt couplets landward until they transitioned into peat-peat couplets. Figure 4.7 presents the stratigraphy of cores taken in September 2023 alongside those from the older Coral Lane transect (Hamilton et al. 2005). In three of the cores taken at Ocean View in September 2023, a peat-silt couplet is evident at -1 to -1.4 m MHHW (1.9 to 2.3 m below the surface). This same peat-silt couplet was identified in all the Coral Lane transect cores and was dated by Hamilton et al. (2005) to 1520-1333 cal yr BP. The silt layer transitions up core into a unit of turfa peat that gradually transitions into sphagnum peat, associated with post-seismic uplift following co-seismic subsidence. In all the cores I described in September 2023, this sphagnum peat is overlain by turfa peat, marked by a sharp boundary at –0.3 to -0.45 m MHHW (132 cm below the sediment surface in the sample core). This peat-peat couplet can be traced horizontally seaward where it is represented as a peat-silt contact (beyond the seaward limit of cores in Figure 4.7) and was dated by Hamilton et al. (2005) to 946-739 cal yr BP. More recently, Barclay et al. (2024) used tree ring data from Girdwood to date this contact representing EQ1 to 785 ± 10 cal yr BP. The turfa layer above the peat-peat contact is eventually overlain by a silt layer at approximately 60 cm below the surface in the sample core, also marked by a sharp boundary. This peat-silt couplet seen in all cores on the transect formed during co-seismic subsidence associated with the 1964 CE earthquake (Hamilton et al. 2005).

4.3.2. Ocean View core XRF and CT results

The stratigraphy at Ocean View reveals subtle transitions between Sphagnum and Turfa peat between the ~1500 BP event and the 1964 CE event. To better understand changes within the peat layers, the sample core was analysed using X-ray fluorescence (XRF) scanning (Figure 4.8). High concentrations of elements such as aluminium, silicon, calcium, and iron were observed at depths of approximately 190-210 cm. High levels of aluminium are typically

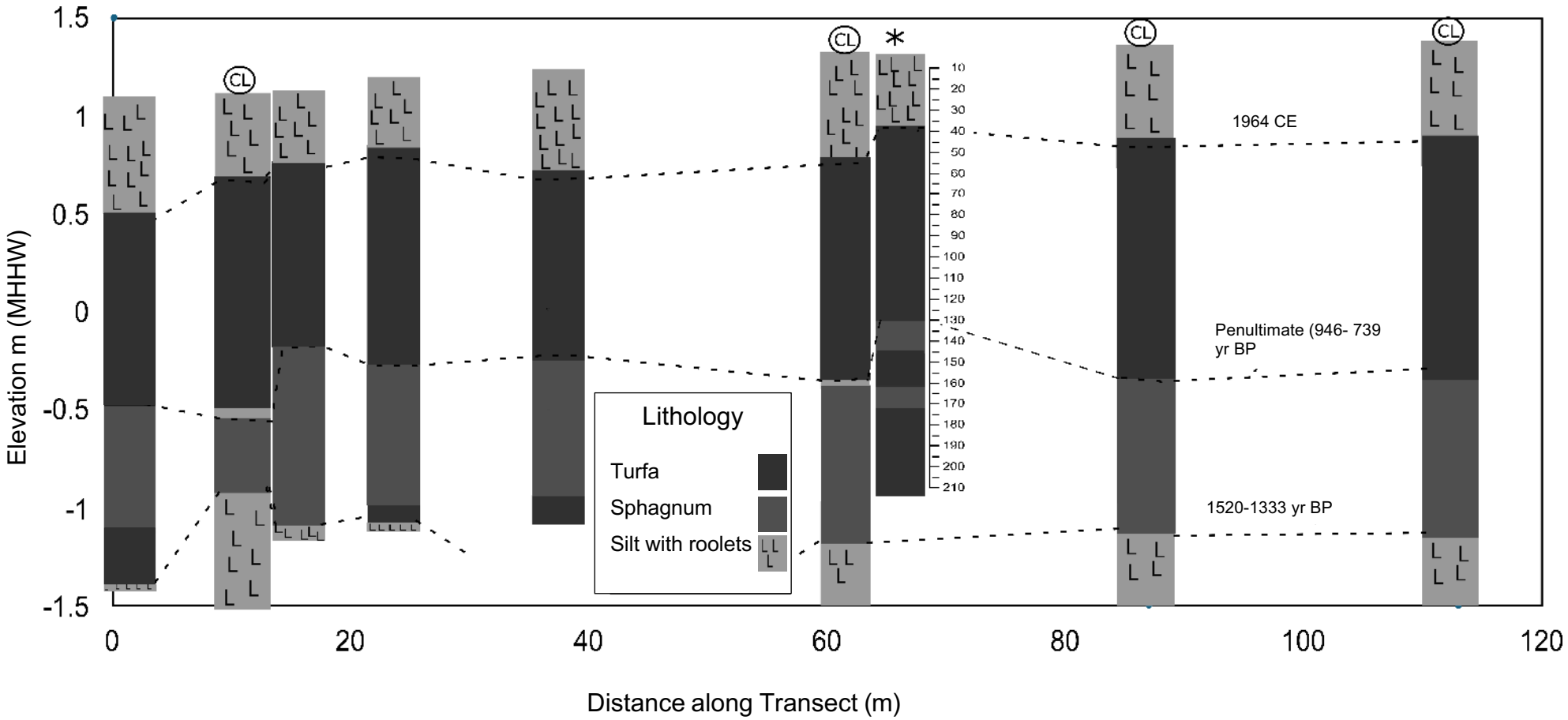

Figure 4.7. Stratigraphy of cores collected at Ocean View in September 2023, alongside cores from the Coral Lane transect obtained by Hamilton et al. (2005). The transect is seaward to landward left to right across the page. The cores labelled with "CL" correspond to those from the older Coral Lane transect. The remaining cores are those taken in September 2023. Dashed lines represent interpreted correlation of units across merged transect, where events ages are directly from Hamilton et al. (2005). The star indicates the fossil core used for diatom analysis and palaeomarsh surface reconstructions (Core 5 in figure 3.2). Varying 'L' sizes hold no significance in diagram.

associated with fresh water terrestrial environments, as aluminium is a major component of clay minerals and silicate rocks. Similarly, iron and silicon are also indicative of fresh water terrestrial environments, with iron linked to sediments from weathered rocks and silicon related to the presence of quartz and silicate minerals (Rothwell and Croudace, 2015). Based on the high concentrations of iron, aluminium, and silicon between 190-210 cm, it can be inferred that thesediments at these depths were deposited in a freshwater terrestrial environment. As the core depth decreases, the concentrations of these elements diminish, suggesting a shift towards a more marine-influenced environment. Notably, high concentrations of sulphur and calcium are also present at 190-210 cm, which, Rothwell and Croudace (2015) suggest is associated with a marine environment due to the presence of biogenic carbonate minerals such as calcite and aragonite from shells and coral fragments. However, calcium can also be influenced by limestone or carbonate-rich terrestrial sources, so its presence does not necessarily contradict the inference of a terrestrial depositional environment. Throughout the rest of the core, the elemental composition shows low levels of terrestrial elements, indicating a stronger marine influence. A minor peak in aluminium and silicon at approximately 138 cm suggests a slight terrestrial influence. The variations in elemental composition do not correspond with visible changes in the stratigraphy, and thus do not provide additional corroborating evidence for the shifts in depositional environment inferred from the stratigraphy.

Additionally, variations in the CT results in Figure 4.8 show subtle variations in the density of the sediment core, representing differences in sediment composition throughout the core. A subtle change in density can be identified at 150 cm, where the sediment shows a higher density, potentially representative of a silt layer. Peat has a lower density than silt, due to its organic composition and high water content, whereas silt can be associated with higher densities, since it is composed of fine mineral material. A second layer can also be seen at approximately 160 cm, which coincides with a peak in calcium, indicating a marine influenced environment. Additionally, as the core depth increases, the high concentrations of sulphur and calcium present at 190-210 cm coincide with a section of higher density seen within the CT scan, reinforcing the argument for a more marine influenced environment at the bottom of the core. No notable changes in density are identified at the peat – peat contact at 132 cm.

4.3.3. Ocean View bio- stratigraphy

Sampling intervals for diatom analysis varied according to the stratigraphy of the core. For the majority of the core, samples were collected at 4 cm intervals to accommodate time constraints while ensuring comprehensive coverage. However, at depths where notable changes in diatom assemblages were observed, the sampling frequency was increased to 1 cm intervals (16-25 cm,

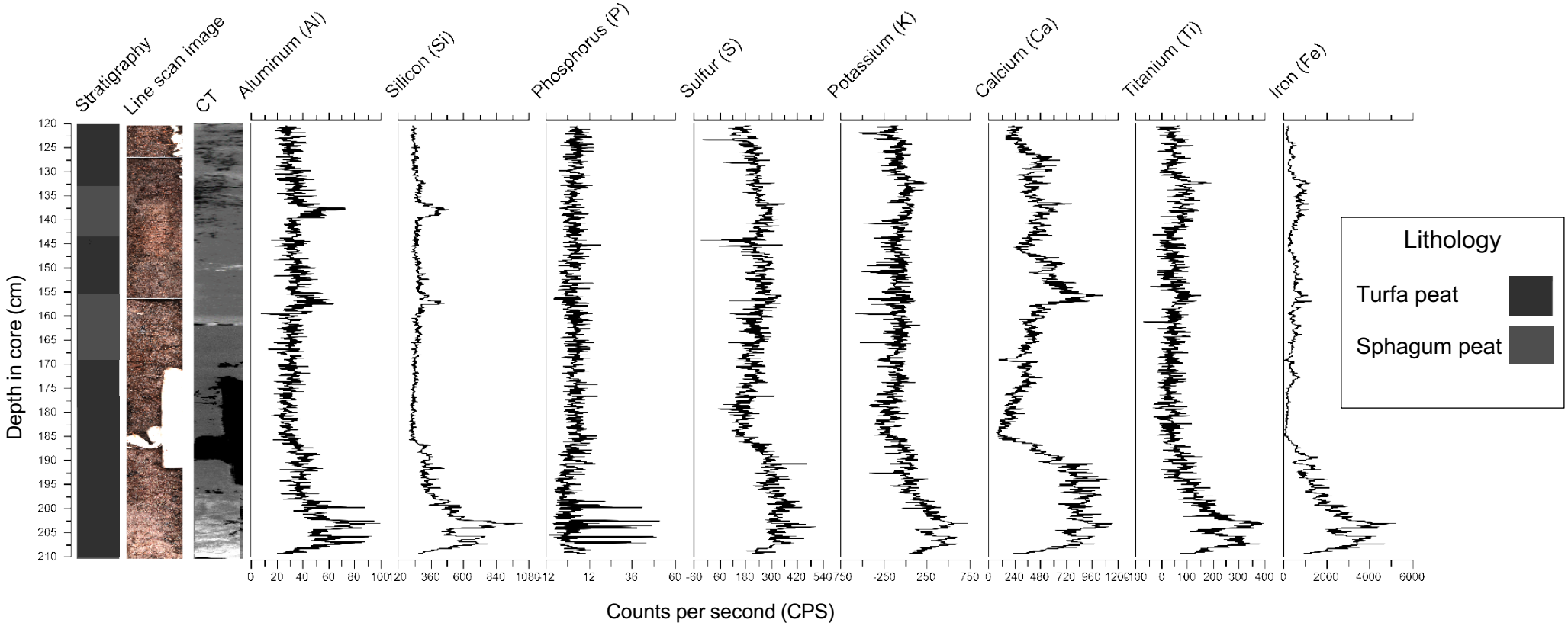

Figure 4.8. Elemental compositions within the fossil core at Ocean View, as determined by X-ray fluorescence (XRF). The elements are quantified in counts per second (CPS). The CT scan is also shown. Lighter sections are indicative of higher densities, whereas darker sections are indicative of lower densitiy material.

130-134 cm, and 198-203 cm). In total, 68 samples were analysed. Figure 4.9 illustrates the bio- stratigraphy of the fossil core from Ocean View, showing diatoms that constitute at least 5% of the total diatom valves, along with summary salinity classes based on the halobian classification. Zones generated through stratigraphically constrained cluster analysis facilitate the description of diatom assemblages throughout the core. A minimum of 250 diatoms per sample were counted.

Zone A (203-197 cm): Characterized by a dominance of oligohalobian-indifferent and halophobe species, including *Tabellaria flocculosa* (max 28%), *Synendra ulna* (max 12%), *Eunotia pectinalis* (max 11%), and *Navicula pupula* (max 16%). The notably high abundance of the halophobe species *Tabellaria flocculosa* indicates a depositional environment characterized by freshwater conditions.

Zone B (197-167 cm): Dominated by oligohalobian-indifferent and halophobe species similar to those in Zone A but at reduced abundances, including *Tabellaria flocculosa* (max 15.7%), *Synedra ulna* (max 6%), *Eunotia pectinalis* (max 6.9%), and *Navicula pupula* (max 15%). The reduced abundances of fresher species suggest a slight positive sea level tendency.

Zone C (167-134 cm): A marked transition occurs at the boundary between Zones B and C, characterized by the abrupt disappearance of oligohalobian-indifferent and halophobe species, such as *Tabellaria flocculosa* and *Synedra ulna*. These species are replaced by high abundances of polyhalobian, mesohalobian, and oligohalobian-halophile species, with some oligohalobian-indifferent species. Species with the highest abundances include *Navicula cari* var. *cinta* (max 24%), *Denticula subtilis* (max 15%), and *Navicula peregrina* (max 18%). This abrupt shift from predominantly freshwater to marine species may indicate a sudden rise in relative sea level (RSL) (positive sea level tendency), potentially associated with co-seismic subsidence. Throughout zone C, there is little variability in diatom assemblages which is consistent with the litho- stratigraphy which suggests minimal change.

Zone D (134-130 cm): A significant increase in *Navicula peregrina* is observed between 135 cm and 130 cm, with the abundance of this species peaking at 48% at 132 cm. Additionally, sudden increases in *Delpheneis surirella* and *Paralia sulcata* are also evident. A pronounced spike in the oligohalobian-indifferent species *Pinnularia microstauron* (14.8% at 132 cm) is apparent between 135 cm and 130 cm, which is atypical given the otherwise marine-associated spikes in species. However, *Pinnularia microstauron* is known for its adaptability to a broad range of environmental conditions, allowing it to inhabit much of the environmental gradient. The brief period of increased marine influence is succeeded by a return to the diatom abundances characteristic of Zone C, indicating a sudden rise in sea level, followed by a return to previous

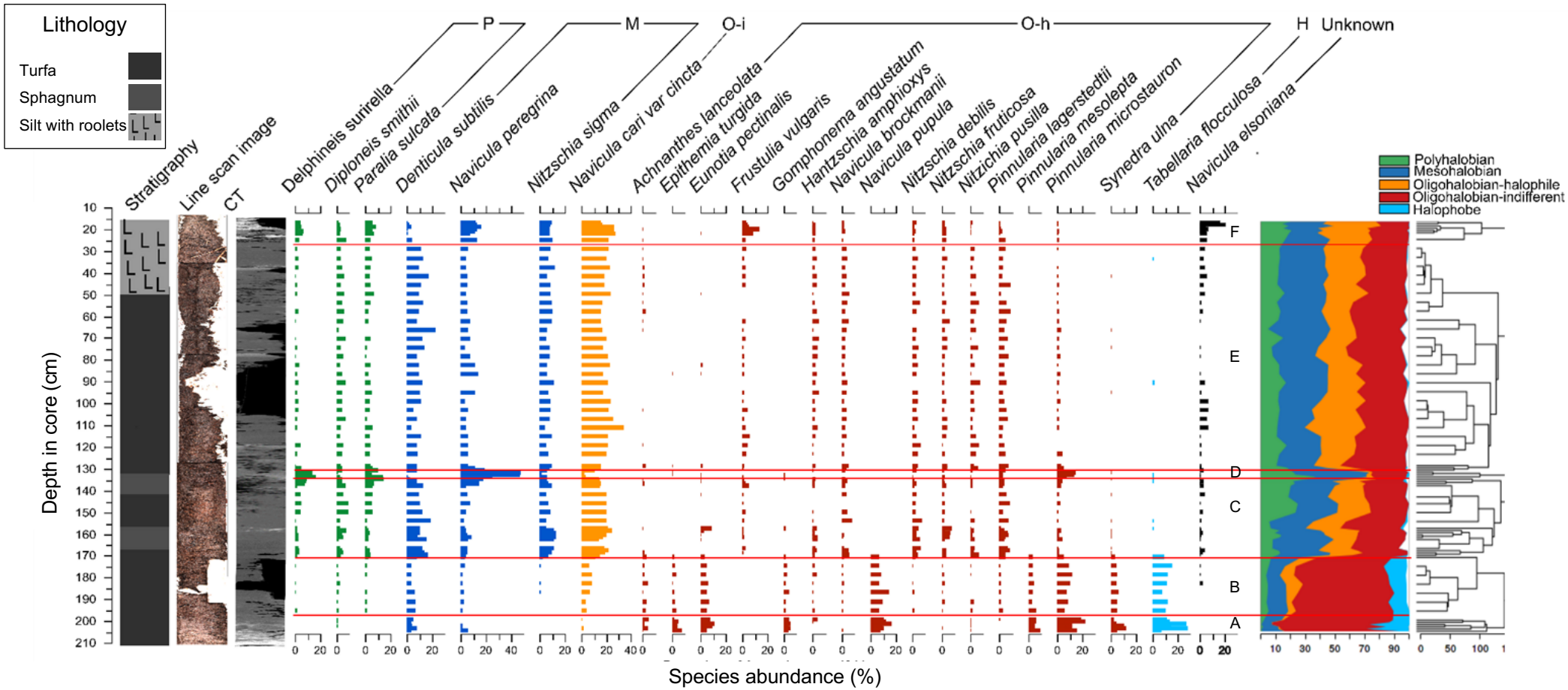

Figure 4.9. Ocean View fossil core diatom assemblages (> 5%). Summary salinity classes: Polyhalobian (P), Mesohalobian (M), Oligohalobian-halophile (O-h), Oligohalobian-indifferent (O-i), Halophobe (H). The total of each summary salinity class is also shown. The red lines show the zones produced by the dendogram. The stratigraphy, line scan image and CT scan are shown alongside the diatom assemblage data. Letters correlate to the zones.

conditions. This zone correlates with the peat-peat contact within the stratigraphy, likely corresponding to EQ1 at 132 cm.

Zone E (130-29 cm): Diatom assemblages in zone E return to those characteristic of Zone C, with a dominance of polyhalobian, mesohalobian, and oligohalobian-halophile diatoms, alongside some oligohalobian-indifferent species. This shift suggests a return to a depositional environment comparable to that preceding EQ1. The diatom abundances remain stable throughout this zone, indicating a consistent and stable environment.

Zone F (29-20 cm): There is a sudden increase in polyhalobian, mesohalobian and oligohalobian-halophile diatoms identified in zone E at approximately 28 cm. Notable species include *Navicula elsoniana* (max 20%), *Navicula cari* var. *cincta* (max 28%), *Navicula peregrina* (max 17%), and *Paralia sulcata* (max 8.8%), indicating a marked rise in marine influence. The increase in marine species, together with an abrupt change in lithology from peat to organic silt suggests a positive sea level tendency, likely associated with the 1964 CE earthquake.

4.3.4. Ocean View Core Chronology

Eleven samples from the Ocean View core were dated at the National Ocean Sciences Accelerator Mass Spectrometry Facility (NOSAMS) in Woods Hole, USA (Table 4.2). Dates from NOSAMS were modelled using the software Oxcal (P_sequence, v4.4, Bronk Ramsey, 2009a) (Figure 4.10). Of the 11 dates modelled, one date at 156 cm was deemed an outlier when modelled. Wood fragments dated at a depth of 132-133 cm (immediately below the peat – peat contact) coincide with the abrupt increase in *Navicula peregrina* and the abrupt boundary between sphagnum to turfa peat. Oxcal yielded a modelled date for EQ1 at 857-789 cal BP, which agrees well with previous ages from this location (946-739 cal yr BP- Hamilton et al. 2005) and the more recent tree ring dating at Girdwood (785 ± 10 cal yr BP, Barclay et al. (2024)). The observed changes in litho- and bio- stratigraphy, along with the similarity to dates from other studies, suggest that an abrupt change (likely representitive of EQ1) is recorded within the stratigraphy at a depth of 132 cm. Between this abrupt change and the 1964 CE earthquake (132–29 cm) the rate of deposition is 0.12 +/- 0.02 cm/year. The rate of deposition significantly increases following the 1964 CE earthquake to the top of the core (29–0 cm), with a rate of 0.49 +/- 0.005 cm/year.

4.3.5. Ocean View core reconstruction of Palaeomarsh Surface Elevation and Relative Sea Level

Palaeomarsh Surface Elevation (PMSE) and RSL was only reconstructed within the peat section

Sample ID	Laboratory number	Material dated	Lab-reported age (14C yr B.P.)	Callibrated age 2σ cal yr B.P.)	Modelled age (2σ cal yr B.P.)	± Error (2σ cal yr B.P.)
OV23/17A (40cm)	OS-180365	Plant/Wood	120 ± 30	271-10	265-13	126
OV23/17A (60cm)	OS-180423	Plant/Wood	255 ± 20	422-153	422-155	134
OV23/17A (80cm)	OS-180424	Plant/Wood	440 ± 25	526-473	526-471	28
OV23/17A (100cm)	OS-180425	Plant/Wood	615 ± 20	650-551	611-548	32
OV23/17A (120cm)	OS-180366	Plant/Wood	585 ± 20	641-542	644-593	26
OV23/17A (132cm)	OS-180419	Plant/Wood	950 ± 20	918-793	857-789	34
OV23/17A (146cm)	OS-180420	Plant/Wood	965 ± 20	925-793	889-811	39
OV23/17A (156cm)	OS-180421	Plant/Wood	860 ± 20	792-722	902-871	16
OV17/17A (160cm)	OS-180422	Plant/Wood	1000 ± 20	959-802	956-903	27
OV17/17A (169cm)	OS-180426	Plant/Wood	1090 ± 20	1058-935	1052-930	61
OV17/17A (198cm)	OS-180364	Plant/Wood	1180 ± 35	1241-975	1180-998	91

Table 4.2. ^{14}C dates from the Ocean View core. Calibrated age is using standard 14C terrestrial calibration in OxCal, modelled age is produced using a P sequence model in OxCal (P_sequence, v4.4, Bronk Ramsey, 2009a) for 11 macrofossil samples within the Ocean View core (not including age at 156 cm which was rejected by the P_sequence model as an outlier during model development).

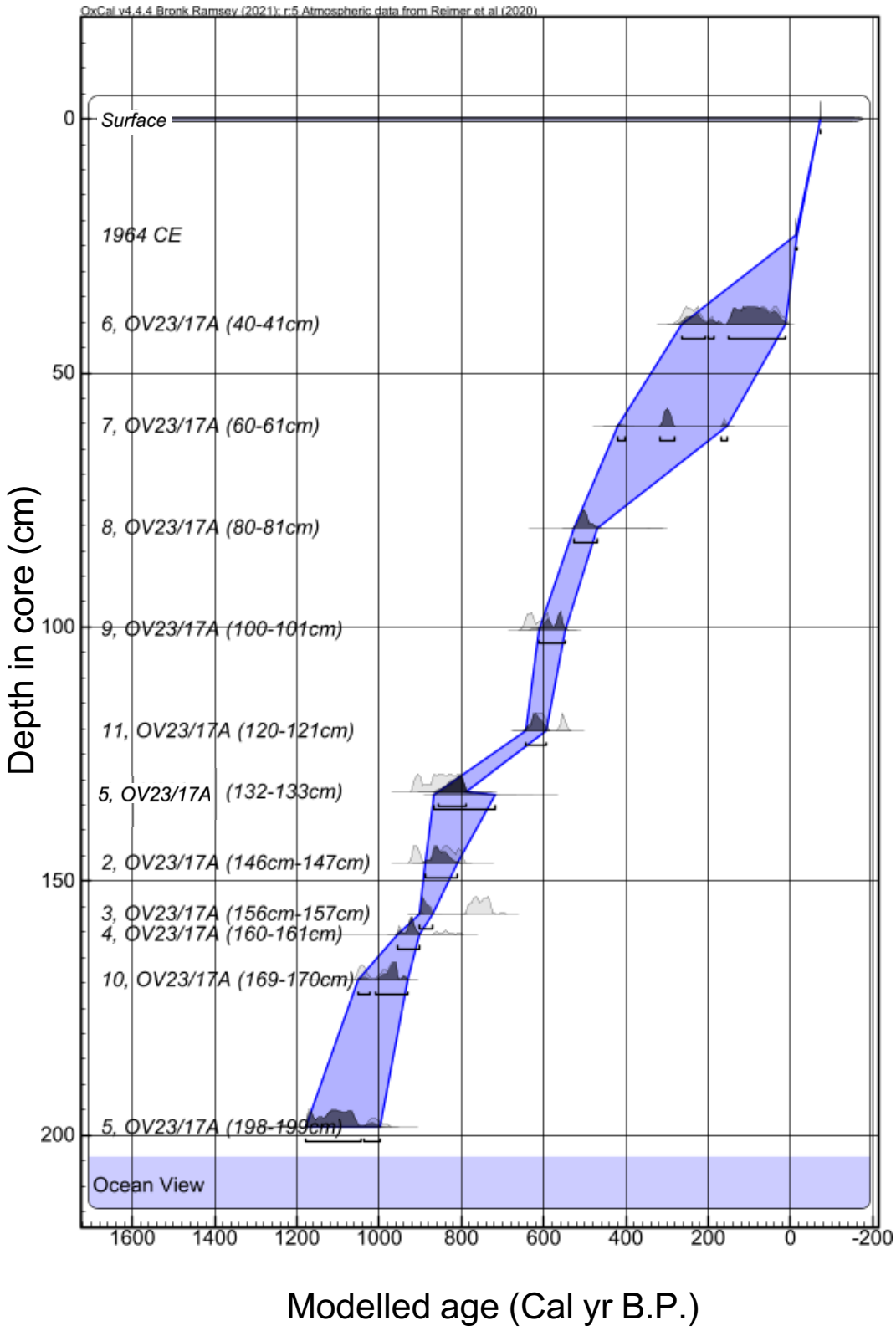

Figure 4.10. P-sequence age-depth model produced in Oxcal (P_sequence, v4.4, Bronk Ramsey, 2009a) for the Ocean View core. OxCal's individual unmodelled probability distribution curves are shown in light gray, and modeled probability distributions are shown in dark gray. The blue shaded area indicates the fitted model with 95% confidence ranges.

of the core from Ocean View (30-203 cm), since the > 225 SWLI and > 180 SWLI training sets are not suitable for reconstructing RSL within silt layers (which usually form below 180 SWLI). Thus, the transition into and within the top silt layer of the core which I hypothesise is from after the 1964 CE event (0–30 cm) was not reconstructed. For all reconstructions, errors are stated to 1σ.

4.3.5.1. Palaeomarsh surface elevation using the Full Alaskan training sets

Across all sub divisions using the Full Alaskan training set, the reconstructions show similar patterns, but the magnitude of PMSE change varies depending on the training set employed by the transfer function model. Only the subdivided training sets are shown in the reconstructions in Figure 4.11. The models using the 225-250 SWLI training set reconstruct the smallest variations in PMSE through the core, with values ranging from 1.1 to 1.4 m above MHHW (0.3 m range) and little variability between models (Figure 4.11a). In contrast, the Full AK > 180 SWLI and 100-250 SWLI training sets reconstruct variability in elevation of 1.3 m and 2.6 m through the core, and more variability between different models (Figure 4.11a). Models using all three training sets identify the sedimentary signature of EQ1 at 132 cm, characterized by a pronounced decline in PMSE followed by a return to prior elevations (Figure 4.11a). Table 4.3 shows the magnitude of the PMSE change associated with EQ1 at 132 cm using the WAPLS component 2 model. Land level estimates at 130 and 134 cm were compared as for every model they show the largest amounts of deformation. The WAPLS model using the 100-250 SWLI training set reconstructs an elevation decrease of approximately 0.99 ± 0.55 m, whereas the > 180 SWLI and 225-250 SWLI training sets record a fall of 0.55 ± 0.45 m and 0.08 ± 0.15 m respectively.

4.3.5.2. Palaeomarsh surface elevation using the Upper Turnagain Arm training sets

The reconstructed PMSE using the Upper Turnagain Arm training sets show similar results to the Full Alaskan reconstructions. Only the subdivided training sets were used in the reconstructions (Figure 4.11b). Whilst all reconstructions using the Upper Turnagain Arm training sets produce similar reconstructions, the magnitude of PMSE change varies according to the different training sets employed, in the same way as the Full Alaskan training sets (Figure 4.11b). The models using the > 225 SWLI training set show the smallest variations in surface elevation, with values between 1.1 m - 1.3 m above MHHW (0.2 m range). In contrast, the > 180 SWLI and 100-250 SWLI training sets reconstruct elevation variation of 0.8 m and 1.7 m above MHHW, respectively (Figure 4.11b). In general,

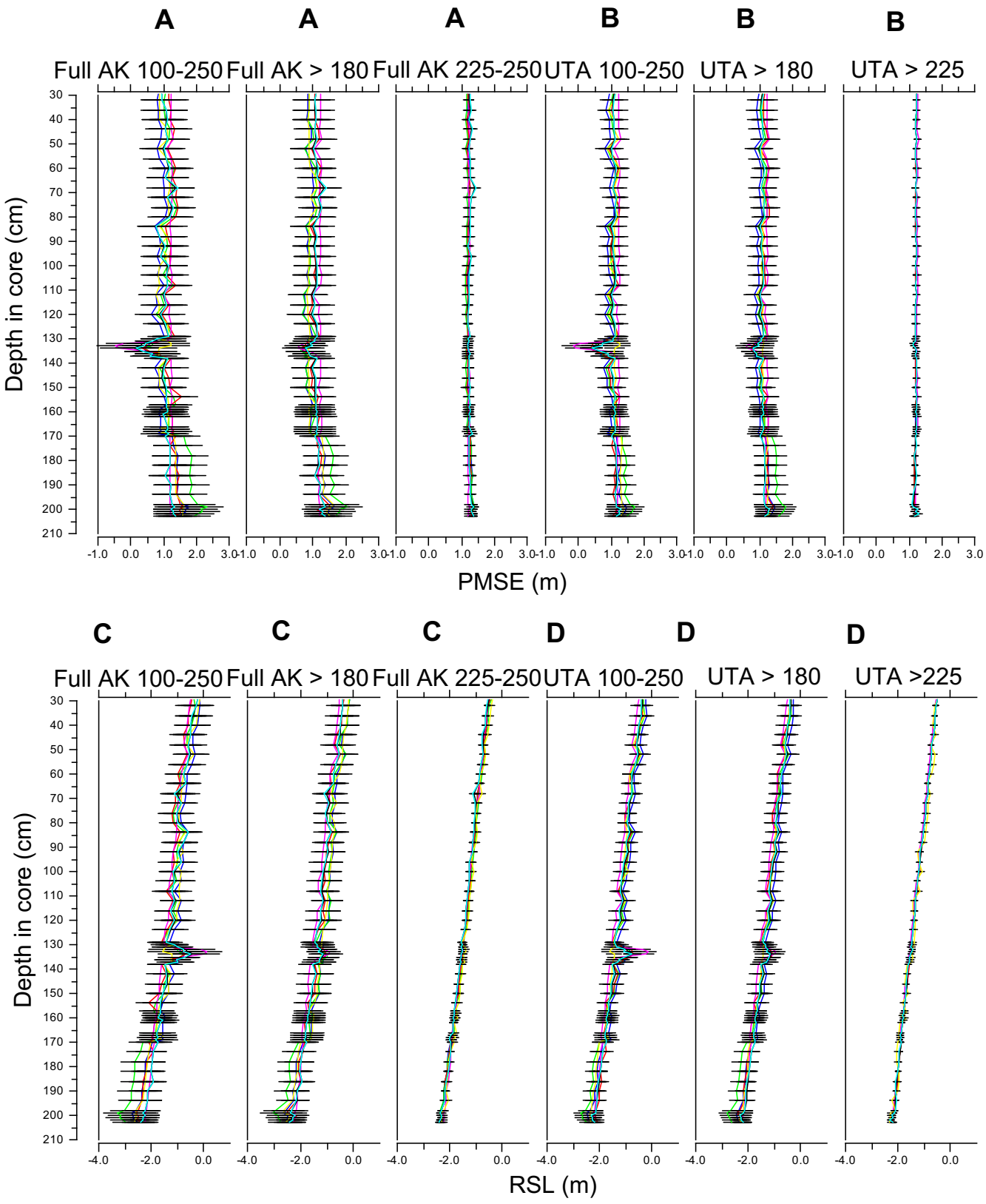

Figure 4.11. Ocean View fossil core palaeomarsh surface elevation and relative sea level reconstructions. A) Reconstructed palaeomarsh surface elevation (PMSE) (m) against core depth (cm) using Full Alaskan training sets. B) Reconstructed palaeomarsh surface elevation (PMSE) (m) against core depth (cm) using Upper Turnagain Arm training sets. C) Reconstructed relative sea level (RSL) (m) against core depth (cm) using Full Alaskan training sets. D) Reconstructed relative sea level (RSL) (m) against core depth (cm) using Upper Turnagain Arm training sets. Blue = WA (Inverse), Green = WA (Classical), Red = WA-LPS, Pink = MAT, Yellow = ML, Black = LW-WA (Inverse), Turquoise = LW-WA (Classical). Horizontal lines show average uncertainity of all 7 models (uncertainity is to 1σ).

A

Training set used in reconstruction	PMSE at 130cm	PMSE at 134cm	Change in Elevation (cm)	Sample specific error +- (cm)	Modern Analogue at 130cm	Modern Analogue at 134cm
Full AK 100-250	1.34	0.34	99	55	Good	Close
UTA 100-250	1.22	0.37	85	28	Close	Poor
Full AK >180	1.22	0.66	55	45	Good	Poor
UTA > 180	1.27	0.75	52	31	Close	Poor
Full AK > 225	1.11	1.09	2	17	Close	Poor
UTA > 225	1.21	1.15	5	9	Close	Poor
Full AK 225 - 250	1.18	1.10	8	15	Close	Close

B

Training set used in reconstruction	RSL at 130cm	RSL at 134cm	Change in RSL (cm)	Sample specific error +- (cm)	Modern Analogue at 130cm	Modern Analogue at 134cm
Full AK 100-250	-1.63	-0.68	94	55	Good	Close
UTA 100-250	-1.51	-0.71	80	28	Close	Poor
Full AK >180	-1.51	-1.00	50	45	Good	Poor
UTA > 180	-1.56	-1.09	47	31	Close	Poor
Full AK > 225	-1.41	-1.43	2	17	Close	Poor
UTA > 225	-1.48	-1.57	8	9	Close	Poor
Full AK 225 -250	-1.41	-1.48	6	15	Close	Close

Table 4.3. Reconstructed palaeomarsh suface elevation (PMSE) (A) and relative sea level (RSL) (B) associated with EQ1. 130 and 134 cm are used as they show the largest change in land level. Sample errors are to 1σ.

the Upper Turnagain Arm training sets reconstruct smaller elevation ranges than the Full Alaskan training sets. Models using all three training sets identify the sedimentary signature of EQ1, characterized by a pronounced decline in PMSE followed by a return to prior elevations between 134-130 cm depth. For the 100-250 SWLI, > 180 SWLI and > 225 SWLI training sets, the change in elevation recording EQ1 around 132 cm using the WAPLS component 2 model are -0.85 ± 0.28 m, -0.52 ± 0.31 m and -0.05 ±0.09 m above MHHW respectively.

4.3.5.3. Relative sea level reconstruction using the Full Alaskan training sets.

For all reconstructions using the Full Alaskan training sets, there is a gradual RSL rise throughout the core. The WA-PLS component 2 model using the 225- 250 SWLI training set records a RSL rise of 0.06 ± 0.15 m during EQ1 (Figure 4.11c). When more samples and a larger modern elevation range are included within the transfer function, e.g. when using the > 180 SWLI training set (WA-PLS component 2) the RSL rise increases to 0.5 ± 0.45 m (Figure 4.11c). RSL rise at the time of EQ1 is even larger when using the 100- 250 SWLI training set, recording a rise of 0.94 ± 0.55 m (WA-PLS component 2).

4.3.5.4. Relative sea level reconstruction using the Upper Turnagain Arm training sets

The Upper Turnagain Arm training sets reconstruct similar patterns in RSL as the Full Alaskan training sets. For all reconstructions using the WAPLS model and the Upper Turnagain Arm training sets, there is a gradual RSL rise throughout the core (Figure 4.11d). The > 225 SWLI training set produces the smallest rise in RSL during EQ1, with a change of 0.08 ±0.09 m using the WA-PLS component 2 model (Figure 4.11d). The UTA > 180 SWLI training set produces a RSL rise of 0.47 ± 0.31 m, whilst the 100-250 SWLI training set produces a RSL rise of 0.8 ± 0.28 m using the WA-PLS component 2 model (Figure 4.11d). Figure 4.12 shows the diatom assemblage alongside the RSL reconstructions for WA-PLS component 2.

4.3.6. Modern Analogues for Ocean View fossil data

The Modern Analogue Technique was run to compare each modern training set to the fossil Ocean View data to define for each model output the number of ‘good’ or ‘close’ modern analogues within the Ocean View reconstruction. For the 61 samples within the Ocean View fossil core reconstruction, the Full Alaskan training sets had more ‘good’ and ‘close’ modern analogues than the Upper Turnagain Arm training sets. The Full AK 100-250 SWLI, > 180 SWLI and 225-250 SWLI training sets had 45, 16 and 23 ‘good’ modern analogues respectively. The Upper Turnagain Arm training sets provided no ‘good’ modern analogues for the fossil data.

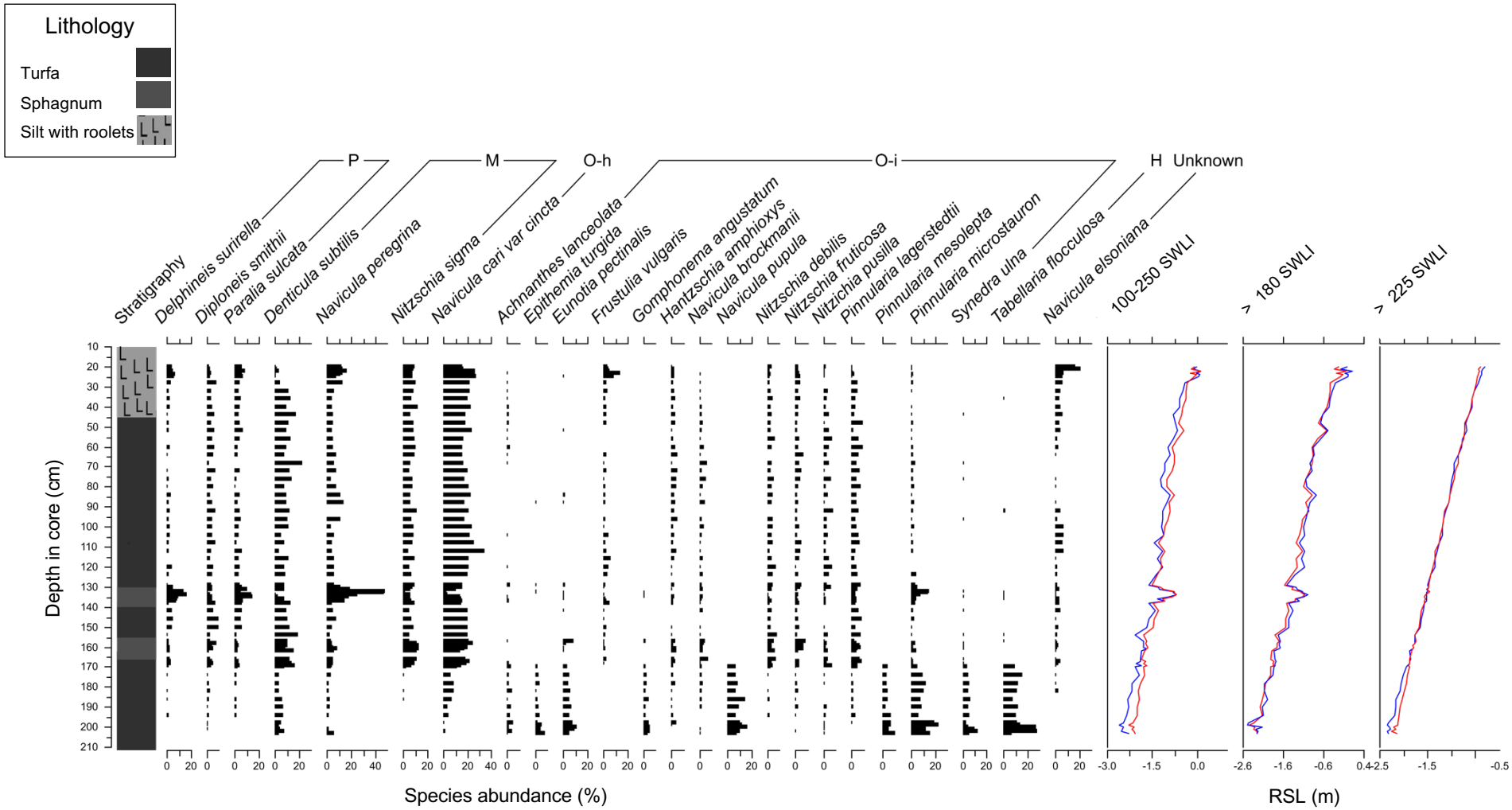

Figure 4.12. Ocean View fossil core diatom assemblage data (> 5%) alongside the stratigraphy and relative sea level reconstruction using WAPLS component 2 for 6 training sets. Summary salinity classes: polyhalobian (P), mesohalobian (M), oligohalobian-halophile (O-h), oligohalobian-indifferent (O-i), halophobe (H). Relative sea level (RSL) (m) is shown against depth in core (cm). Blue = Full AK reconstructions. Red = UTA reconstructions.

However, all of the Upper Turnagain Arm training sets show a reasonable number of 'close' modern analogues. Table 4.4 shows the number of 'good' and 'close' modern analogues for each training set. The 5th and 20th percentiles of training set dissimilarities for each training set can be found in Appendix 3.

Training set	Good modern analogue	Close modern analogue
Full AK 100-250	23	61
Full AK > 180	16	60
Full AK > 225	23	60
Full AK 225-250	45	61
UTA 100-250	0	45
UTA > 180	0	44
UTA > 225	0	47

Table 4.4. Number of 'good' and 'close' modern analogues in the Ocean View reconstruction.

4.3.7. Ocean View summary

The results from fossil core provide lithological and bio- stratigraphical evidence of co- seismic subsidence within a peat-forming environment at Ocean View (Figure 4.12). A change in the stratigraphy from sphagnum to turfa peat at 132 cm coincides with a spike in the abundance of *Navicula peregrina*. The age-depth model for the sample core places this litho- and bio-stratigraphic change at 132 cm at 857-789 cal yr BP. Transfer function-based reconstructions indicate a fall in PMSE and a rise in RSL at ~132 cm in all models I have developed, with a plausible magnitude of 8 cm +/- 15 cm (PMSE) using the WAPLS model with the Full AK 225-250 training set. However, the magnitude of the change in PMSE is dependent on the training set used by each transfer function model (Table 4.3, Figure 4.12).

4.4. Fossil results from Girdwood

4.4.1. Girdwood core litho- stratigraphy

The litho- stratigraphy of Girdwood Marsh is characterised by multiple peat-silt couplets. 24 cores, each ~2 m deep, collected from three transects across the marsh at Girdwood reveal a silt unit at the top of each core, underlain by a peat unit with a sharp boundary between them (Figure 4.13). This peat unit was buried by silt during co-seismic subsidence associated with the 1964 CE earthquake. In transect one, four cores document an additional peat-silt couplet at approximately 200 cm depth formed during EQ1 (Hamilton et al. 2005). Two additional transects were taken perpendicular to these cores to trace the lateral extent of this EQ1 event peat-silt couplet. However, within the additional transects, this peat-silt couplet was only identified in one core (the sample core; core one from Transect two (T2/1), (Figure 4.13).

The transects collected in September 2023 extend from the marsh front to the rear of the marsh at Girdwood with the intention to trace the peat-silt couplet associated with the EQ1 event landward until it became a peat-peat couplet. However, while the peat-silt couplet from EQ1 was identified, a change to a peat-peat couplet was not evident inland. Transect one reached the present-day highest marsh zone where marine inundation is very infrequent and the underlying topography shallowed. The EQ1 peat-silt couplet is still present in core 13 of Transect one (Figure 4.13). A beaver dam isolated cores 14-16 on Transect one from the rest of the transect. The complicated nature of the environment including ponded water and inflow from Tidewater Slough is reflected in the stratigraphy of these three cores. The litho- stratigraphy consists of up to ten distinct sediment layers, including gyttja, organic peat, and silts, which make it hard to see if any sedimentary signature (e.g. a peat-peat contact) of co-seismic subsidence is present.

4.4.2. Girdwood bio- stratigraphy

Sampling intervals for diatom analysis in core T2/1 varied according to the stratigraphy of the core. For much of the core, samples were collected at 4 cm intervals. However, at depths where notable changes in diatom assemblages were observed (32-40 cm), the sampling frequency was increased to 1 cm intervals. In total, 52 diatom samples were counted. Figure 4.14 illustrates the bio- stratigraphy of the fossil core, with diatoms that constitute at least 5% of the total diatom valves, along with summary salinity classes based on halobian classification. The zones generated through stratigraphically constrained cluster analysis facilitate the description of diatom assemblages throughout the core. In most instances, a minimum of 250 diatoms per sample were counted.

Zone A (220-138 cm): The first sample in zone A is dominated by oligohalobian-indifferent species, including high abundances of *Staurosirella pinnata* (max 31.7%) and *Fragilariforma virescens* (max 30%). This sample comes from the upper limit of a lower peat layer recorded in

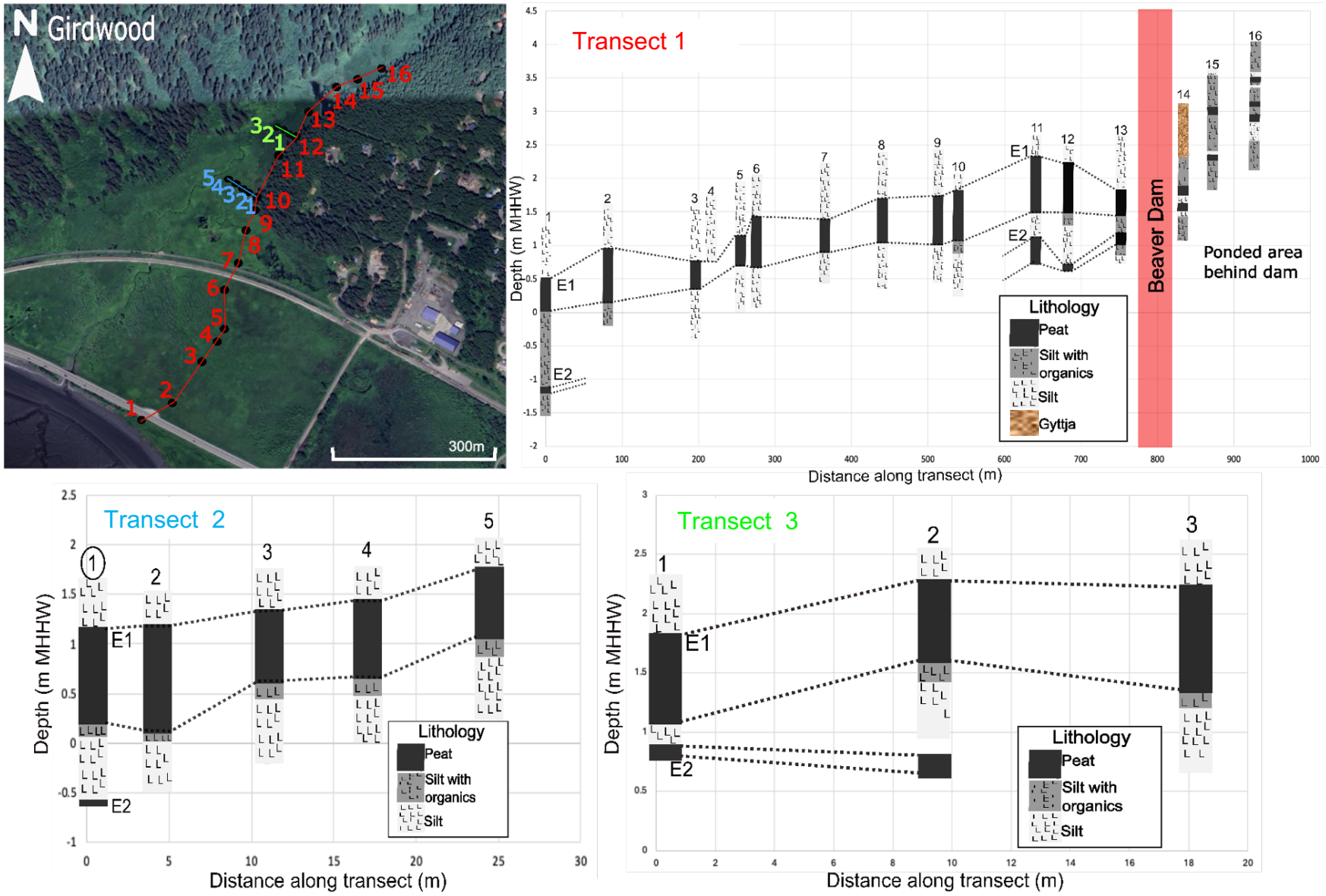

Figure 4.13. Litho- stratigraphy for 3 transects taken across Girdwood marsh. 'E1' and 'E2' represent the inferred 1964 CE and EQ1 respectively. The '1' circled on transect two highlights the Girdwood fossil core used in analysis (core T2.1). On inset map, Red = Transect one. Blue = Transect two. Green = Transect 3.

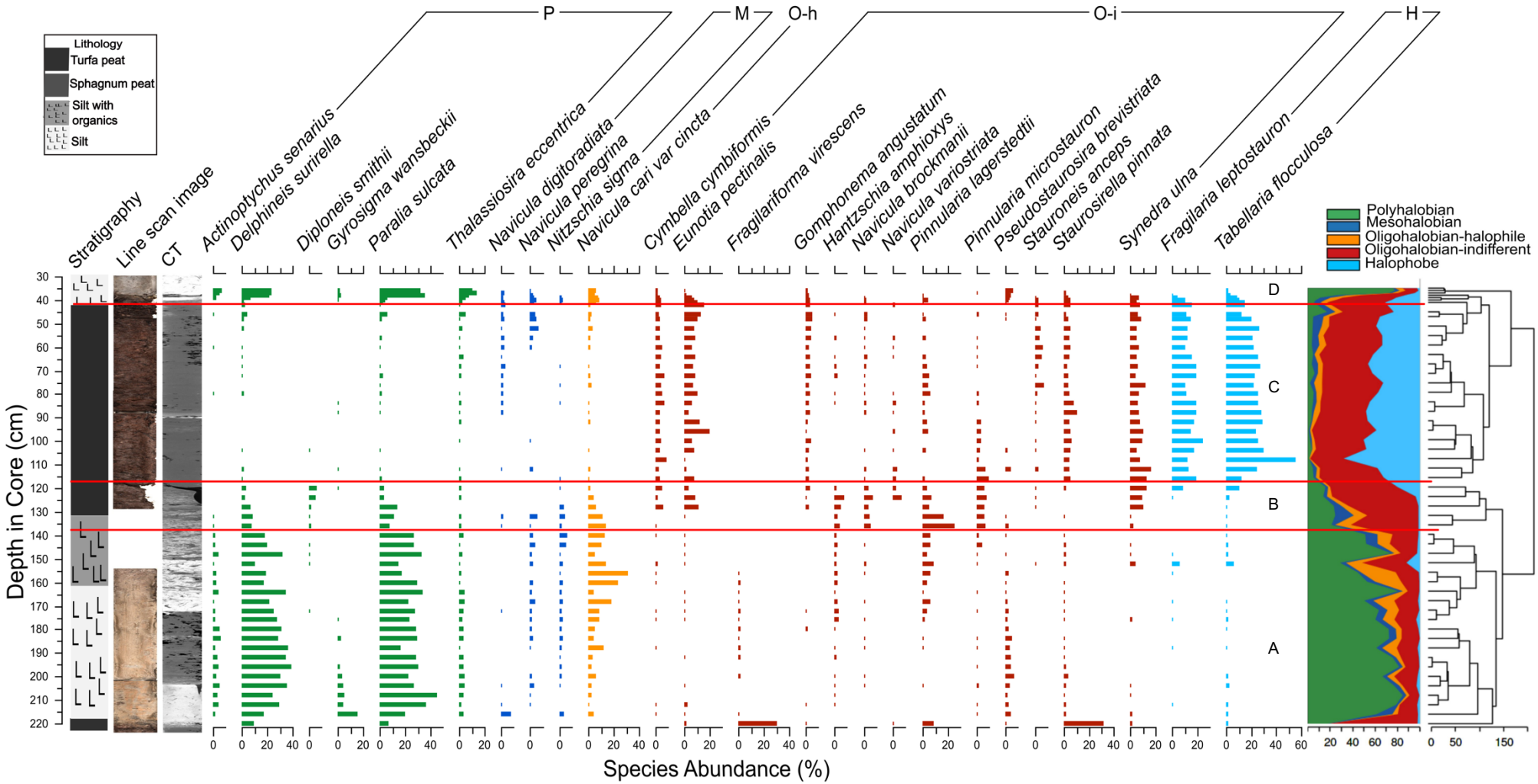

Figure 4.14. Girdwood fossil core (T2/1) diatom assembalage data (> 5% total diatom valves). Summary salinity classes: Polyhalobian (P), Mesohalobian (M), Oligohalobian- halophile (O-h Oligohalobian-indifferent (O-i) and halophobe (H). The stratigraphy, line scan image, CT scan and stratigraphically constrained cluster analysis results are shown alongside the diatom assemblage data. Letters correlate to the zones.

the stratigraphy. The rest of zone A is dominated by polyhalobian species, with high abundances of *Paralia sulcata* (max 45%) and *Delphineis surirella* (max 36%). A marked shift in species composition suggests a sudden transition from a freshwater to a marine environment, and a rise in RSL. The large change in the diatom assemblage at 218 cm coincides with a change in the stratigraphy, where the peat layer is succeeded by a silt layer, forming a peat - silt couplet. Based on previously dated deposits at the marsh front by Shennan and Hamilton (2006) which I traced inland to the sample core location, I infer that this peat- silt couplet is evidence of EQ1.

Zone B (138-118 cm): Zone B is a transition zone from polyhalobian species such as *Paralia sulcata* to halaphobe species such as *Tabellaria flocculosa* (max 15%), *Fragilaria leptostauron* (max 10%)*, Synedra ulna* (max 16%), and Eunotia pectinalis (max 5%). This change from polyhalobian species in zone A suggests a negative sea level tendency, associated with post-seismic uplift following EQ1. This transition is reflected in the stratigraphy as the silt layer gradually turns into a peat layer.

Zone C (118 – 40): Zone C is made up of halaphobe species such as *Tabellaria flocculosa* (max 15%), *Fragilaria leptostauron* (max 10%)*, Synedra ulna* (max 16%), and Eunotia pectinalis (max 5%). This is indicative of a fresh water environment and post seismic uplift.

Zone D (40-36 cm): Zone C has a sudden increase in polyhalobian, mesohalobian, and oligohalobian-halophile diatoms, including *Paralia sulcata* (max 35%) and *Thalassiosira eccentric*a (max 13.5%), indicating an increase in marine influence. There is a decline in halophobe species such as *Tabellaria flocculosa* (10% at 40 cm, 1% at 36 cm) and *Fragilaria leptostauron* (max 1.5%), which are replaced by polyhalobian species. The decline of freshwater species, coupled with the rise in marine species and an abrupt lithological shift from peat to silt which was traced from the marsh front, suggests a positive sea-level tendency associated with the 1964 CE earthquake.

4.4.3. Girdwood reconstruction of Palaeomarsh surface elevation and Relative sea level

4.4.3.1. Palaeomarsh surface elevation using the Full Alaskan training sets

The three subdivided Full Alaskan training set transfer functions were applied to the peat section of the Girdwood core (130 – 40 cm, approximate age 515-318 cal yr BP to 1964 CE based on dates from a marsh front core at Girdwood in Hamilton and Shennan, 2005) with the aim of reconstructing changes in PMSE during the period of peat formation between the EQ1 and 1964 CE events. For all reconstructions, erros are stated to 1σ. Across all models using the Full

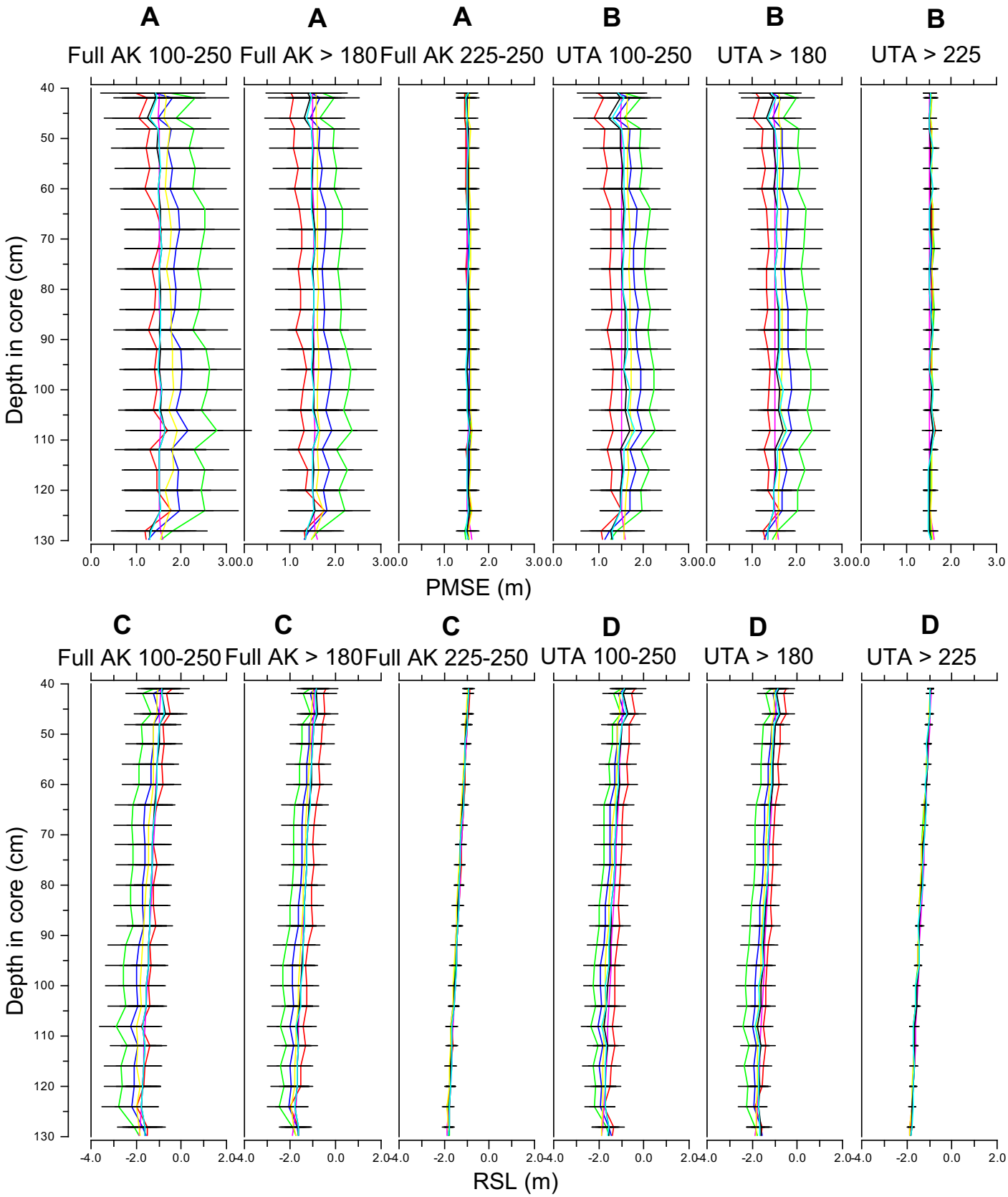

Figure 4.15. Girdwood T2/1 fossil core palaeomarsh surface elevation and relative se level (RSL) reconstructions. A) Reconstructed palaeomarsh surface elevation (PMSE) (m) against core depth (cm) using Full Alaskan training sets. B) Reconstructed palaeomarsh surface elevation (PMSE) (m) against core depth (cm) using Upper Turnagain Arm training sets. C) Reconstructed relative sea level (RSL) (m) against core depth (cm) using Full Alaskan training sets. D) Reconstructed relative sea level (RSL) (m) against core depth (cm) using Upper Turnagain Arm training sets. Blue = WA (Inverse), Green = WA (Classical), Red = WA-PLS, Pink = MAT, Yellow = ML, Black = LW-WA (Inverse), Turquoise = LW-WA (Classical). Horizontal lines show average uncertainity of all 7 models (uncertainity is to 1σ).

Alaskan training sets, no abrupt changes in PMSE are observed throughout the peat section of the Girdwood core (Figure 4.15a). As is seen in the Ocean View core reconstructions, training sets with more samples reconstruct a wider elevation range between different model reconstructions. The Full Alaskan 225-250 SWLI training set shows very little variability between models. In contrast, the Full Alaskan > 180 SWLI and 100-250 SWLI show greater variability between models, with a range of ~1.3 m between reconstructions using the Full AK 100-250 training set, and ~0.9 m range when using the Full AK > 180 SWLI training set (Figure 4.15a).

4.4.3.2. Palaeomarsh surface elevation using the Upper Turnagain Arm sets

No notable changes are seen in PMSE throughout the peat reconstructed from models using the UTA training sets (Figure 4.15b). The different training sets reconstruct similar PMSE, however, as the training sets incorporate more samples, the transfer function models reconstruct a wider elevation range, as is seen when using the Full AK training sets (Figure 4.15b).The Upper Turnagain Arm > 225 SWLI training set shows very little variability between models, whereas the Upper Turnagain Arm > 180 SWLI and 100-250 SWLI training sets show a greater variability. The range in elevation between the WA and WA-PLS models for the > 180 SWLI and 100-250 SWLI training sets are 0.6 m and 0.5 m respectively (Figure 4.15b).

4.4.3.3. Relative sea level using the Full Alaskan training sets

Figure 4.15c shows reconstructed RSL using the different models. All models using the Full Alaskan training sets yield similar RSL reconstructions, with RSL rising from ~-2 m to -1 m MHHW through the core section, with no sudden changes in RSL identified. However, similar to the PMSE reconstruction, the five types of transfer functions used display increasing reconstruction range as training set size increases. The > 225 SWLI training set shows very little between model variance. For the > 180 SWLI training set, the WA and WA- PLS reconstructions produce RSL values of around -2.2 m above MHHW and -1.8 m above MHHW (range 0.4 m). The 100-250 SWLI training set reconstructs RSL between -2.4 m and -1.7 m above MHHW (range 0.7 m) for the WA and WA-PLS models respectively. Figure 4.16 shows the RSL alongside the diatom assemblages.

4.4.3.4. Relative Sea Level using the Upper Turnagain Arm training sets

Very similar results are seen within the Upper Turnagain Arm training set as the Full Alaska training sets. No rapid changes in RSL are evident within the core section, with RSL slowing rising from ~–2 m to ~-1 m MHHW up core (Figure 3.16d). Similar to the Full Alaska training sets, as sample size increases so does the variability between model reconstructions. However, this variability is smaller than between the models in the Full Alaska training sets. The WA and

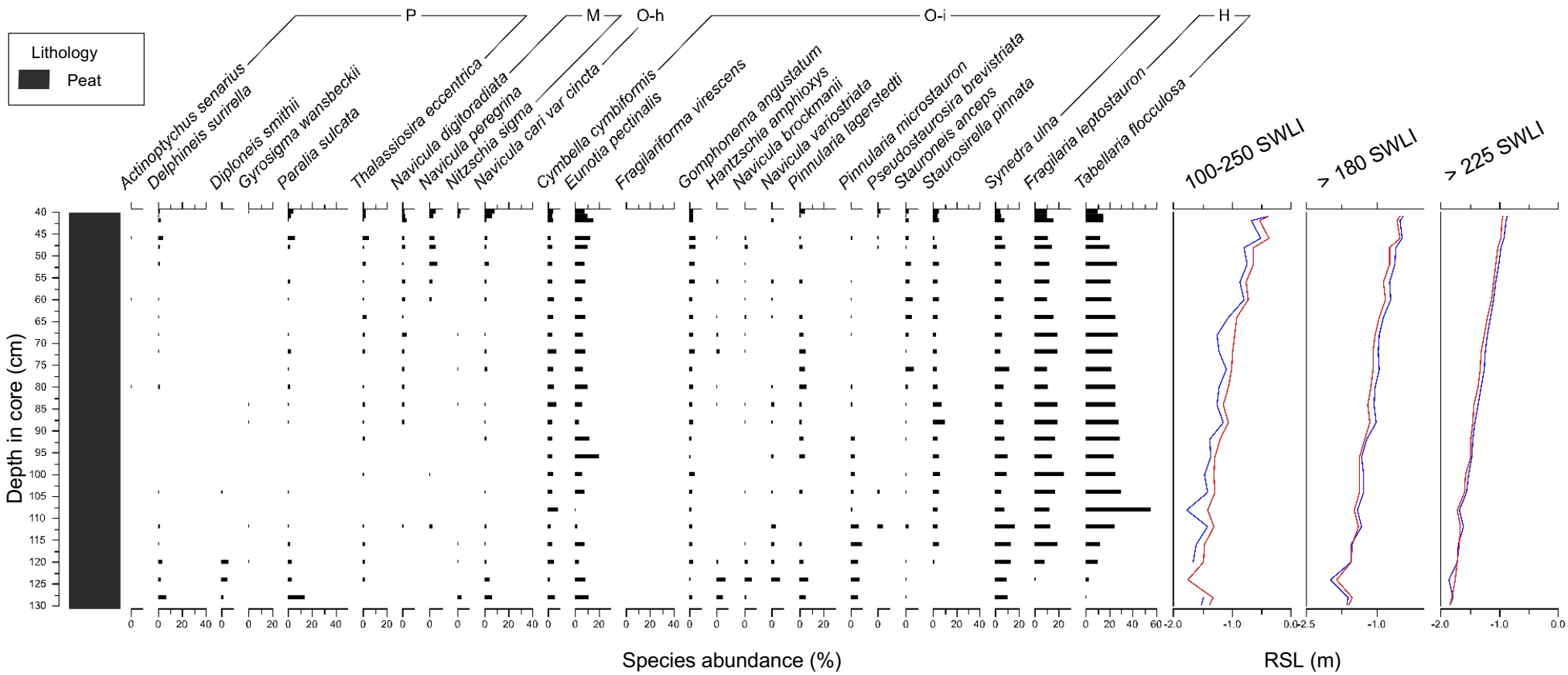

Figure 4.16. Diatom assemblage data (> 5%) within the peat section of the Girdwood fossil core. The relative sea level (RSL) (m) reconstruction for WAPLS component 2 is shown alongside. Summary salinity classes: Polyhalobian (P), Mesohalobian (M), Oligohalobian-halophile (O-h Oligohalobian-indifferent (O-i) and halophobe (H).). Blue = Full AK reconstructions. Red = UTA reconstructions.

WAPLS models for the > 180 SWLI training set produce RSL values around – 2.1 m and -1.8 m respectively. The WA and WAPLS models for the 100-250 SWLI training set produce RSL values around -2.2 m and -1.7 m respectively. Figure 3.17 shows the RSL alongside the diatom assemblages.

4.4.4. Modern Analogues for Girdwood fossil data

For the 29 samples within the Girdwood fossil core reconstruction, every training set except UTA > 225 SWLI gives all as 'close' modern analogues. The UTA > 225 SWLI has 28 'close' modern analogues. However, the Full Alaska training sets had more of the higher confidence 'good' modern analogues to the fossil data than the Upper Turnagain Arm training sets. The Full AK 100-250 SWLI, > 180 SWLI and 225-250 SWLI models have 22, 20 and 26 'good' modern analogues respectively. The Upper Turnagain Arm 100-250 SWLI, >180 SWLI and >225 SWLI models have 6, 4 and 0 'good' modern analogues respectively. Table 4.5 shows the number of 'good' and 'close' modern analogues for each training set. The 5th and 20th percentiles of training set dissimilarities for each training set can be found in the appendix.

Training set	Good modern analogue	Close modern analogue
Full AK 100-250	22	29
Full AK > 180	20	29
Full AK > 225	28	29
Full AK 225-250	26	29
UTA 100-250	6	29
UTA > 180	4	29
UTA > 225	0	28

Table 4.5. Number of 'good' and 'close' modern analogues in the Girdwood reconstruction.

4.4.5. Girdwood results summary

Coring transects at Girdwood designed to spatially extend the record of the EQ1 peat-silt couplet found at the marsh front did not result in this couplet changing to a peat-peat couplet landward. The river valley of Tidewater Slough is generally flat and was probably flooded up to core 16 in 1964 CE, as evidenced by an up to ~80 cm cap of silt above the 1964 CE peat surface even in cores at the upstream end of the transect (Figure 4.13). Similarly, the record of EQ1 here is a peat-silt couplet along the whole transect, with the most landward cores again complicated by the presence of a beaver dam. The lithological, bio- stratigraphical and transfer function model

results from the peat section of the Girdwood core provide no evidence of rapid land level changes during the time period of peat formation (at least c. 515- 318 cal yr BP to 1964 CE from previous dating of peat formation at the marsh front between the EQ1 and 1964 CE events by Hamilton et al. (2005)). The transfer function models all reconstruct gradual RSL rise through the peat section of the Girdwood fossil core.

Chapter 5: Discussion

This thesis presents high-resolution microfossil analyses of peat material from the high marsh zone in south-central Alaska, aimed at better understanding the litho- and bio- stratigraphic imprint of land-level changes in the peat-forming environment at Ocean View, Anchorage, and earthquakes causing similar amounts of land-level change in peat-forming environments at Girdwood.

This discussion addresses the main research questions outlined in Chapter 2: How do new high marsh modern diatom samples collected at Girdwood in 2023 compare to data in the existing modern training set described by Shennan et al. (2018) and high marsh diatoms regionally and globally? 2. Is EQ1 detectable within a peat-peat contact at Ocean View? 3. If it is, how does the training set selection influence the magnitude of the reconstructed surface deformation? 4. Is there evidence of decimetre-scale surface deformation caused by additional earthquakes other than EQ1 at Ocean View or Girdwood? The discussion also situates the findings within the broader context of palaeoseismological research, to identify areas for future research.

5.1. RQ 1 - Comparison of new and existing modern diatom data

Initial findings suggest that the new Girdwood samples taken in September 2023 align well with the existing training set from Shennan et al. (2018), indicating that the local diatom assemblages are consistent with broader regional patterns. The new modern samples occupy a SWLI range from 230.5 to 238 which is above HAT at Anchorage (217 SWLI units). There are 89 samples above 230 SWLI units in the existing training set, with the uppermost sample in the existing training set at 302.1 SWLI units. The new samples occupy an environmental zone which includes peat-forming environments dominated by *Sphagnum* moss (Transect one) and waterlogged high marsh dominated by *Triglochin* and sedges (Transect two).

When considering species with > 30% abundance, no new species not already present in the Full Alaskan training set are found in the new Girdwood samples. Of 28 species found with abundances above 30% in the Full Alaskan training set, 11 of these species also have abundances above 30% in the new Girdwood samples.

Whilst most species in the new samples show remarkable resemblance to the species in the Full Alaskan training set at the same SWLI elevation, there are discrepancies. For example, high abundances of *Fragilaria leptostauron* (> 30%) are found within Transect two at Girdwood (Figure 4.2), whereas much smaller abundances (< 5%) are found in the Full Alaskan training set (Figure 4.3). Morales and Manoylov (2006) suggest *Fragilaria leptostauron* (also known as *Staurosirella leptostauron*) is widely distributed across various regions in the United States,

including Idaho, Wyoming, and Alaska, and that it has a broad ecological range, being present in oligotrophic to highly eutrophic and in fresh to brackish waters. Its high abundance in Transect two at Girdwood may reflect the nature of the environment here which was waterlogged high marsh. The fact that this species has very low abundances in the rest of the training set (Transect one at Girdwood and the Shennan et al. (2018) data)) suggests that it prefers waterlogged environments, and modern sampling at other locations in the training set may not have included similar waterlogged environments above HAT.

A second species at high abundances in Transect two of the new Girdwood samples (> 30%) but at lower abundances in the Full Alaskan training set (< 15%) is *Staurosirella pinnata*. Several studies note the presence of the species in freshwater lacustrine settings, with the species found across lakes in Canada (Finkelstein and Gajewski, 2008) Greenland (Cremer et al. 2001) and Argentina (Hassan et al. 2006).

The modern sampling undertaken above HAT at Girdwood highlights that diatoms that live in high marshes that are only very occasionally inundated by marine water may not reflect the general principle that diatom species change with increasing elevation. Instead, the high abundances of *Fragilaria leptostauron*, *Staurosirella pinnata*, and freshwater species such as *Tabellaria flocculosa* and *Synedra ulna*, may reflect the environment within the marsh where the modern samples were taken at Girdwood. The two new transects exhibit significantly different diatom assemblages, without showing significant differences in elevation, with Transect one being more similar to the Shennan et al. (2018) data. Hamilton (2003) notes that Girdwood is less appropriate for collecting modern samples from higher elevations because of the Seward Highway and Alaska Railroad which both cross the marsh. The marsh behind the railroad is largely cut off from the estuary, with tidal flow restricted to the Tidewater Slough channel. The railroad levees also cause ponding of freshwater towards the rear of the marsh, creating a waterlogged high marsh environment which is reflected in different dominant diatom species here compared to similar elevations elsewhere at Girdwood and at other sites in south-central Alaska.

5.2. RQ 2 – Is EQ1 recorded in a peat-peat couplet at Ocean View?

This study identifies a sphagnum peat-turfa peat couplet that most likely represents EQ1 at Ocean View, Anchorage. New AMS ages on plant macrofossils indicate that the sediment at the peat-peat contact was deposited between 857 and 789 cal. yr BP. This agrees with a previous estimate obtained from salt marsh sediments at Ocean View (~850 cal. yr BP; Hamilton and Shennan, 2005) and with a more recent estimate using tree rings at Girdwood (785 ± 10 cal. yr

BP; Barclay et al. 2024). The amount of subsidence originally suggested for this event at Ocean View was ~0.2 m (Shennan and Hamilton, 2006).

The sphagnum peat-turfa peat couplet at Ocean View is marked by a distinct shift in diatom assemblages across the contact (Figure 5.1). This assemblage change serves as an analogue when investigating peat records for evidence of small (<0.2-0.3m) subsidence elsewhere. There is a pronounced increase in *Navicula peregrina*, which peaks at 48% abundance (Figure 5.1), alongside an increase in *Delphineis surirella*, *Paralia sulcata* and *Pinnularia microstauron* and a decrease in *Navicula cari var cincta, Nitschia sigma, Pinnularia lagerstedtii* and *Denticula subtilis*. This differs from the peat- silt contact (Peat D, OV6) analysed by Hamilton et al. (2005) in their Shore Drive, Ocean View transect at the EQ1 contact, where high abundances of *Diploneis ovalis, Epithemia turgida, Pinnularia intermedia* and *Rhopalodia gibba* in the underlying peat are replaced by polyhalobous and mesohalobous diatoms such as *Delphineis surirella*, *Achnanthes delicatula, Cyclotella striata and Rhopalodia operculata* in the overlying silt. This may be because the marsh surface elevation immediately prior to the earthquake would have been lower in the Hamilton et al. (2005) core and hence subsidence would have lowered the marsh surface sufficiently to deposit silt which is not seen in this study.

The sharp increase in *Navicula peregrina* which is the 'signature' of the EQ1 event in the new core, suggests a pronounced drop in PMSE as *Navicula peregrina* is predominantly found on tidal flats in south-central Alaska (Shennan et al. 1999). However, the transfer function results for the Full Alaskan 225- 250 SWLI model suggest only an 0.08 m +/- 0.15 m drop in land level, with close modern analogues across the contact. This agrees with the lithology of the core, which remains as peat with no discernible minerogenic content after the event. This suggests that the elevation drop must have been short-lived, or the spike in poly- and meso-halobian species was caused by short-lived wave action (e.g. a tsunami), with peat continuing to form in the years immediately after the event.

Additionally, before reaching its peak abundance of 48% at 132 cm (Figure 4.1), the results show that *Navicula peregrina* increases in the years immediately prior to the drop in elevation, providing potential evidence of a preseismic signal. The idea of a 'preseismic signal' in Alaskan salt marshes was introduced by Shennan and Hamilton (2006) who suggest that all of the peat–silt couplets used within the study that record great earthquakes in the last 3300 years show evidence of pre seismic land subsidence. However, research surrounding preseismic signals is lacking, and thus I cannot confidently conclude the increase in *Navicula peregrina* is evidence of a preseismic signal. An alternative explanation for the increase in *Navicula peregrina* immediately prior to the peat-peat contact at 132 cm may be a result of sediment mixing across

the contact. Whilst Shennan and Hamilton (2006) argue for evidence of preseismic signals within Alaskan salt marsh diatoms, they also note the effect of sediment mixing across sedimentary contacts as a possibility for the changes in elevation reconstructed immediately before great earthquakes. Variations in the density of turfa and sphagnum peat, sedimentation rates, tidal fluctuations and bioturbation can all cause sediment mixing across coseismic contacts within salt marsh sediments.

The results of this thesis have implications for palaeosiesmological research, as it challenges the necessity of meeting the criteria outlined by Nelson et al. (1996) to detect vertical land displacement caused by earthquakes in Alaska. The 4th criteria outlined by Nelson et al. (1996) states that peat-silt contacts are laterally extensive with a sharp contact. Moreover, Shennan et al. (2016) argues that a detection limit of 0.1 – 0.2 m is possible, but states that at all the sites they visited in south-central Alaska, stratigraphic evidence of relative land subsidence was indicated by the presence of peat-silt couplets.

Condradictory to Nelson et al (1996) and Shennan et al. (2016), this study shows that land-level change associated with earthquakes can be recorded within marsh sediments at a peat-peat couplet, instead of a peat-silt couplet. However, whilst a peat-silt couplet does not need to be present to record earthquakes, without tracing the known peat-silt couplet inland until it changed to a peat-peat couplet, the EQ1 event would have been hard to detect. Previous research (Hamilton et al. 2005) allowed me to correlate the peat-peat contact to EQ1 and thus provide confidence regarding the depth in core of the EQ1 event. Consequently, I suggest that the ability to detect a known earthquake at a peat-peat contact (as opposed to non-seismic displacement), requires the identification of a lithological boundary which is traced from peat-silt contacts formed lower in the intertidal zone. Research by Brader et al. (2021) found similar results with regards to lithological constraints when establishing detection limits associated with the 2016 Chiloé earthquake. Still, Brader et al. (2021) also note that tsunami deposits may overcome the lithological constraints needed by identifying tsunami deposits as a guide for diatom sampling in instances of small magnitude co-seismic deformation. However, for this study, I identified no tsunami deposits in our fossil cores.

5.3. RQ 3 - How does training set selection influence the magnitude of reconstructed surface deformation?

Investigation of EQ1 at Ocean View demonstrates that the magnitude of subsidence reconstructed by the transfer function varies significantly according to the choice of modern training set. For

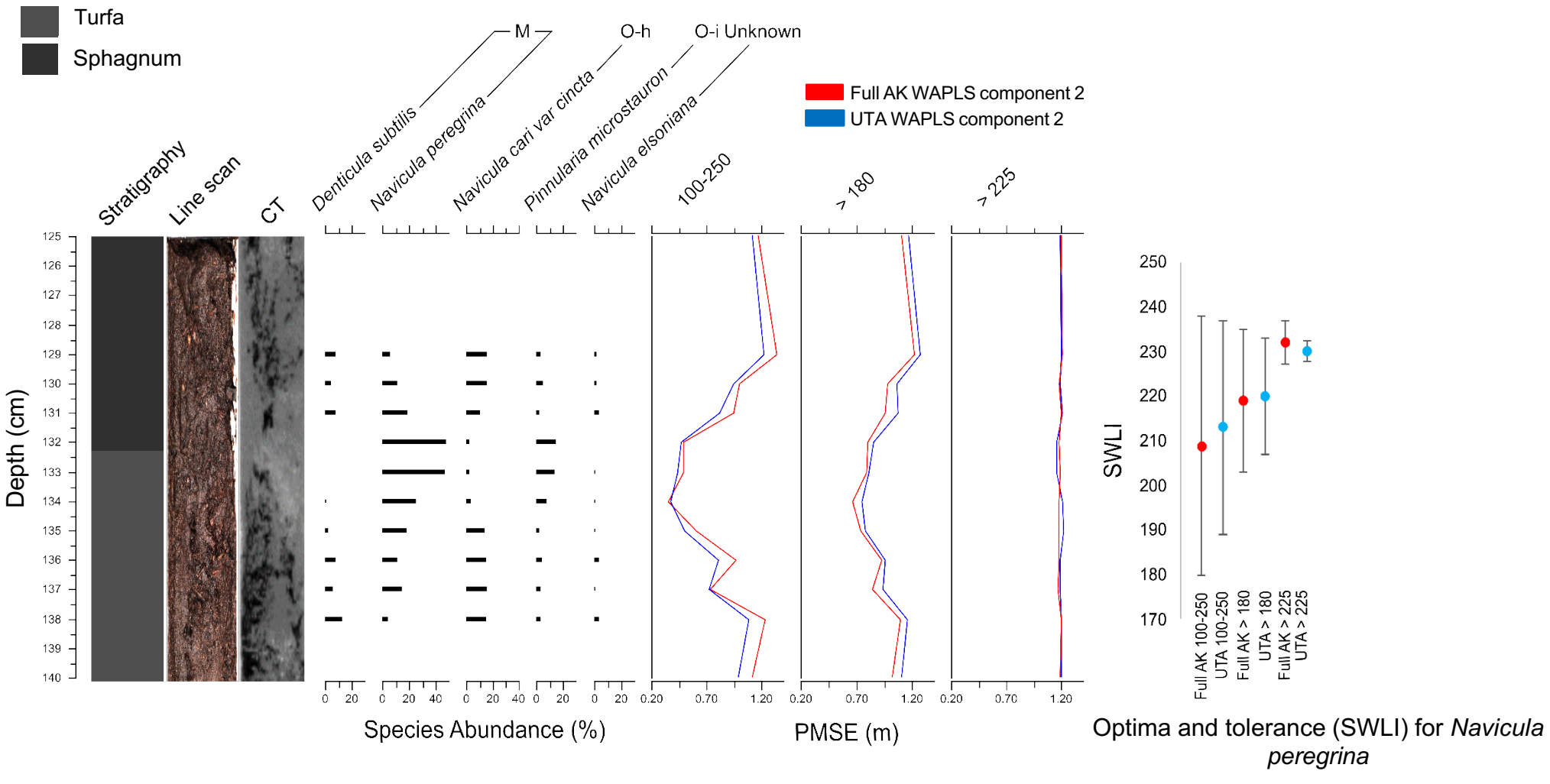

Figure 5.1 shows the stratigraphy, diatoms (> 25%) and reconstructed PMSE during EQ1 at Ocean View. The Optima (circle) and tolerance (lines) are shown alongside. It is evident that the optima decreases and the tolerance increases, the training set size also increases, and this is causing the increasing magnitude of the PMSE.

comparison with the new results presented here, Shennan and Hamilton (2006) reconstructed 0.2 m subsidence from the peat-silt couplet at Ocean View.

5.3.1. Subdividing training sets based on core lithology

As the number of samples and the environmental gradient length in the training set increases, the magnitude of reconstructed land-level changes associated with EQ1 also increases. The Full Alaskan 225-250 SWLI and Upper Turnagain Arm > 225 SWLI training sets reconstruct RSL changes of 0.08 m and 0.06 m respectively, for EQ1. The > 225 and 225-250 SWLI training sets were created to reconstruct peat sections, and they yield the lowest RMSEP values of the models developed in this study by excluding lower marsh elevations. The > 225 and 225-250 SWLI training sets are the only training sets applied in the transfer function models that result in reconstructed subsidence estimates of less than 0.1 m for EQ1.

However, these reconstructions demonstrate the difficulties in differentiating between co-seismic subsidence and non-seismic displacement when detecting small level land changes. Our results for the > 225 and 225-250 SWLI models indicate that EQ1 does not exhibit a significant fall in PMSE or a rise in RSL compared to the variability observed throughout the rest of the core – and thus it may not be possible to differentiate between seismic and non-seismic displacement. For example, Hamilton et al. (2005) found potential evidence of a co-seismic event in the stratigraphy at Girdwood in a peat layer formed between 2472-2763 cal yr BP. However, they note the difficulties with reconstructing low magnitude land subsidence, suggesting that since the elevation changes are small, co-seismic subsidence may be indistinguishable from non-seismic relative sea-level change. Instead, they suggest the simplest explanation for the RSL oscillation, which is distinguishable from natural variability caused from atmospheric-ocean factors, is that isostatic movements (which are independent of co-seismic processes) occurred during the Little Ice Age, 650– 100 cal. yr BP causing land level changes. The result of this thesis emphasises the findings of Shennan et al. (2016), who suggests the attribution of decimetre scale subsidence to a seismogenic source is not feasible without a lithological constraint (i.e. a peat-silt contact from which to trace a landward peat-peat contact).

The > 180 SWLI training sets reconstruct larger subsidence associated with EQ1, with a change in RSL of 0.5 ± 0.45 m and 0.47 ± 0.31 m for the Full Alaskan and Upper Turnagain Arm training sets respectively. The > 180 SWLI training set was created to reconstruct samples composed of 'silts with rootlets'. Given that these training sets encompass more samples from lower elevations in the environmental gradient, it is expected that the > 180 SWLI models will produce larger estimates of co-sesimic subsidence then the > 225 SWLI models. The core

analysed in this study does not contain any silt with rootlets below the EQ1 event contact, so it is expected that a transfer function which includes these modern environments will overpredict the magnitude of the land subsidence because the transfer function uses longer distributions of key species along the environmental gradient than if a shortened gradient is used (i.e.. > 225/225- 250 SWLI units) (Figure 5.2). The 100-250 SWLI training sets reconstruct the largest magnitudes of subsidence, with the Full Alaskan and Upper Turnagain Arm training sets reconstructing subsidence of 0.94 ± 0.55 m and 0. 8 ± 0.09 m, respectively. These training sets were designed to be used across peat-silt couplets, thus also incorporating SWLI elevations from the lower end of the environmental gradient.

Given that the fall in PMSE / rise in RSL at the EQ1 event is driven largely by a spike in *Navicula peregrina*, a species predominantly found at low elevations on tidal flats (Shennan et al. 1999), it is expected that the 100-250 SWLI training set would produce the largest magnitudes of PMSE fall/RSL rise. This is reflected in the optimum SWLI value for *Navicula peregrina*, which is at lower elevations as more samples lower in the environmental gradient are included (Figure 5.2) (See Appendix 4 for all species optima and tolerance values). The 100-250 SWLI transfer functions produce similar results to those produced by Watcham et al. (2013), who argue that there was 0.9 ± 0.4 m of subsidence during EQ1 at Ocean View when applying a sub- regional (Cook inlet) training set to fossil samples from core OV6. However, I argue that due to a high percentage of poor analogues in the Watcham et al. (2013) training sets, I must treat their results with caution. For ~0.9 m of subsidence to have occurred at the new core site, and the environment to have remained as 'peat-forming' (ie. above 225 SWLI, above 0.7-1 m above MHHW) post-event, the sediment surface pre-event must have been at least 1.6 m above MHHW (0.7 m MHHW + 0.9 m). This means the pre-event sediment surface would have to have been at least 278 SWLI. Looking at the Alaska Full training set, modern samples at around this elevation have <5 % poly and mesohalobian diatom species within them. The samples immediately below the EQ1 contact in the fossil core from Ocean View have 30-50 % poly and mesohalobian species within them (Figure 5.1), suggesting the palaeomarsh surface before EQ1 was in the range between 225-240 SWLI. On this basis I reject the estimate of 0.9 m of subsidence during EQ1 before making a quantitative estimate using a transfer function.

Whilst transfer function model selection has a significant influence on the magnitude of the reconstructed surface deformation associated with EQ1, all of the training sets reconstruct the same sign (submergence), which supports the findings outlined by Shennan et al. (2016), who investigated detection limits in south-central Alaska to update the criteria outlined by Nelson et al. (1996). Shennan et al. (2016) suggests that one of the criteria for attributing small amounts

of land subsidence to seismic activity is that quantitative estimates of elevation change across the contact from several different independent transfer function models all indicate the same sign. Therefore, it can be concluded that whilst different models produce different magnitudes of change, the models are consistently reconstructing submergence at EQ1.

In summary I recommend using the Full AK 225-250 SWLI training set for reconstructing subsidence in peat-forming environments, as it provides the most analogues when compared other training sets, shows a similar magnitude of subsidence during EQ1 to that recorded by Hamilton and Shennan (2005) and supports the theoretical framework of using a peat only model.

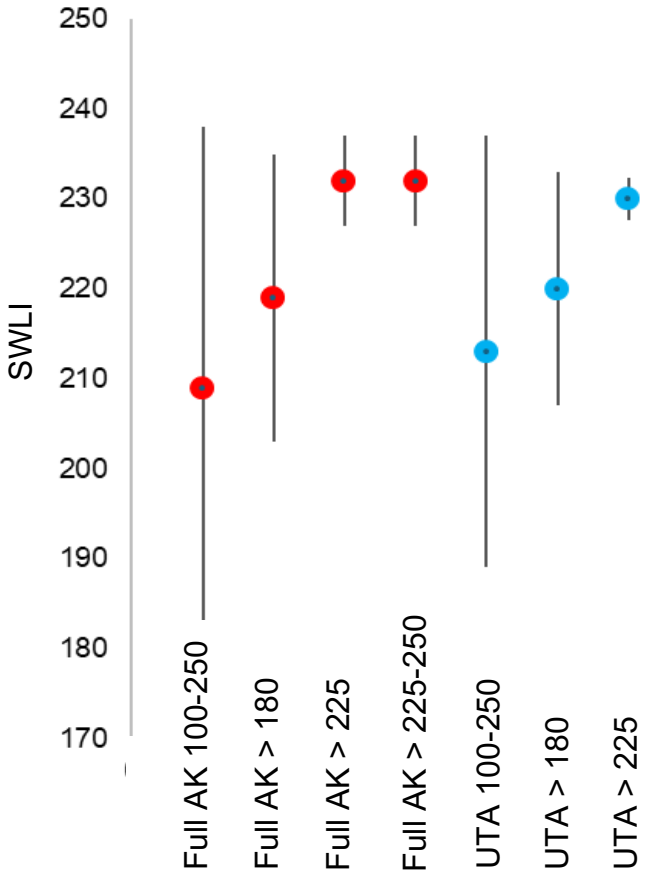

Figure 5.2. Optima (circles) and tolerance (error bars) for *Navicula peregrina* created using the Weighted Averaging model using 7 different training sets.

5.3.2. Local vs regional training sets

The local training set, comprising sites from Upper Turnagain Arm (Hope, Ocean View, and Girdwood), was anticipated to produce lower RMSEP values than the regional training set, due to some less important environmental variables (e.g., grain size) being more consistent across samples at sites in closer proximity, thereby minimizing the influence of factors other than

elevation (Kemp, 2015). This study has shown that when running the various transfer function models, the local training sets show a significant reduction in RMSEP values compared to the regional training sets (e.g. Full AK training set RMSEP is 29.8 SWLI units, UTA training set RMSEP is 9.4 SWLI units, Table 4.1). However, whilst RMSEP for the local training set is lower, the local training sets yield a smaller number of 'good' or 'close' modern analogues than the regional training sets. This is seen particularly across the EQ1 event where the Full AK 100-250 model is 'close' before the event and 'good' after, whilst the AK 100-250 model is 'poor' before the event and 'close' after (Table 4.3). The issues with local training sets producing poor modern analogues have also been noted in previous studies, such as by Watcham et al. (2013) who investigated scale considerations for using diatom training sets in Alaska. For example, the > 225 SWLI Full Alaskan model has 26 close modern analogues when reconstructing the Ocean View fossil core, whereas when the UTA > 225 training set is applied, the number of close modern analogues is zero. This pattern is consistent across all training sets, with regional training sets consistently providing more modern analogues than local ones. Although RMSEP decreases with local training sets, the lack of modern analogues indicates that regional training sets are more appropriate for this study.

5.4. RQ4 - Is there evidence of decimetre-scale surface deformation caused by additional earthquakes other than EQ1 at Ocean View or Girdwood?

5.4.1. Evidence of additional earthquakes at Ocean View

Whilst evidence of EQ1 is seen in the form of a peat-peat boundary, a spike in *Navicula peregrina* and other mesohalobian species and a transfer-function predicted rapid fall in PMSE and rise in RSL, there appears to be no evidence of other earthquakes recorded in the peat core from Ocean View between the 1500 cal. yr BP and 1964 CE events. Apart from EQ1, only one other notable change in diatom assemblages and PMSE/RSL is observed in the Ocean View core (figure 4.13). The base of the core (167-203 cm) has diatom assemblages that are markedly different from the rest of the core, characterized by a dominance of freshwater species such as *Tabellaria flocculosa* and *Synedra ulna*. Based on previous studies where these species are found, this section of the core likely reflects a terrestrial environment (Hustedt 1930, Krammer and Lange-Bertalot 1991). The change from this *Tabellaria flocculosa*- dominated assemblage to a *Navicula cari var cincta*-dominated assemblage at around 167 cm is reconstructed by some models as a decrease in PMSE and a rise in RSL which may at first glance appear to be evidence for co-seismic subsidence (Figures 4.10 and 4.12a). However, it is more likely that this shift in diatom species and PMSE/RSL reflects a change in environmental conditions as opposed to

changes in elevation. *Tabellaria flocculosa*, which dominates this section of the core, can be associated with standing water bodies (Hamilton et al. 2023), like the environment seen in transect two of the Girdwood moderns, where surface samples were collected in ponded water and *Tabellaria flocculosa* is dominant (Figure 4.2). The decrease in marine diatoms from 167 cm up core may therefore be due to slow but continuous inter- seismic uplift or another geomorphic process unrelated to the earthquake deformation cycle, which may have changed the marsh from a more waterlogged to better drained system over time. A more drained system will be less saline in nature, and therefore provide conditions for the increase in fresh water diatoms, and decrease in marine diatoms. The lack of stratigraphic variation in this section of the core further supports the idea that it is unlikely to be recording earthquake-related land subsidence.

5.4.2. Evidence of additional earthquakes at Girdwood

EQ1 and 1964 CE earthquake are both recorded as peat-silt couplets at Girdwood (Hamilton and Shennan 2005). The stratigraphy between these two events in the sample core consists of silt (218-130 cm) and peat (130-42 cm). In the silt layer (218-130 cm), even if there were smaller earthquakes which occurred during silt deposition, they would not be easy to identify because of the dominance of planktonic diatom species such as *Paralia sulcata*, which does not have tight elevation tolerances (Figure 4.15). Bartsch-Winkler and Schmoll (1992) suggest that if all or part of a submerged marsh did not become re-established before the next subsidence event, evidence of that event would be lacking or very difficult to identify. In addition, there are no spikes in *Navicula peregrina* or other poly- or mesohalobian species in the peat layer (130-42 cm, Figure 4.15). This lack of evidence for rapid increases in marine diatoms suggests that there were no ~0.2 m magnitude subsidence events between 515-318 cal yr BP (dated base of peat layer, Hamilton and Shennan 2005) and 1964 CE (top of peat layer). This assumes that the signature of EQ1 subsidence in the peat-forming environment at Ocean View is a good analogue for similar-sized events at other sites in south-central Alaska.

5.4.3. Implications for seismic hazards

Apart from EQ1 identified at the peat-peat boundary at Ocean View, no additional seismic events were detected between EQ1 and 1964 CE events at Ocean View or Girdwood. The results suggest several possibilities: either no earthquakes ≤ Mw 8 occurred between the 1964 CE event and EQ1, and thus stress accumulation on the megathrust is likely released during infrequent but great earthquakes rather than frequent smaller events, or earthquakes of a smaller magnitude are not preserved due to the creation and/or preservation threshold not being exceeded. However, this study disproves the second possibility, since I now know from the results of this thesis that low magnitude events can be preserved in fossil peats. Additionally, the results could

be a consequence of varying slip distributions on the fault. Whilst great earthquakes such as the 1964 CE and EQ1 events can be identified in the bio- and litho-stratigraphy, additional earthquakes may not be recorded if they have a different slip distribution. This also poses the possibility that additional earthquakes may be recorded within the stratigraphy at other sites within south-central Alaska not analysed in this thesis. Thus, the geological history of Mw 7–7.9 earthquakes in south-central Alaska remains poorly understood. Briggs et al. (2023) note the discrepancies between the recurrence interval of earthquakes in the Prince William Sound using their geodetic data vs observed geological data. They suggest the geodetic estimate for Mw ≥ 8 earthquakes is only ~200-300 years, whereas Shennan et al. (2014) suggest the geological estimate for the recurrence interval is 594 ± ~20 years. To explain the geologic record, one possible cause is that smaller earthquakes (≤ Mw 8) still remain undetected in paleoseismic records from coastal marshes in the region.

Tidal marsh records from other marshes in south-central Alaska may similarly underestimate or fail to record large (Mw 7-7.9) earthquakes. Consequently, if recurrence intervals are calculated or seismic hazard assessments are developed based on coastal marsh palaeoseismology; this limitation must be taken into consideration. The underrepresentation of major earthquakes also limits the ability to assess the role of smaller earthquakes in releasing accumulated strain (Brader et al. 2021). While the current recurrence interval for a magnitude 9 earthquake in south-central Alaska is estimated at every 650 years, the interval between the 1964 CE earthquake and EQ1 is approximately 785 ± 10 years (Barclay et al. 2024). This thesis, therefore, does not provide additional insight into whether this irregular time interval reflects natural variability in the time-dependent behaviour of the megathrust or if it is related to smaller earthquakes occurring in the Prince William Sound segment during the interseismic period, which may have released stress on the megathrust. It does however provide important new insights into the signature of a small subsidence event in a high marsh which may give future researchers confidence to look for smaller events in other high marsh settings in south-central Alaska.

Chapter 6: Conclusions and Future Research

6.1. Summary of findings

This project aimed to investigate whether a peat-peat contact from EQ1 provides diatom evidence of submergence, and whether this signature can be seen elsewhere as evidence of submergence <0.2 m, potentially from previously undetected earthquakes in the range between Mw 7-7.9.

At Ocean View, I traced a peat-silt couplet into the high marsh until it transitioned into a peat-peat couplet, representing EQ1. I did this as the high marsh consists of peat-forming communities where the most precise quantitative estimates of vertical deformation can be reconstructed. AMS dating, the pronounced spike in *Navicula peregrina* and other mesohalobian diatoms, a sudden fall in PMSE and rise in RSL at this peat-peat contact all provide evidence of EQ1. Using the Full Alaskan 225-250 SWLI training set, multiple models reconstructed subsidence to be ~0.1 m +/- 0.15 m. However, the magnitude of subsidence is dependent on the training set used, as magnitude increases as more modern samples lower in the environmental gradient are included. Nonetheless, this study has shown evidence of a known earthquake at a peat-peat contact, with all transfer functions showing the same sign of change (subsidence). I recommend using the Full AK > 225- 250 training set to reconstruct subsidence at Ocean View, since it predicted a similar amount of subsidence to previous studies (Hamilton et al. 2005) and provided 'good' and 'close' analogues for the fossil samples. No diatom evidence for additional earthquakes were identified in the peat core from Ocean View.

No peat-peat contact was identified for EQ1 in the stratigraphy at Girdwood. Instead, EQ1 is seen as a peat-silt contact. No evidence of smaller earthquakes was found in the peat layer at Girdwood, which represents the time period between 515-318 cal. yr BP and 1964 CE.

This study has implications for palaeoseismological research. Firstly, it highlights the dependency of the reconstructions on the training set used, and therefore it is important to be able to justify restricting the elevation range of the training set using an independent constraint (e.g. lithology), as constraining the training set will significantly influence the magnitude of reconstructed co-seismic subsidence. It also draws attention to the difficulties in differentiating seismic vs non-seismic activity when reconstructing submergence events ~0.1 m, because some changes in diatom assemblages may be unrelated to co-seismic activity. Furthermore, this study challenges the necessity of meeting the criteria outlined by Nelson et al. (1996), whereby a great earthquake is manifested in the form of a long-lasting change in PMSE and RSL over a peat-silt couplet. Instead, this study has shown that a great earthquake can be

recorded by a peat-peat couplet, and by a temporary change in PMSE and RSL over a limited time period (a few years). Finally, this thesis highlights that when reconstructing PMSE and RSL in high marsh environments the diatom communities there may vary because of local conditions (e.g. waterlogging) as well as elevation change, and therefore a large training set which includes samples from a wide range of environments in the intertidal zone is necessary to ensure good modern analogues for fossil samples.

6.2. Future research

The results from this thesis can be used as a guideline for framing future research. This thesis shows that it is possible to identify coseismic events using diatoms in peat sequences, and that the large training set of Alaskan diatoms which already exists is useful for developing quantitative PMSE and RSL reconstructions across peat-peat contacts. Therefore the same methodology could be rolled out at other high marsh sites in South Central Alaska to look for smaller events that may have occurred in the time periods between documented Great earthquakes.

An important conclusion from the diatom work in this thesis is that it is worth exploring in future using different microfossil groups such as foraminifera to compare to results derived from diatom-based transfer functions. This thesis indicates that many diatom species in the modern samples, such as *Navicula peregrina*, exhibit broad ecological tolerances. *Navicula peregrina* appears across a wide SWLI range, including tidal flats and low marsh environments. However, in the Ocean View fossil core, which is made entirely of peat, and thus formed at SWLI values above 225, *Navicula peregrina* dominates abundances (max 48%) at the peat-peat contact of EQ1. Using the lithologically constrained training sets reduces the length of the environmental gradient in which a species is found, and thus if only one extreme end of the distribution is included (i.e. > 225), the model may not capture the full range of diatom responses across the environmental gradient. As a result, the training sets may over or under predict the magnitude of subsidence at EQ1. Future research should investigate using other microfossils that have smaller tolerances in high marsh environments to ensure that transfer function-based reconstructions are not model-dependent. Then, the environmental gradient can be justifiably constrained to high marsh environments if the dominant species used in the reconstruction are only found in the high marsh. Instead of diatoms, which have broad tolerances in Alaskan marshes due to the large tidal ranges (8 m at Ocean View, 9.2 m at Girdwood), studies expanding on this work could investigate the use of foraminifera to determine detection limits in peat environments. Furthermore, Cahill et al. (2016) found that six

of the eight most dominant foraminifera in 12 saltmarshes in southern New Jersey, USA, do not conform to the unimodal, Gaussian response curve assumed in Weighted Averaging transfer function models. Consequently, future research should consider the use of Bayesian transfer function models which do not require unimodal microfossil response curves, since dominant species like *Navicula peregrina* have also been shown elsewhere do not always conform to a unimodal distribution (Laird and Edgar, 1992, Potapova et al. 2004).

In conclusion, this thesis has aimed to identify and reconstruct the magnitude of earthquake (EQ1, ~771 cal yr BP) at Ocean View for the first time from a high marsh, peat-forming environment. Modern diatom data suggests that the high marsh is where the highest precision PMSE reconstructions are possible, and therefore also a lower detection limit should be achievable. Using AMS dating, shifts in diatom assemblages and a series of transfer function models, a pronounced fall in PMSE provides evidence of the ~771 cal yr BP earthquake in the high marsh at Ocean View which is not visible in the stratigraphy alone. This study also shows that the magnitude of the reconstructed subsidence is dependent on transfer function model selection. A regional peat only modern training set in conjunction with a WA-PLS transfer function provides the most plausible amount of subsidence (~0.1 m) for the ~771 cal yr BP earthquake whilst providing good analogues before and after the event. Applying this newly developed methodology to a mainly peat core from the high marsh at Girdwood, there is there is no diatom evidence for additional earthquakes in the period between 515-318 cal yr BP (dated base of peat layer, Hamilton and Shennan 2005) and 1964. This may be correct but there is still the possibility that diatoms are not sufficiently sensitive to small amounts of subsidence in some settings, leading to the suggestion that future work could both roll out the methodology developed in this thesis to other coastal high marsh settings in South Central Alaska to identify hitherto unidentified smaller events that may occur between Great earthquakes, but also to investigate the potential for other high marsh microfossils such as foraminifera to provide complementary data on PMSE changes that may provide even lower detection limits than are possible using diatom data.

Appendix

Training set	Model	R2	RMSEP
Full AK	WA_Inv	0.54787	31.1489
Full AK	WA_Cla	0.548937	38.0845
Full AK	WATOL_Inv	0.500124	33.3089
Full AK	WATOL_Cla	0.502031	39.4878
Full AK	WAPLS Component 1	0.546668	31.1978
Full AK	WAPLS Component 2	0.605867	29.8207
Full AK	WAPLS Component 3	0.620589	30.5011
Full AK	WAPLS Component 4	0.629438	31.067
Full AK	WAPLS Component 5	0.623085	32.0638
Full AK	MAT	0.765158	24.5895
Full AK	WMAT	0.797348	22.8129
Full AK	Est_ML	0.527352	34.6231
Full AK	LWWA_Inv	0.779141	23.0107
Full AK	LWWA_Cla	0.784859	23.0353
Full AK 100-250	WA_Inv	0.75281	16.1425
Full AK 100-250	WA_Cla	0.753592	17.1362
Full AK 100-250	WATOL_Inv	0.578302	22.116
Full AK 100-250	WATOL_Cla	0.578517	26.3294
Full AK 100-250	WAPLS Component 1	0.753019	16.1677
Full AK 100-250	WAPLS Component 2	0.816876	14.1209
Full AK 100-250	WAPLS Component 3	0.828668	13.9847
Full AK 100-250	WAPLS Component 4	0.833588	14.1708
Full AK 100-250	WAPLS Component 5	0.840603	14.3086
Full AK 100-250	MAT	0.745408	17.1243
Full AK 100-250	WMAT	0.77993	15.945
Full AK 100-250	Est_ML	0.774304	18.1151
Full AK 100-250	LWWA_Inv	0.824699	14.1745
Full AK 100-250	LWWA_Cla	0.827455	14.2374
Full AK >180	WA_Inv	0.572311	13.0257
Full AK >180	WA_Cla	0.574143	15.2757
Full AK >180	WATOL_Inv	0.547075	13.792
Full AK >180	WATOL_Cla	0.548708	16.03
Full AK >180	WAPLS Component 1	0.571629	13.0379
Full AK >180	WAPLS Component 2	0.6705	11.8367
Full AK >180	WAPLS Component 3	0.687169	11.8912
Full AK >180	WAPLS Component 4	0.690209	12.3409
Full AK >180	WAPLS Component 5	0.693006	12.7689
Full AK >180	MAT	0.696386	11.7943
Full AK >180	WMAT	0.733401	11.0913
Full AK >180	Est_ML	0.656971	12.9077
Full AK >180	LWWA_Inv	0.763898	10.4228
Full AK >180	LWWA_Cla	0.777884	10.2138
Full AK > 250	WA_Inv	0.505563	8.98269
Full AK > 250	WA_Cla	0.51231	9.92466
Full AK > 250	WATOL_Inv	0.411493	9.90756
Full AK > 250	WATOL_Cla	0.420436	10.7242
Full AK > 250	WAPLS Component 1	0.498345	9.04077
Full AK > 250	WAPLS Component 2	0.567951	8.7866
Full AK > 250	WAPLS Component 3	0.576159	8.972
Full AK > 250	WAPLS Component 4	0.569186	9.24326
Full AK > 250	WAPLS Component 5	0.560678	9.53882
Full AK > 250	MAT	0.557013	8.8442
Full AK > 250	WMAT	0.596287	8.46372
Full AK > 250	Est_ML	0.49186	9.31569
Full AK > 250	LWWA_Inv	0.581864	8.42457
Full AK > 250	LWWA_Cla	0.583403	8.49098
Full AK 225-250	WA_Inv	0.483163	4.39401
Full AK 225-250	WA_Cla	0.487365	5.00037
Full AK 225-250	WATOL_Inv	0.532467	4.30875
Full AK 225-250	WATOL_Cla	0.535787	4.74153
Full AK 225-250	WAPLS Component 1	0.481658	4.38859
Full AK 225-250	WAPLS Component 2	0.508211	4.51564
Full AK 225-250	WAPLS Component 3	0.527434	4.55093
Full AK 225-250	WAPLS Component 4	0.530776	4.65618
Full AK 225-250	WAPLS Component 5	0.522482	4.8234
Full AK 225-250	MAT	0.556049	4.12966
Full AK 225-250	WMAT	0.58876	3.96915
Full AK 225-250	Est_ML	0.545398	4.67965
Full AK 225-250	LWWA_Inv	0.579061	4.00395
Full AK 225-250	LWWA_Cla	0.576548	4.08668

Appendix 1, Table A. Transfer function performance results for the Full Alaskan training set. RMSEP = Root Mean Square Error of Prediction. WA_Inv = Weighted Averaging Inversed. WA_Cla = Weighted Averaging Classical. WATOL_Inv = Weighted Avergaing Tolerenace Inversed. WATOL_Cla = Weighted Averaging Classical. WAPLS = Weighted Avergaing Least Partial Squares. MAT = Modern Anaologue Technique, WMAT = Weighted Modern Analogue Technique. EST_ML = Maximum Liklihood. LWWA_Inv = Locally Weighted - Weighted Averaging Inverse. LWWA_Cla = Locally Weighted - Weighted Averaging Classical.

Training set	Model	R2	RMSEP
UTA	WA_Inv	0.77499	10.9216
UTA	WA_Cla	0.77683	11.4636
UTA	WATOL_Inv	0.75621	12.7041
UTA	WATOL_Cla	0.75662	12.844
UTA	WAPLS Component 1	0.77488	10.9235
UTA	WAPLS Component 2	0.83865	9.4698
UTA	WAPLS Component 3	0.87119	8.87164
UTA	WAPLS Component 4	0.87792	8.83878
UTA	WAPLS Component 5	0.88028	9.20563
UTA	MAT	0.80794	10.9567
UTA	WMAT	0.83402	10.1203
UTA	Est_ML	0.81935	10.7972
UTA	LWWA_Inv	0.87954	8.48126
UTA	LWWA_Cla	0.88253	8.55267
UTA 100-250	WA_Inv	0.77499	10.9216
UTA 100-250	WA_Cla	0.77683	11.4636
UTA 100-250	WATOL_Inv	0.75621	12.7041
UTA 100-250	WATOL_Cla	0.75662	12.844
UTA 100-250	WAPLS Component 1	0.77488	10.9235
UTA 100-250	WAPLS Component 2	0.83865	9.4698
UTA 100-250	WALPS Component 3	0.87119	8.87164
UTA 100-250	WALPS Component 4	0.87792	8.83878
UTA 100-250	WAPLPS Component 5	0.88028	9.20563
UTA 100-250	MAT	0.80794	10.9567
UTA 100-250	WMAT	0.83402	10.1203
UTA 100-250	Est_ML	0.81935	10.7972
UTA 100-250	LWWA_Inv	0.87954	8.48126
UTA 100-250	LWWA_Cla	0.88253	8.55267
UTA > 180	WA_Inv	0.60408	9.40096
UTA > 180	WA_Cla	0.60816	10.5635
UTA > 180	WATOL_Inv	0.65142	9.31003
UTA > 180	WATOL_Cla	0.65385	9.5856
UTA > 180	WAPLS Component 1	0.60421	9.39718
UTA > 180	WAPLS Component 2	0.72086	8.16385
UTA > 180	WALPS Component 3	0.79459	7.38401
UTA > 180	WALPS Component 4	0.81316	7.20368
UTA > 180	WAPLPS Component 5	0.81367	7.40194
UTA > 180	MAT	0.6893	8.72095
UTA > 180	WMAT	0.72585	8.22877
UTA > 180	Est_ML	0.73881	8.44791
UTA > 180	LWWA_Inv	0.78702	7.41519
UTA > 180	LWWA_Cla	0.7999	7.31112
UTA > 225	WA_Inv	0.41496	2.72996
UTA > 225	WA_Cla	0.42595	2.90362
UTA > 225	WATOL_Inv	0.45642	2.73216
UTA > 225	WATOL_Cla	0.46316	2.89786
UTA > 225	WAPLS Component 1	0.42019	2.70836
UTA > 225	WAPLS Component 2	0.48498	2.53577
UTA > 225	WALPS Component 3	0.46207	2.65872
UTA > 225	WALPS Component 4	0.44522	2.73949
UTA > 225	WAPLPS Component 5	0.42914	2.82729
UTA > 225	MAT	0.35633	2.81833
UTA > 225	WMAT	0.43201	2.64279
UTA > 225	Est_ML	0.41278	3.16952
UTA > 225	LWWA_Inv	0.43431	2.64712
UTA > 225	LWWA_Cla	0.40649	2.8505

Appendix 2, Table B. Transfer function performance results for the Upper Turnagain Arm training set. RMSEP = Root Mean Square Error of Prediction. WA_Inv = Weighted Averaging Inversed. WA_Cla = Weighted Averaging Classical. WATOL_Inv = Weighted Avergaing Tolerenace Inversed. WATOL_Cla = Weighted Averaging Classical. WAPLS = Weighted Avergaing Least Partial Squares. MAT = Modern Anaologue Technique, WMAT = Weighted Modern Analogue Technique. EST_ML = Maximum Liklihood. LWWA_Inv = Locally Weighted - Weighted Averaging Inverse. LWWA_Cla = Locally Weighted - Weighted Averaging Classical.

Training set	5th percentile	20th percentile
Full AK 100-250	55.406	91.0176
Full AK > 180	70.5676	114.535
Full AK > 225	85.3434	129.821
Full AK 225-250	82.9122	126.912
UTA 100-250	55.406	91.0176
UTA > 180	53.9679	89.1037
UTA > 225	47.4361	95.0968

Appendix 3. Table of the 5th and 20th percentiles of dissimilarity calculated using MAT for each training set.

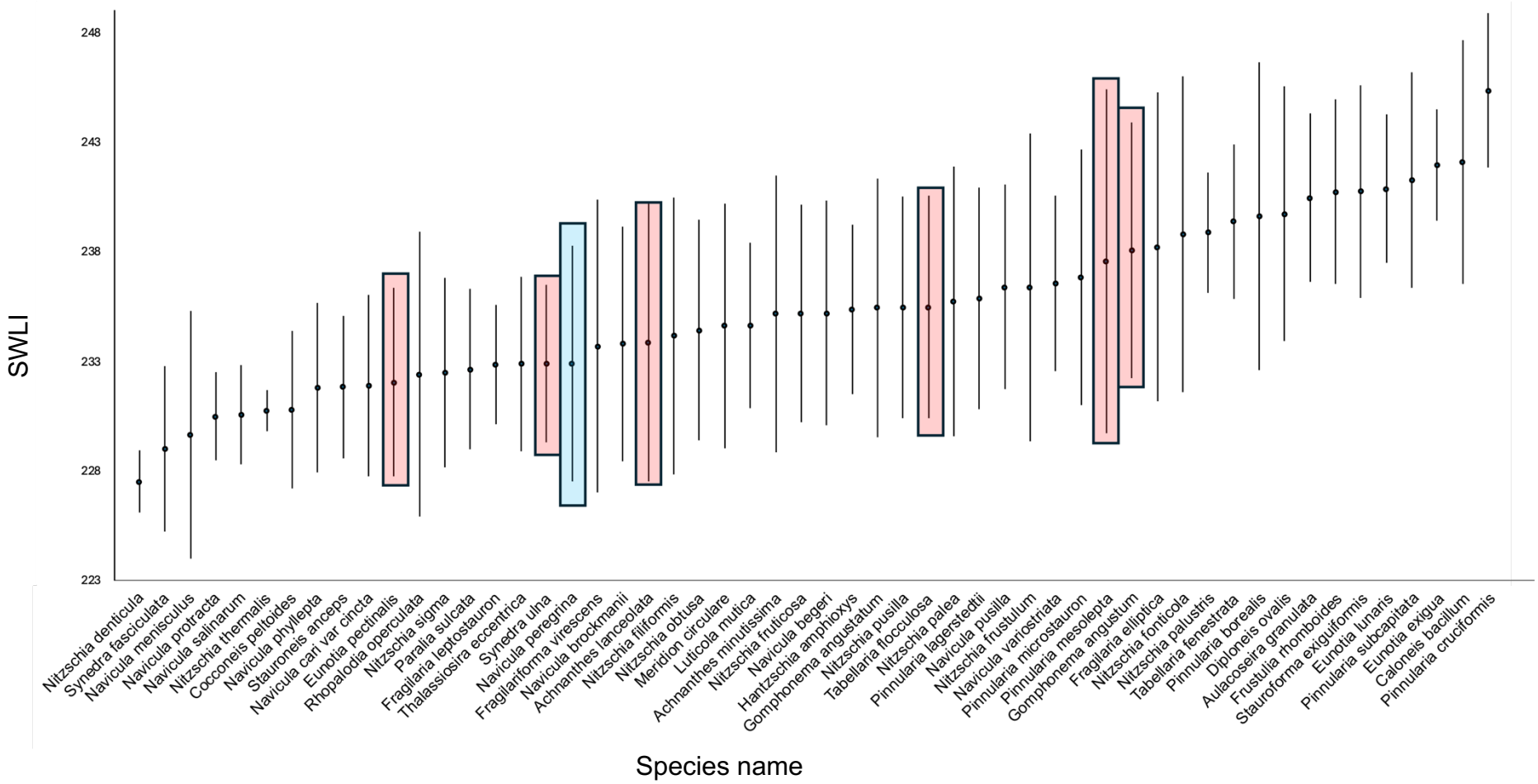

Appendix 4a. Optima (circle) and tolerance (line) for each species > 10% in the Full AK 225-250 dataset. Notable species found in the core section 167-203cm are highlighted in red. *Navicula peregrina* is highlighted in blue.

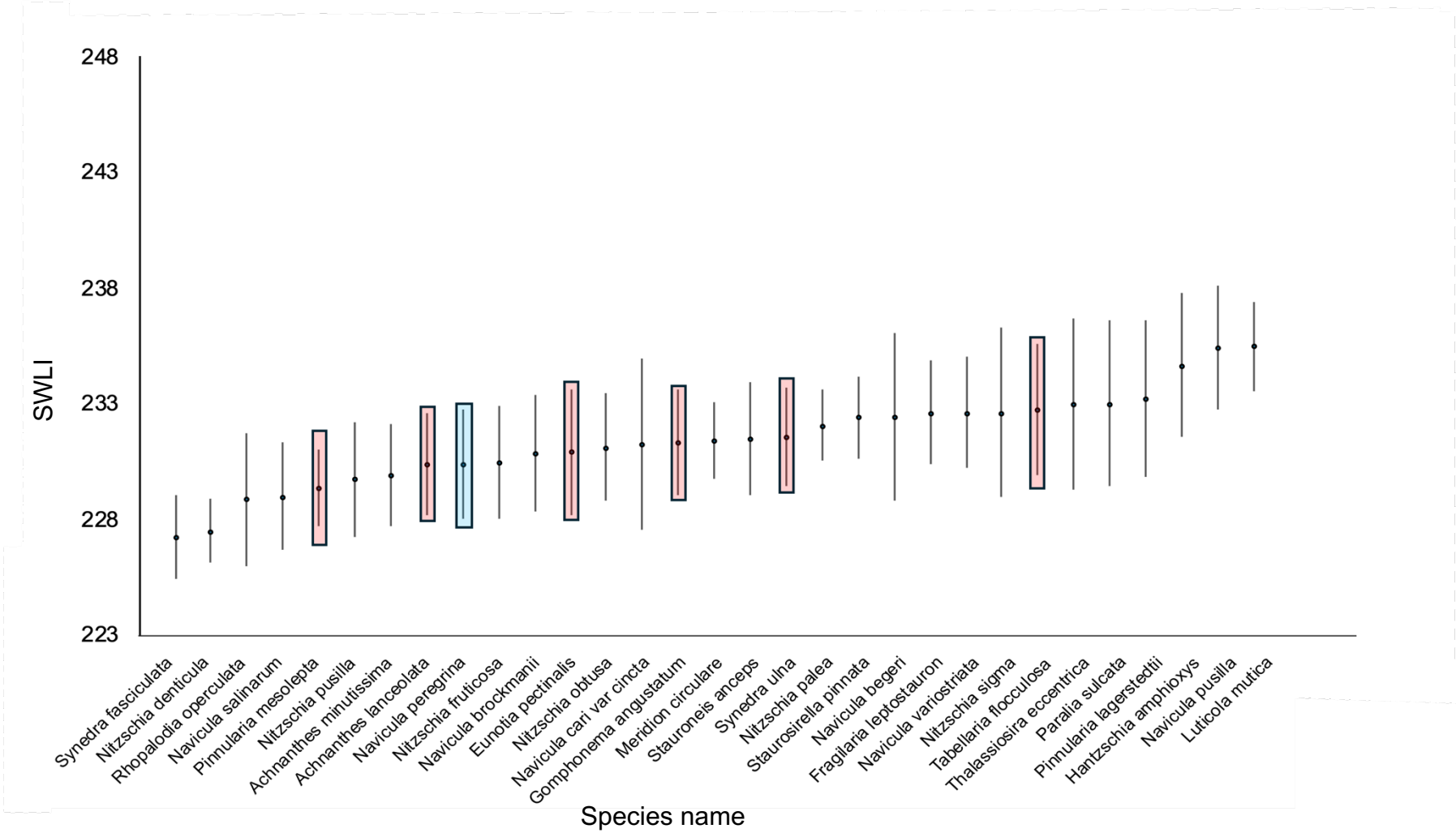

Appendix 4b. Optima (circles) and tolerance (lines) for species > 10% in the UTA 225-250 training set has also been plotted. The species overall have lower optima and a smaller tolerance. Notable species found in the core section 167-203cm are highlighted in red. *Navicula peregrina* is highlighted in blue.

List of References

Allen, J.R.L., 2000. Late Flandrian (Holocene) tidal palaeochannels, Gwent Levels (Severn Estuary), SW Britain: character, evolution and relation to shore. *Marine Geology*, *162*(2-4), pp.353-380.

Barclay, D.J., Haeussler, P.J. and Witter, R.C., 2024. Dating the penultimate great earthquake in south-central Alaska using tree-ring crossdating and radiocarbon wiggle- matching. *Quaternary Science Advances*, *13*, p.100142.

Barlow, N., 2010. *Glacial isostatic adjustment and relative sea level change over the last earthquake cycle in upper Cook Inlet, Alaska, USA* (Doctoral dissertation, Durham University).

Bartsch-Winkler, S. and Schmoll, H.R., 1992. Utility of radiocarbon-dated stratigraphy in determining late Holocene earthquake recurrence intervals, upper Cook Inlet region, Alaska. *Geological Society of America Bulletin*, *104*(6), pp.684-694.

Bender, A.M., Witter, R.C. and Rogers, M., 2015. Testing the use of bulk organic δ13C, δ15N, and Corg: Ntot ratios to estimate subsidence during the 1964 great Alaska earthquake. *Quaternary Science Reviews*, *113*, pp.134-146.

Bennett, K.D., 1996. Determination of the number of zones in a biostratigraphical sequence. *New Phytologist*, *132*(1), pp.155-170.

Bertness, M.D., Ewanchuk, P.J. and Silliman, B.R., 2002. Anthropogenic modification of New England salt marsh landscapes. *Proceedings of the National Academy of Sciences*, *99*(3), pp.1395-1398.

Birks, H.J.B., 1995. Quantitative palaeoenvironmental reconstructions. *Statistical modelling of quaternary science data. Technical guide*, *5*, pp.161-254.

Brader, M., Garrett, E., Melnick, D. and Shennan, I., 2021. Sensitivity of tidal marshes as recorders of major megathrust earthquakes: constraints from the 25 December 2016 Mw 7.6 Chiloé earthquake, Chile. *Journal of Quaternary Science*, *36*(6), pp.991- 1002.

Briggs, R., 2017. SSA Annual Meeting Report. *Seismological Research Letters*, 88(5), pp. 1341–1376. https://doi.org/10.1785/0220170121

Briggs, R., Witter, R., Freymueller, J., Powers, P., Haeussler, P., Ross, S., Dura, T., Engelhart, S., Koehler, R. and Thio, H.K., 2023. An Alaska-Aleutian subduction zone interface earthquake recurrence model from geology and geodesy. *American Geophysical Union.*

Briggs, R. W., & Barnhart, W. D. (2017). "The contribution of local sea level changes to long-term global trends." *Geophysical Research Letters,* 44(16), 8461–8469.

Brocher, T.M., Filson, J.R., Fuis, G.S., Haeussler, P.J., Holzer, T.L., Plafker, G. and Blair, J.L., 2014. *The 1964 great Alaska earthquake and tsunamis: A modern perspective and enduring legacies* (No. 2014-3018). US Geological Survey.

Brown, L.D., Reilinger, R.E., Holdahl, S.R. and Balazs, E.I., 1977. Postseismic crustal uplift near Anchorage, Alaska. *Journal of Geophysical Research*, *82*(23), pp.3369- 3378.

Cahill, N., Kemp, A.C., Horton, B.P. and Parnell, A.C., 2016. A Bayesian hierarchical model for reconstructing relative sea level: from raw data to rates of change. *Climate of the Past*, *12*(2), pp.525-542.

Cohen, S.C. and Freymueller, J.T., 1997. Deformation of the Kenai Peninsula, Alaska. *Journal of Geophysical Research: Solid Earth*, *102*(B9), pp.20479-20487.

Combellick, R.A. and Reger, R.D., 1994. *Sedimentological and radiocarbon-age data for tidal marshes along eastern and upper Cook Inlet, Alaska* (Vol. 93, No. 83). State of Alaska, Department of Natural Resources, Division of Geological and Geophysical Surveys.

Combellick, R.A., 1997. Evidence of prehistoric great earthquakes in the Cook Inlet region, Alaska. *Guide to the Geology of the Kenai Peninsula, Alaska, Alaska Geological Society.*

Cremer, H., Wagner, B., Melles, M. and Hubberten, H.W., 2001. The postglacial environmental development of Raffles Sø, East Greenland: inferences from a 10,000 year diatom record. *Journal of Paleolimnology*, *26*, pp.67-87.

Engelhart, S.E., Horton, B.P., Nelson, A.R., Hawkes, A.D., Witter, R.C., Wang, K., Wang, P.L. and Vane, C.H., 2013. Testing the use of microfossils to reconstruct great earthquakes at Cascadia. *Geology*, *41*(10), pp.1067-1070.

Fatela, F. and Taborda, R., 2002. Confidence limits of species proportions in microfossil assemblages. *Marine Micropaleontology*, *45*(2), pp.169-174.

Finkelstein, S.A. and Gajewski, K., 2008. Responses of Fragilarioid-dominated diatom assemblages in a small Arctic lake to Holocene climatic changes, Russell Island, Nunavut, Canada. *Journal of Paleolimnology*, *40*, pp.1079-1095.

Grimm, E.C., 1987. CONISS: a FORTRAN 77 program for stratigraphically constrained cluster analysis by the method of incremental sum of squares. *Computers & geosciences*, *13*(1), pp.13-35.

Hamilton, S.L., 2003. *Late Holocene relative sea-level changes and earthquakes around the upper Cook Inlet, Alaska, USA* (Doctoral dissertation, Durham University).

Hamilton, S. and Shennan, I., 2005. Late Holocene relative sea-level changes and the earthquake deformation cycle around upper Cook Inlet, Alaska. *Quaternary Science Reviews*, *24*(12-13), pp.1479-1498.

Hamilton, S., Shennan, I., Combellick, R., Mulholland, J. and Noble, C., 2005. Evidence for two great earthquakes at Anchorage, Alaska and implications for multiple great earthquakes through the Holocene. *Quaternary Science Reviews*, *24*(18-19), pp.2050-2068.

Hamilton, V.A., Lee, S.S., Rober, A.R., Furey, P.C., Manoylov, K.M. and Wyatt, K.H., 2023. A Voucher Flora of Diatoms from Fens in the Tanana River Floodplain, Alaska. *Water*, *15*(15), p.2803.

Hartley, B., Barber, H.G., Carter, J.R. and Sims, P.A., 1996. An atlas of British diatoms. *British Phycological Society.*

Hassan, G.S., Espinosa, M.A. and Isla, F.I., 2006. Modern diatom assemblages in surface sediments from estuarine systemsin the southeastern buenos aires Province, Argentina. *Journal of Paleolimnology*, *35*, pp.39-53.

Hatté, C. and Jull, A.J.T., 2007. RADIOCARBON DATING| plant macrofossils. *Encyclopedia of Quaternary Science*, pp.2958 2965.

Hemphill-Haley, E., 1993. *Taxonomy of recent and fossil (Holocene) diatoms (Bacillariophyta) from northern Willapa Bay, Washington* (No. 93-289). US Geological Survey.

Horton, B.P. and Sawai, Y., 2010. Diatoms as indicators of former sea levels, earthquakes, tsunamis, and hurricanes. *The diatoms: applications for the Environmental and Earth Sciences*, *2*, pp.357-372.

Hustedt, F., 1930. Bacillariophyta (diatomeae). *Die Susswasser-Flora Mitteleuropas*, *10*, pp.1-446.

Hustedt, F. and Aleem, A.A., 1951. Littoral diatoms from the Salstone, near Plymouth. *Journal of the Marine Biological Association of the United Kingdom*, *30*(1), pp.177-196.

Hutson, W.H., 1980. The Agulhas Current during the Late Pleistocene: Analysis of modern faunal analogs. *Science*, *207*(4426), pp.64-66.

Imbrie, J., Kipp, N.G., (1971). A new micropaleontological method for quantitative paleoclimatology: application to a Late Pleistocene Caribbean core.

Turekian, K.K., *The Late Cenozoic Glacial Ages Yale University Press New Haven* , pp.71–181.

Janigian, G., 2018. *A stratigraphic and microfossil record of coseismic land-level changes and tsunami deposits from Old Harbor, Central Kodiak Island, Alaska*. University of Rhode Island.

Juggins, S., 2001. The European diatom database. *User Guide, Version*, *1*, p.72.

Juggins, S., 2018. C2 Version 1.8. Software for ecological and palaeoecological data analysis and visualisation. Newcastle University, Newcastle upon Tyne, UK.

Juggins, S., Simpson, G.L. and Telford, R.J., 2015. Taxon selection using statistical learning techniques to improve transfer function prediction. The Holocene, 25(1), pp.130-136.

Kemp, A.C. and Telford, R.J., 2015. Transfer functions. *Handbook of sea-level research*, pp.470-499.

Krammer, K. and Lange-Bertalot, H., 1991. *Bacillariopyceae: 4. Teil: Achnanthaceae, Literaturverzeichnis*. Gustav Fischer.

Laird, K. and Edgar, R.K., 1992. Spatial distribution of diatoms in the surficial sediments of a New England salt marsh. Diatom Research, 7(2), pp.267-279.

Morales, E.A. and Manoylov, K.M., 2006. Morphological studies on selected taxa in the genus Staurosirella Williams et Round (Bacillariophyceae) from rivers in North America. *Diatom research*, *21*(2), pp.343-364.

Mueller, C.S., Briggs, R.W., Wesson, R.L. and Petersen, M.D., 2015. Updating the USGS seismic hazard maps for Alaska. *Quaternary Science Reviews*, *113*, pp.39-47.

Nelson, A.R., Jennings, A.E. and Kashima, K., 1996. An earthquake history derived from stratigraphic and microfossil evidence of relative sea-level change at Coos Bay, southern coastal Oregon. *Geological Society of America Bulletin*, *108*(2), pp.141-154.

NOAA Tides & Currents, 2023. Datums for 9455920, Anchorage, AK. [online] Available at: https://tidesandcurrents.noaa.gov/datums.html?id=9455920 [Accessed 20 September 2024].

Palmer, A.J. and Abbott, W.H., 1986. Diatoms as indicators of sea-level change. In *Sea-level Research: A Manual for the Collection and Evaluation of Data* (pp. 457- 487). Dordrecht: Springer Netherlands.

Patterson, R.T., Hutchinson, I., Guilbault, J.P. and Clague, J.J., 2000. A comparison of the vertical zonation of diatom, Foraminifera, and macrophyte assemblages in a coastal marsh;

implications for greater paleo-sea level resolution. *Micropaleontology*, *46*(3), pp.229-244.

Pilarczyk, J.E., Dura, T., Horton, B.P., Engelhart, S.E., Kemp, A.C. and Sawai, Y., 2014. Microfossils from coastal environments as indicators of paleo-earthquakes, tsunamis and storms. *Palaeogeography, Palaeoclimatology, Palaeoecology*, *413*, pp.144-157.

Plafker, G., 1965. Tectonic Deformation Associated with the 1964 Alaska Earthquake: The earthquake of 27 March 1964 resulted in observable crustal deformation of unprecedented areal extent. *Science*, *148*(3678), pp.1675-1687.

Plafker, G., 1969. *Tectonics of the March 27, 1964, Alaska earthquake* (No. 543-I). US Government Printing Office.

Plafker, G., Lajoie, K.R. and Rubin, M., 1992. Determining recurrence intervals of great subduction zone earthquakes in southern Alaska by radiocarbon dating. In *Radiocarbon After Four Decades: An Interdisciplinary Perspective* (pp. 436-453). New York, NY: Springer New York.

Potapova, M.G., Charles, D.F., Ponader, K.C. and Winter, D.M., 2004. Quantifying species indicator values for trophic diatom indices: a comparison of approaches. Hydrobiologia, 517, pp.25-41.

Ramsey, C.B., 2009. Bayesian analysis of radiocarbon dates. *Radiocarbon*, *51*(1), pp.337-360.

Rasband, W.S., ImageJ, U. S. National Institutes of Health, Bethesda, Maryland, USA, http://rsb.info.nih.gov/ij/, 1997-2007.

Reimer, P.J., Austin, W.E., Bard, E., Bayliss, A., Blackwell, P.G., Ramsey, C.B., Butzin, M., Cheng, H., Edwards, R.L., Friedrich, M. and Grootes, P.M., 2020. The IntCal20 Northern Hemisphere radiocarbon age calibration curve (0–55 cal kBP). *Radiocarbon*, *62*(4), pp.725-757.

Rothwell, R.G. and Croudace, I.W., 2015. Twenty years of XRF core scanning marine sediments: what do geochemical proxies tell us?. Micro-XRF Studies of Sediment Cores: Applications of a non-destructive tool for the environmental sciences, pp.25- 102.

Sancetta, C., 1979. Use of semiquantitative microfossil data for paleoceanography. Geology, 7(2), pp.88-92.

Savage, J.C. and Plafker, G., 1991. Tide gage measurements of uplift along the south coast of Alaska. *Journal of Geophysical Research: Solid Earth*, *96*(B3), pp.4325-4335.

Scholl, D.W., 1964. Recent sedimentary record in mangrove swamps and rise in sea level over the southwestern coast of Florida: Part 2. *Marine Geology*, *2*(4), pp.343-364.

Scott, D.B. and Medioli, F.S., 1980. Living vs. total foraminiferal populations: their relative usefulness in paleoecology. *Journal of Paleontology*, pp.814-831.

Scott, D.B. and Medioli, F.S., 1986. Foraminifera as sea-level indicators. In *Sea-level research: A manual for the collection and evaluation of data* (pp. 435-456). Dordrecht: Springer Netherlands.

Shennan, I. and Hamilton, S., 2006. Coseismic and pre-seismic subsidence associated with great earthquakes in Alaska. *Quaternary Science Reviews*, *25*(1-2), pp.1-8.

Shennan, I., Barlow, N. and Combellick, R., 2008. Paleoseismological records of multiple great earthquakes in southcentral Alaska: A 4000-year record at Girdwood. *Geophysical Monograph Series*, 179, pp.185-199.

Shennan, I., Barlow, N., Carver, G., Davies, F., Garrett, E. and Hocking, E., 2014. Great tsunamigenic earthquakes during the past 1000 yr on the Alaska megathrust. *Geology*, *42*(8), pp.687-690.

Shennan, I., Bruhn, R. and Plafker, G., 2009. Multi-segment earthquakes and tsunami potential of the Aleutian megathrust. *Quaternary Science Reviews*, *28*(1-2), pp.7-13.

Shennan, I., Bruhn, R., Barlow, N., Good, K. and Hocking, E., 2014. Late Holocene great earthquakes in the eastern part of the Aleutian megathrust. *Quaternary Science Reviews*, *84*, pp.86-97.

Shennan, I., Brader, M.D., Barlow, N.L., Davies, F.P., Longley, C. and Tunstall, N., 2018. Late Holocene paleoseismology of Shuyak Island, Alaska. *Quaternary Science Reviews*, *201*, pp.380-395.

Shennan, I., Garrett, E. and Barlow, N., 2016. Detection limits of tidal-wetland sequences to identify variable rupture modes of megathrust earthquakes. *Quaternary Science Reviews*, *150*, pp.1-30.

Shennan, I., Scott, D.B., Rutherford, M. and Zong, Y., 1999. Microfossil analysis of sediments representing the 1964 earthquake, exposed at Girdwood Flats, Alaska, USA. *Quaternary International*, *60*(1), pp.55-73.

Suito, H. and Freymueller, J.T., 2009. A viscoelastic and afterslip postseismic deformation model for the 1964 Alaska earthquake. *Journal of Geophysical Research: Solid Earth*, *114*(B11).

Ter Braak, C.J. and Juggins, S., 1993. Weighted averaging partial least squares regression (WA-PLS): an improved method for reconstructing environmental variables from species assemblages. In *Twelfth international diatom symposium: Proceedings of the twelfth international diatom symposium, Renesse, The Netherlands, 30 August–5 September 1992* (pp. 485-502). Springer Netherlands.

Ter Braak, C.J. and Prentice, I.C., 1988. A theory of gradient analysis. In *Advances in ecological research* (Vol. 18, pp. 271-317). Academic Press.

Ter Braak, C.J. and van Dame, H., 1989. Inferring pH from diatoms: a comparison of old and new calibration methods. *Hydrobiologia*, *178*, pp.209-223.

Troels-Smith, J., 1955. Karakterisering af løse jordarter. *Danmarks Geologiske Undersøgelse IV. Række*, *3*(10), pp.1-73.

VAN DER WERFF, A. and H. HULS, 1957–1974. Diatomeeënflora van Nederland. Abcoude, De Hoef.

Wang, P.L., Engelhart, S.E., Wang, K., Hawkes, A.D., Horton, B.P., Nelson, A.R. and Witter, R.C., 2013. Heterogeneous rupture in the great Cascadia earthquake of 1700 inferred from coastal subsidence estimates. *Journal of Geophysical Research: Solid Earth*, *118*(5), pp.2460-2473.

Watcham, E.P., Shennan, I. and Barlow, N.L., 2013. Scale considerations in using diatoms as indicators of sea-level change: Lessons from Alaska. *Journal of Quaternary Science*, *28*(2), pp.165-179.

Wesson et al 2007. U.S. Geological Survey Open-File Report, pp. 1-33.

Wright, A.J., Edwards, R.J. and van de Plassche, O., 2011. Reassessing transfer- function performance in sea-level reconstruction based on benthic salt-marsh foraminifera from the Atlantic coast of NE North America. *Marine Micropaleontology*, *81*(1-2), pp.43-62.

Zong, Y., Shennan, I., Combellick, R.A., Hamilton, S.L. and Rutherford, M.M., 2003. Microfossil evidence for land movements associated with the AD 1964 Alaska earthquake. *The Holocene*, *13*(1), pp.7-20.

Zweck, C., Freymueller, J.T. and Cohen, S.C., 2002. Three-dimensional elastic dislocation modeling of the postseismic response to the 1964 Alaska earthquake. *Journal of Geophysical Research: Solid Earth*, *107*(B4), pp.E